Characterization of Flavivirus Host-Cell Interactions

By

David Lin

A dissertation submitted in partial fulfillment
of the requirements for the degree of
Doctor of Philosophy
(Microbiology and Immunology)
in The University of Michigan
2018

Doctoral Committee:

Associate Professor Andrew W. Tai, Chair
Professor David Ginsburg
Professor Akira Ono
Professor Katherine R. Spindler
Professor Billy Tsai

David L. Lin

davlin@umich.edu

ORCID iD: 0000-0001-5607-2781

Dedication

This work is dedicated to Katherine Rose Imai Nakama, who has provided invaluable encouragement during this journey. Her influence has been incredibly meaningful, and extends beyond just her support of my career decisions.

Acknowledgments

I thank Andrew Tai, my thesis advisor, for his guidance and supervision. He provided me a long leash, with which I was able to explore several avenues of research, helping me develop the skills necessary to become an independent researcher. I am extremely fortunate to have been his first graduate student.

I also greatly appreciate the feedback from my committee members, Dr. David Ginsburg, Dr. Akira Ono, Dr. Katherine R. Spindler, and Dr. Billy Tsai. Their support and guidance during committee meetings, joint laboratory meetings, and one-on-one meetings were critical to my growth as a scientist. I also thank the members of their labs, especially for commiserating through the graduate school experience.

I am also grateful to all the previous members of the lab for providing an enjoyable laboratory environment, and for their scientific support. I especially would like to thank Dr. Hongliang Wang for his help in the lab, and for our entertaining discussions both about science and life in general.

The various projects I pursued could not have been completed without critical contributions from other scientists. The characterization of MAGT1 was a collaborative effort with the labs of Dr. Reid Gilmore and Dr. Margaret R. MacDonald. I would like to thank Dr. Natalia Cherepanova, who performed the pulse chase experiments demonstrating the glycosylation of NS1, and Dr. Leonia Bozzacco for flow cytometry experiments establishing the OST as a critical host factor for DENV and ZIKV. I also thank Stephanie Azzopardi from the MacDonald lab, who helped perform flow cytometry experiments to show that NS1 mutants could function as dominant-negative inhibitors across flavivirus species. Additionally, I thank Natalie McMyn for aiding in the cloning and construction of several NS1 mutants.

The work to characterize the EMC as a flavivirus host factor was a collaborative effort with the lab of Billy Tsai. Dr. Takamasa Inoue, Dr. Yu-Jie Chen, and Aaron Chang

from the Tsai lab performed experiments to demonstrate that expression of Zika virus non-structural proteins are dependent on the EMC. Additionally, they performed experiments to establish a role for ER-associated degradation mediated removal of NS4B.

This work was funded by the National Institutes of Health grant R01DK097374 (Andrew W. Tai), the Molecular Mechanisms of Microbial Pathogenesis Training Program T32AI007528 (David L. Lin), and the Training in Basic and Translational Digestive Sciences grant T32DK094775 (David L. Lin).

Table of Contents

List of Figures

List of Tables

ABSTRACT

Dengue virus (DENV) is the most prevalent arbovirus globally, infecting an estimated 400 million people each year. DENV belongs to the *Flaviviridae* family of viruses, and is closely related to Zika virus (ZIKV), West Nile virus (WNV), and yellow fever virus (YFV). To date, there are no approved antivirals for the treatment of dengue, in part due to the poor understanding of DENV replication and interactions with its host cell. We performed a genome-wide CRISPR-Cas9 knockout screen in human hepatoma Huh-7 cells to identify host dependency factors for DENV and reveal potential therapeutic targets. We found that two major protein complexes are necessary for DENV replication, the oligosaccharyltransferase (OST) complex and the endoplasmic reticulum membrane protein complex (EMC).

We show that two mammalian OST complexes that incorporate either STT3A or STT3B, the catalytic subunits responsible for N-linked glycosylation, are necessary for DENV replication. However, the enzymatic activity of these subunits is not essential for replication. We found that expression of MAGT1 or its homolog TUSC3 is dependent on expression of STT3B, and that cells lacking MAGT1/TUSC3 are protected from DENV infection. Mutagenesis studies of MAGT1 revealed that a conserved CxxC motif shared among oxidoreductases is required for efficient DENV infection, suggesting that MAGT1 acts as an oxidoreductase to support DENV infection. We also provide evidence that the STT3B/MAGT1 OST complex interacts with NS4B and may be important for its biogenesis and folding.

We also show that the EMC, which contains ten subunits EMC1 through EMC10, is also necessary for DENV replication. The EMC has been proposed to function as a chaperone and insertase for transmembrane proteins. We found that cells lacking the EMC support significantly reduced levels of flavivirus NS4A and NS4B, both of which

are multi-pass transmembrane proteins that contain domains with marginal hydrophobicity. Importantly, we demonstrate an interaction between the EMC and NS4B, but not NS1 or NS2B, during viral replication. We show that deletion or mutagenesis of two marginally hydrophobic domains of NS4B render its expression no longer dependent on the EMC. Taken together, our data suggest that the EMC promotes the expression of NS4B via an interaction with marginally hydrophobic domains, a feature that may apply to other cellular EMC substrates as well.

In a tangentially related project, we found that exogenous expression of a hypoglycosylated N207A mutant of DENV NS1 blocked DENV infection in a dominant-negative fashion. Similarly, we found that expression of an N130A mutant of ZIKV NS1 inhibited both DENV and ZIKV infection. Immunofluorescence microscopy revealed that these NS1 mutants exhibited a filamentous phenotype upon flavivirus infection, rather than the punctate distribution of wild-type NS1. We further designed NS1 mutants that were able to inhibit DENV, YFV, and ZIKV infection, and we speculate that they may also prevent infection by other flaviviruses. While the mechanism of inhibition is still unclear, these mutants may be useful tools to study the role of NS1 in flavivirus replication, and potentially in preventing flavivirus transmission. Our novel findings demonstrate cross-flavivirus dominant-negative inhibition of replication by NS1 mutants.

In summary, these findings provide a deeper understanding of flavivirus biology and help elucidate the roles of these cellular complexes in viral replication.

CHAPTER I

Introduction

Dengue disease

Dengue virus (DENV) is the etiologic agent of dengue fever, which can manifest with a spectrum of acute symptoms such as a fever, rash, joint pains, vomiting, with less than 5% of dengue infections resulting in severe illness called dengue hemorrhagic fever or dengue shock syndrome. Dengue virus is transmitted primarily by the *Aedes aegypti* mosquito, which is geographically restricted to subtropical regions of the world (1). Unfortunately, projections estimate that climate change will result in the expansion of the Aedes vector range, leading to the increased incidence of dengue and other arboviruses (2-4). There are four DENV serotypes that co-circulate in regions with endemic DENV(5). Genetically related flaviviruses, such as Zika virus (ZIKV), yellow fever virus (YFV), and West Nile virus (WNV) are also transmitted by mosquito, and often cause symptoms similar to dengue. Approximately 80% of DENV infections are asymptomatic, with an estimated 400 million people each year becoming infected by DENV, and approximately 100 million presenting with disease (6). To date, no approved antivirals exist for the treatment of dengue, due at least in part to the poor understanding of the DENV host-cell biology.

Dengue virus

Dengue virus (DENV) is an enveloped positive sense-single stranded RNA virus of the genus *Flavivirus*. Like all other viruses, DENV is an intracellular obligate parasite dependent on a host cell for reproduction. The DENV infection cycle is initiated by binding to the host cell surface, which has been shown to be cell type and serotype specific, with a number of putative receptors that mediate virus entry (7). The virion is

internalized via endocytosis, and a reduction in pH by the vacuolar-type H^+-ATPase complex within the endosome triggers a conformational change in the viral structural protein E, inducing fusion of the viral envelope with the endosomal membrane (8). The viral capsid carrying the positive-sense genome delivers the genome to the cytosol where it is translated at the endoplasmic reticulum (ER).

All flaviviruses contain a similar genetic organization, having a single open reading frame that is translated as a polyprotein and cleaved into ten individual proteins (Figure 1.1). At the N-terminus of the polyprotein are the three structural proteins that comprise the virion, and toward the C-terminus are the seven non-structural (NS) proteins, NS1, NS2A, NS2B, NS3, NS4A, NS4B, and NS5, which are necessary and sufficient to drive replication of the flavivirus genome (Figure 1.1) (9, 10). Cleavage of the polyprotein is mediated by various proteases, including the host signalase complex, the viral NS2B-NS3 protease, and a still unidentified protease that cleaves between NS1 and NS2A (11, 12). Of the seven non-structural proteins, only the NS2B-NS3 protease/helicase and NS5 RNA-dependent RNA polymerase and methyltransferase have known enzymatic functions (13-16). The other NS proteins lacking known enzymatic functions, NS1, NS2A, NS4A, and NS4B, have been proposed to carry out other pro-viral functions necessary for replication, such as immune evasion and remodeling of the ER membrane necessary for the establishment of the flavivirus replicase, also known as the replication organelle (RO) (9, 17, 18).

Genome replication of virtually all positive-sense RNA viruses occurs on a host-derived membrane, such as the ER, rather than freely in the cytoplasm (19). In general, RO morphology is virus-dependent and can be divided into two types. For instance, DENV induces vesicular invaginations of the ER membrane, while HCV infection leads to the formation of double membrane vesicles that protrude from the ER (20). In the case of DENV, the vesicular RO encompasses the viral genome and replicative intermediates such as double-stranded RNA (dsRNA) (Figure 1.2) (19-21). Additionally, some ER-resident cellular machinery is recruited to the RO and has been shown to be important for viral replication.

During infection, flaviviruses selectively repress host translation, strongly favoring viral translation (22). Not surprisingly, the cellular co-translational machinery including the Sec61 translocon, the oligosaccharyltransferase (OST) complex, and the endoplasmic reticulum membrane protein complex (EMC) are required for flavivirus replication (12, 23-26). Importantly, the OST localizes to the RO, though its function during flavivirus replication is still unclear (26). A review of these major protein complexes will be discussed later in this chapter.

The localization of the non-enzymatic non-structural proteins to the RO suggests that they likely participate in genome replication, possibly through rearranging the ER membrane to generate ROs. However, their specific roles in this process are poorly understood. While multiple non-structural proteins antagonize innate immune pathways, these non-structural proteins also play more direct roles in supporting viral replication (18). The behavior and roles of NS1, NS4A, and NS4B in flavivirus replication are further discussed below.

NS1

Flavivirus NS1 is a 352 amino acid glycoprotein whose structure is highly conserved across flaviviruses, despite significant sequence variation. The 24 C-terminal amino acids from E protein serve as a signal sequence for the insertion of NS1 into the ER lumen, where NS1 is glycosylated by the oligosaccharyltransferase (OST) complex at positions N130 and N207 with high-mannose carbohydrates (27-29). The function of NS1 glycosylation has not been elucidated, though multiple studies have shown that NS1 glycosylation is essential for efficient genome replication. Hypoglycosylation of NS1 by mutation to the N130 and N207 sequons have varying virus-specific effects, usually resulting in attenuation of viral replication (30-34). In addition, glycosylation at N207 has been reported to mediate oligomer stability and heat sensitivity (29, 32, 35). Viruses harboring mutations to both glycosylation sites were genetically unstable, further reinforcing the importance of glycosylation in replication (31, 33).

The NS1 monomer harbors 12 cysteines that form 6 intramolecular disulfide bonds necessary for NS1 folding and viral propagation (36, 37). The short-lived

monomer rapidly homo-dimerizes in the ER lumen within 20 minutes of translation (38). The highly conserved structure of the NS1 dimer can be separated into three structural domains: a short β-roll (1-29), a wing domain (30-180), and the β-ladder (Figure 1.3) (181-352) (39). The β-roll consists of two intertwined β-hairpins that have been proposed to mediate NS1 dimerization, lipid interaction, and association with other NS proteins (Figure 1.3) (39-41). The β-ladder consists of 18 anti-parallel β-strands that resemble a ladder along the length of the dimer (39). A discontinuous connector sits against the β-roll, joining the wing domain with the β-roll, and forming a hydrophobic spike that has been proposed to mediate membrane interactions (39, 41, 42). The wing is further comprised of an α/β subdomain and a disordered wing tip that is necessary for its interaction with the DENV virion during viral assembly (40).

While evidence suggests dimerization is necessary for its function, a single report has described a replication-competent Kunjin virus encoding a monomeric NS1 harboring an L250P mutation (43). However, studies with other viruses have failed to recapitulate this effect, and attempts to destabilize the DENV NS1 dimer by mutagenesis have not been successful (32, 44, 45). The NS1 dimer is primarily localized to the RO, localizing with dsRNA and other non-structural proteins, suggesting a role for NS1 in genome replication (46). Despite considerable effort, studies have yet to yield significant advances in the understanding of NS1 function. Being an ER lumenal protein, NS1 is physically excluded from the interior of the RO, making it unlikely that NS1 interacts directly with the cytoplasmic-facing replication machinery. Instead, NS1 associates with NS4A, NS4B, and host factors to assist in replication. Evidence of a biochemical interaction between NS1 and NS4A was first identified in Kunjin virus, and further reinforced using YFV, by using both genetic and biochemical techniques (17, 46, 47). However, the same has not been conclusively shown for DENV. In addition, passage of WNV harboring inhibitory NS1 mutations led to adaptive mutations in NS4B, suggesting an interaction between the two proteins (41). Other evidence using mass-spectrometry of NS1-interacting proteins during viral infection has further reinforced that NS1 and NS4B are likely associated during infection (28, 48, 49). It is possible that this

interaction between NS1 and NS4B induces conformational changes that drive RO formation, and regulate viral replication.

NS1 may also recruit cellular pro-viral factors within the ER lumen to the RO to facilitate viral replication. Efforts to identify these NS1-interacting factors have revealed a number of proteins that may interact with NS1 during viral infection such as the OST, ribosomal machinery, vimentin, and the chaperonin-containing TCP-1 (CCT) complex (also known as the TRiC) (26, 28, 50, 51). While NS1 no doubt interacts with cellular machinery, the nature of its interactions and whether they are important for viral replication is still unclear.

In addition to participating in genome replication at the flavivirus RO, NS1 plays a role in viral assembly through its interactions with E and M glycoproteins during infection (40). A fraction of NS1 is also secreted from the cell as a hexamer (35). Surprisingly, the process of NS1 secretion is dispensible for genome replication (40). Soluble hexameric NS1 enhances flavivirus infection when exogenously added to cell culture media (52). Levels of NS1 in patient blood correlate with disease severity, and secreted NS1 has been reported to enhance dengue pathogenesis through interactions with the complement system, and inducing vascular permeability (53-56). In addition, NS1 in host sera enhances flavivirus uptake into naïve mosquitos, also suggesting a role for NS1 in flavivirus transmission (57). In summary, NS1 clearly plays roles in replication, immunity, and disease, but its exact function in each of these processes has yet to be clarified.

NS4A and NS4B

Similar to NS1, NS4A and NS4B localize at the RO during infection, suggesting they participate in viral replication. NS4A is a 127 amino acid multi-pass transmembrane protein with a C-terminal 2kDa peptide, termed 2K, which functions as a signal sequence for NS4B. Cleavage between NS4A and 2k is mediated by the viral NS3 protease, liberating NS4A and 2k-NS4B (58). The N-terminal amphipathic helix is important for NS4A oligomerization and its interaction with NS4B (59-63). NS4A also contains two transmembrane helices with a third ER lumenal helix between the two

transmembrane domains (64). Overexpression of NS4A alone is sufficient to induce membrane rearrangements (65). The combined evidence suggests that NS4A plays a critical role in RO assembly and possibly curvature of the RO.

NS4B is a conserved 248 amino acid protein inserted into the ER lumen. An N-terminal 2K peptide is required for proper insertion of NS4B into the ER membrane, and is cleaved by a host signalase from the mature NS4B (66). NS4B has five putative transmembrane domains, with multiple membrane-associated hydrophobic-rich patches throughout the protein (67). A biochemical study using NS4B fusion proteins and protease protection assays suggested that only three C-terminal helices span the membrane, while the N-terminal two putative transmembrane helices (pTM1 and pTM2) are membrane-associated or reside within the ER lumen (66). By contrast, NMR studies using recombinant NS4B have suggested that the N-terminal helices are embedded in the membrane (68, 69). Indeed, transmembrane prediction tools identify the domains as potential transmembrane helices, but with relatively low probability of being membrane-inserted, an aspect that will be further discussed in Chapter III. Despite attempts to clarify NS4B topology, much of its biochemistry and folding have remained an enigma.

Additionally, DENV-2 NS4B encodes four glycosylation sequons, but is only partially glycosylated during infection (70). Mutagenesis revealed that the two N-terminal sequons located between pTM1 and pTM2 are necessary for efficient replication (70). It is unlikely that NS4B glycosylation is required for proper folding, because only a minor fraction is glycosylated in infected cells. One group has also shown that recombinant NS4B is capable of forming oligomers, though oligomerization has not been definitively shown during infection (71).

Early during infection, NS4B is localized to the perinuclear region of the cell, and later forms distinct foci along with the other NS proteins at the ROs, suggesting a role for NS4B in replication (17, 72). Interactions between NS4B, NS4A, and NS1 may affect NS4B folding, topology, and function (73). NS4B reportedly interacts with NS3, possibly playing a role in coordinating the helicase and protease activities of NS3 (71, 74). NS4B can also be found at the mitochondria, where it inhibits innate immune responses and interacts with ATP synthase machinery, which the authors speculate may be important

for biogenesis of the replication organelle (75). Unfortunately, further interactions between NS4B and host proteins during viral infection have not yet been deeply explored.

NS4B was noted as a “mutational hotspot,” with a high frequency of adaptive mutations (73). A number of mutations across NS4B improve flavivirus replication in cell culture, and others enhance pathogenesis in vivo (76-80). Despite a wide variety of identified NS4B mutations that enhance replication, the mechanism by which NS4B modulates replication is still inconclusive.

The oligosaccharyltransferase complex

DENV, and other flaviviruses, are highly dependent on the ER for replication, since the ER membrane is co-opted to establish the RO (20). Not surprisingly, many ER resident proteins are essential for DENV replication. The two ER complexes that were subjected to extensive study in this work are the OST complex and the EMC.

Protein glycosylation is an important cellular process that mediates protein folding, stability, trafficking, and localization (81). The OST complexes are responsible for asparagine-linked glycosylation, the transfer of oligosaccharides onto target proteins containing N-x-S/T sequons within the ER lumen (82). Vertebrates, insects, and plants express at least two OST isoforms that incorporate either of the paralogous catalytic subunits STT3A or STT3B (83). Both STT3A and STT3B harbor a conserved WWDYG catalytic motif that is required for enzymatic activity (84). Despite their functional redundancy, some cellular substrates are dependent on either STT3A or STT3B for efficient glycosylation, though the determinants that guide OST specificity have yet to be elucidated (82). Additionally, some peptides require both STT3A and STT3B for complete glycosylation, though STT3B has been shown to at least partially compensate in cells lacking STT3A (85).

Data suggest that STT3A is responsible for co-translational glycosylation of target proteins, while STT3B functions post-translationally on sequons skipped by STT3A (85). This difference in functionality is due in part to the isoform-specific subunits that comprise the STT3A or STT3B complexes. The STT3A complex contains two

isoform-specific subunits, KCP2 and DC2 (86). DC2 and KCP2 mediate the interaction between the OST and the Sec61 translocon (87). By contrast, the STT3B complex associates with the thioredoxin homolog MAGT1, or its paralog TUSC3, which both harbor oxidoreductase activity via a conserved CxxC motif (88, 89). The CxxC active site forms mixed disulfides with target proteins in the ER, granting STT3B access to sequons for glycosylation (88). Structural studies of the TUSC3 soluble domain revealed a peptide-binding groove that may guide substrate recognition, though determinants of peptide binding have yet to be identified (89).

Both of the OST complexes are additionally comprised of the shared OST subunits RPN1, RPN2, OST4, OST48, DAD1, and TMEM258 (90-94). The DC2 and KCP2 subunits mediate the interaction between the OST and the Sec61 translocon (87). RPN1 and RPN2 ribophorins link the OST with ribosomal machinery in the cytosol, assisting in co-translational glycosylation (95-97). OST4 and DAD1 may be necessary for OST complex stability, though their functions are still unclear (98, 99). While not all OST subunits have been well characterized, it has become clear that each subunit is necessary for efficient N-linked glycosylation.

The endoplasmic reticulum membrane protein complex (EMC)

The EMC was first identified in yeast, where genetic ablation led to accumulation of misfolded proteins and induction of the unfolded protein response (100). Initially, immunoprecipitation of the complex from yeast established six proteins, EMC1-6, as core EMC components (100). Further studies with mammalian cells revealed four additional potential EMC subunits, EMC7-10, with each EMC subunit 1-10 present in roughly stoichiometric ratios (101, 102). Primary studies identified the EMC as critical for protein folding and ER-associated degradation (ERAD) pathways, though its detailed function was entirely unclear. Studies into the function of the EMC have been hampered in part due to the poor homology between EMC subunits and proteins of known function.

EMC1 is the largest subunit of the complex, 993 amino acids in length, with a single C-terminal transmembrane domain anchoring it to the ER membrane. EMC2 is a cytosolic putative tetratricopeptide repeat protein comprising three degenerate motifs

that have been shown to mediate protein-protein interactions. EMC3 is a multipass transmembrane protein with homology to the bacterial YidC or mitochondrial oxa1 membrane protein insertases (103). EMC4 and EMC6 (TMEM93) are each small (<20 kDa) multipass transmembrane proteins with negligible homology to proteins with known activities, and thus no putative function. EMC5 (MMGT1) is annotated as a magnesium transporter due to its weak homology with MMGT2 and partial localization to Golgi vesicles after overexpression (104). A single study showed that knockdown or overexpression of EMC5 modulates Mg^{2+} transport; however current data suggests that the EMC is necessary for expression of transmembrane proteins, likely those responsible for Mg^{2+} transport (104). Future studies will reveal whether EMC5 homology to other magnesium transporters may provide insight to its function in the EMC.

The data to date support the hypothesis that the EMC functions as a transmembrane chaperone or insertase. Initial evidence supporting this model was that biosynthesis of various transmembrane proteins is dependent on the EMC, including acetylcholine receptors and rhodopsin in *C. elegans* and *Drosophila* respectively (105, 106). Later studies showed that the EMC can function as an insertase, and is sufficient for membrane insertion of an in vitro translated tail-anchored single pass transmembrane protein (107). However, three studies have shown that expression of multipass transmembrane proteins was specifically impaired in cells depleted of the EMC, suggesting the EMC functions as more than a tail-anchored membrane protein insertase (102, 105, 106).

Furthermore, experiments revealed that the EMC participates co-translationally in the biosynthesis of “folding-challenged multipass client proteins” (102). More specifically, these putative EMC clients contain transmembrane domains enriched in charged amino acids and depleted of classic hydrophobic residues usually found in transmembrane helices (102). The authors speculated that the EMC engages these difficult-to-fold transmembrane proteins, delaying their degradation by ERAD, and recruits chaperones to assist in folding (102). In support of this model, another group has shown that the EMC binds HSP90, though the importance of this interaction for EMC function has not been defined (108). Together, these data suggest a specific role for the EMC in the

biogenesis and stability of multipass transmembrane proteins, though some studies have also suggested the EMC plays roles in other cellular processes.

The EMC has also been postulated to function as an ER-mitochondrial tether responsible for lipid transfer. However, this phenotype was only reproducible in the background of yeast harboring multiple EMC knockouts, and ablation of a single EMC subunit did not significantly affect lipid transfer (109). These data are also contradictory to others, where knockout of a single EMC subunit was sufficient to deplete other EMC proteins. One explanation for this contradiction is that depletion of multiple EMC subunits exacerbates the loss of specific transmembrane proteins necessary for ER-mitochondrial tethering and/or lipid transfer.

Other groups have also posited a role for EMC6 in autophagy, since knockdown of EMC6 marginally reduced autophagy compared to control cells when induced by chloroquine (110, 111). These effects may not be EMC6 specific, as the authors did not address whether depletion of other EMC subunits also results in a similar phenotype. Whether the EMC plays a direct role in autophagy has yet to be clarified.

The EMC is important for the propagation of multiple viruses. For polyomavirus SV40, the EMC is necessary for ER membrane penetration and entry, further reinforcing a role for the EMC as a chaperone (112). The EMC has also been identified as a host dependency factor for multiple flaviviruses including WNV, YFV, and ZIKV (12, 25, 26, 113). For DENV, the EMC inhibits at a stage early in the viral life cycle (25). The EMC also associates with the OST, further supporting a potential role for the EMC at the RO (25).

Many questions still remain regarding the EMC and its function. What are determinants that drive EMC dependence of multipass transmembrane proteins? Does the EMC recruit co-chaperones to assist in substrate folding? What is the function of each of the EMC subunits? What role does the EMC play during flavivirus infection?

CRISPR-Cas9 screens

Significant effort has been applied to identify viral host dependency factors, in an effort to develop antiviral therapeutics that target the host rather than viral proteins. High

throughput genome-wide screens have been valuable tools for identifying these host dependency factors. Sessions et al. in 2009 were the first to publish a genome-wide screen using RNA interference to identify DENV host dependency factors (114). However, methods employing interfering RNAs have significant weaknesses, including off-target effects, depletion limits, and low reproducibility (115-117). Recently, tools based on the clustered regularly interspaced short palindromic repeat (CRISPR) Cas9 system have expanded our ability to efficiently and accurately modify genomes.

The CRISPR-Cas9 system involves a Cas9 endonuclease that is guided by a single guide RNA (RNA) molecule, which is composed of a 20 nucleotide targeting RNA (crRNA) fused to a structured RNA that interacts with the Cas9 protein (tracrRNA) (118). Homology between a segment of the genome and the crRNA directs the Cas9 nuclease toward a specific site in the genome, inducing a double-stranded break at a site termed the protospacer adjacent motif (PAM), which is between 3-6 nucleotides from the sgRNA binding site (119). The double-stranded break is repaired either by homologous recombination, or by non-homologous end-joining, which most often results in frameshift mutations, effectively generating a genetic knockout (120). Feng Zhang's group at MIT developed a lentiviral vector library encoding sgRNAs targeting the entire human genome paired with a Cas9 and a puromycin selection marker for the generation of pools of stable knockout human cells (121, 122).

We used this tool to identify host dependency factors necessary for DENV propagation, which launched three intriguing projects that comprise this dissertation.

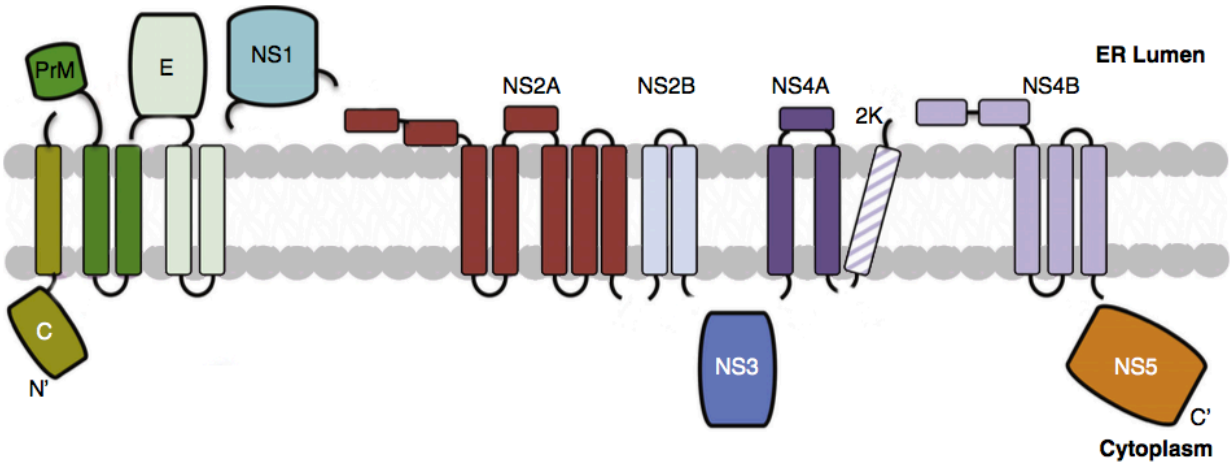

Figure 1.1. The DENV polyprotein. Adapted from (123). DENV is translated as a polyprotein, which is processed at the ER into ten individual proteins. At the N-terminus are the three structural proteins that comprise the DENV virion, C, prM and E. Next are the seven non-structural proteins that are necessary and sufficient for genome replication. NS1 is a soluble ER lumenal protein, NS3 and NS5 are cytosolic proteins, and NS2A, NS2B, NS4A, and NS4B are multi-pass ER transmembrane proteins.

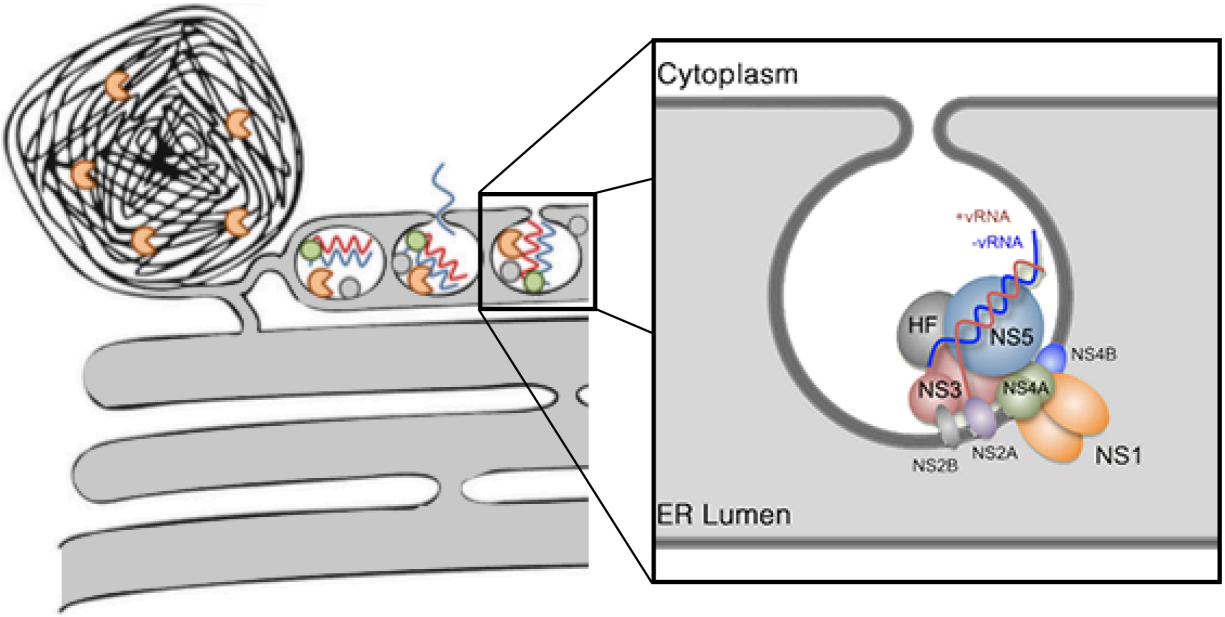

Figure 1.2. The flavivirus replication organelle. Adapted from (20, 124). Dengue infection rearranges the ER membrane into two distinct types: convoluted membranes and vesicular replication organelles (RO) where genome replication occurs. The RO is an invagination of the ER membrane containing each of the non-structural proteins, the double-stranded RNA replicative intermediate, and host-factors (HF).

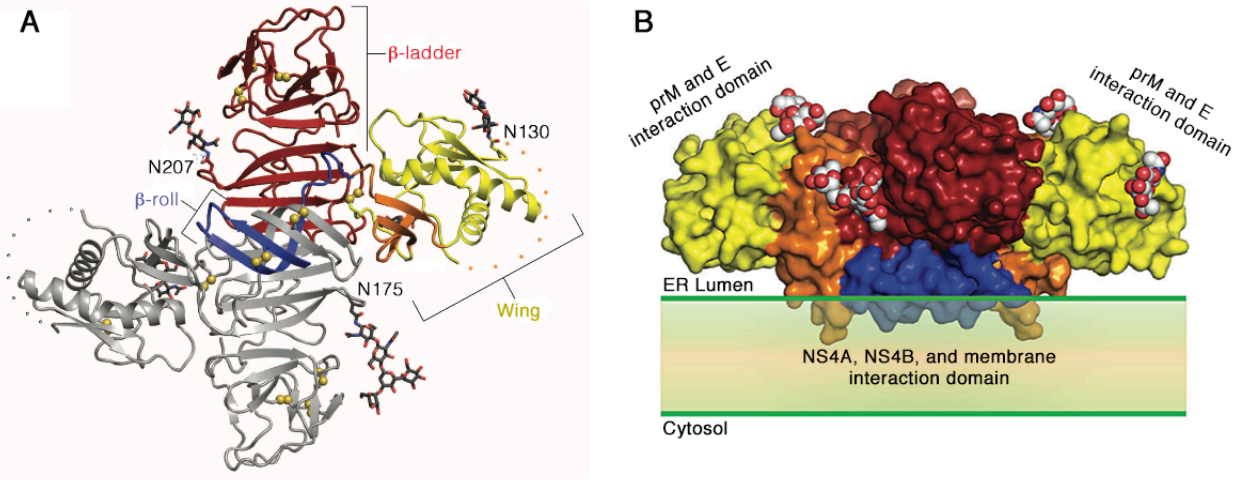

Figure 1.3. Flavivirus NS1. Adapted from (39). In **A**, the crystal structure of the West Nile virus NS1 dimer is shown. One monomer is colored in gray and the other color coded to indicate the three domains of NS1. The three glycosylated asparagines of West Nile virus NS1 are each labeled. In **B**, a surface plot of the same NS1 dimer rotated and embedded on the ER membrane surface. The NS1 β-roll mediates its interaction with NS4A, NS4B, and the ER membrane to support flavivirus replication. The wing domain of NS1 is important for its interaction with structural proteins and virion assembly.

CHAPTER II

Identification and characterization of MAGT1 as a DENV host-dependency factor

This chapter consists of material from a research article in mBio, "Dengue Virus Hijacks a Noncanonical Oxidoreductase Function of a Cellular Oligosaccharyltransferase Complex", written by David L. Lin, Natalia A. Cherepanova, Leonia Bozzacco, Margaret R. MacDonald, Reid Gilmore, and Andrew W. Tai (24).

Dr. Natalia A. Cherepanova performed pulse chase experiments demonstrating that NS1 is unchanged in OST knockout cells. Dr. Leonia Bozzacco performed infection experiments demonstrating that ZIKV is dependent on the OST.

A whole genome CRISPR screen reveals that DENV is dependent on both cellular oligosaccharyltransferase complexes.

We employed a CRISPR-Cas9 pooled screening approach to identify host proteins necessary for DENV-mediated cell death in Huh7.5.1 human hepatoma cells (Figure 2.1A). Among the top-ranked hits from the screen were multiple subunits of the host oligosaccharyltransferase (OST) complexes, including the two catalytic subunits *STT3A* and *STT3B*. Single-guide RNAs (sgRNAs) targeting genes encoding the two unique subunits of the STT3A and STT3B complexes, *DC2* and *MAGT1* respectively, were also significantly enriched in the screen (Figure 2.1B and C). In addition, two shared OST subunits, RPN2 and OST4, were significant hits (Figures 2.1B and C). Alternatively, the screen revealed at least two other major ER resident complexes as DENV host factors, the EMC and the SSR (Figure 2.2). To validate three of the hits from the screen, we generated *STT3A, STT3B* and *MAGT1* knockout Huh7.5.1 cells through stable transduction of the pLENTICRISPRv2 construct encoding both the *S. pyogenes* Cas9 protein and an sgRNA. The knockouts were confirmed by Western blot. Importantly, in *STT3B* knockout cells, MAGT1 protein was also depleted (Figure 2.3A),

as its stability requires interaction with STT3B (88). We then infected these cells with a luciferase reporter dengue virus (luc-DENV), where luciferase activity directly correlates with viral propagation. Three days post-infection, we assessed luciferase activity and saw a significant and marked decrease in luciferase activity in *STT3A, STT3B*, and *MAGT1* knockout cells compared to control cells transduced with a control GFP-targeting sgRNA, demonstrating that protection from DENV-mediated cell death in these knockout cells is mediated by inhibition of DENV infection rather than by a block of cell death signaling pathways (Figure 2.3A). The viability and growth of *STT3A, STT3B*, or *MAGT1* knockout cells was similar to control cells (Figure 2.3E). These data validate the results from the screen and show that *STT3A, STT3B,* and *MAGT1* are all required for efficient DENV propagation.

The catalytic oligosaccharyltransferase activity of the OST complexes is not required for DENV replication.

In order to confirm the specificity of our knockout cell lines, sgRNA-resistant *STT3A and STT3B* were then introduced by lentiviral transduction into the corresponding knockout cell lines to rescue STT3A (Figure 2.3B) or STT3B (Figure 2.3C) expression. Importantly, we found that exogenous expression of STT3B in *STT3B* knockout cells led to restoration of endogenous MAGT1 expression (Figure 2.3C). Exogenous expression of STT3A or STT3B rescued luc-DENV infection in *STT3A*-knockout or *STT3B*-knockout cells, respectively (Figs. 2.3B and C). These data confirm that STT3A and STT3B are specifically required for efficient DENV propagation.

Both STT3A and STT3B are oligosaccharyltransferases necessary for the transfer of glycans to asparagines on target substrates (85). Mutation of a conserved WWDYG motif to WAAYG inactivates oligosaccharyltransferase activity (84). STT3A or STT3B knockout cells expressing catalytically dead STT3A (STT3A-dead) or STT3B (STT3B-dead) were able to support similar levels of DENV infection as their wild-type counterparts, demonstrating that the catalytic activity of STT3A or STT3B is not required for DENV propagation (Figs. 2.3B and C).

We also confirmed that these constructs were indeed catalytically inactive by transfecting the rescued cells with plasmids to express either prosaposin (pSAP) or SHBG, specific N-glycosylation substrates of STT3A and STT3B respectively. By Western blot, a majority of pSAP remained hypoglycosylated, as evidenced by a more rapidly migrating band on SDS-PAGE from both STT3A knockout cells and STT3A-dead expressing cells (Figure 2.3B). Similarly, a fraction of SHBG appeared as a more rapidly migrating hypoglycosylated protein in both *STT3B* knockout cells and STT3B-dead expressing cells (Figure 2.3C). These results demonstrate that glycosylation of STT3A and STT3B specific endogenous substrates remains impaired in STT3A-dead and STT3B-dead expressing cells.

We also transfected a luciferase-DENV replicon into knockout cells to assess whether the specific step of viral replication requires STT3A or STT3B. We found significant decreases in luciferase activity in *STT3A* and *STT3B* knockout cells compared to wild-type control at 48 hours and 72 hours post-transfection (Figure 2.3D). These data confirm that both of the OST complexes are required for DENV replication, consistent with previous data(26). The viability of OST knockout cells was unchanged compared to controls (Figure 2.3E).

Together, these data suggest that STT3B stabilizes MAGT1 and that the canonical oligosaccharyltransferase activity of STT3B-containing OST complexes is not required for DENV propagation. These results support a model where STT3B is required to stabilize MAGT1, which in turn has its own specific function to support DENV replication. Therefore, we explored whether the catalytic activity of MAGT1 is required for DENV replication.

The OSTs are required to support efficient infection by Zika virus but not other flaviviruses

We next asked whether other arboviruses also depend on the same OST complexes, and used flow cytometry to determine whether infection was impaired in STT3A or STT3B knockout cells. We infected cells with DENV-2, Zika virus (ZIKV), West Nile virus (WNV), yellow fever virus (YFV), Sindbis virus (SINV), Venezuelan

Equine Encephalitis virus (VEEV), or Chikungunya virus (CHIKV) and compared the percentage of infected cells in OST knockout cells compared to control. Consistent with our other results, we found that DENV-2 infection was dramatically reduced in OST knockout cells compared to control (Figure 2.4). We also found that ZIKV infection was moderately, but significantly, reduced in STT3A and STT3B knockout cells indicating that the OSTs may also play a role during ZIKV infection (Figure 2.4). However, we did not find a significant decrease in the propagation of the other viruses tested.

The catalytic activities of TUSC3 or MAGT1 are necessary to support DENV propagation

Both MAGT1 and its paralog TUSC3 are thioredoxin homologs that harbor oxidoreductase activity through a conserved catalytic CxxC motif, and interact with STT3B but not STT3A (88). TUSC3 contains a peptide-binding pocket that may interact with proteins in a sequence specific manner (89). Cells lacking both MAGT1 and TUSC3 are unable to fully glycosylate STT3B specific substrates (88). These data support a model where MAGT1 or TUSC3 serve to form a mixed disulfide with a protein substrate, granting STT3B access to glycosylation sites that may otherwise be inaccessible.

In some cell types, TUSC3 expression is upregulated in the absence of MAGT1 (88). Importantly, although TUSC3 has been shown to be expressed in HEK293T cells (88), we found that TUSC3 is not expressed in wild-type or *MAGT1* knockout Huh-7.5.1 cells by immunoblotting (Figure 2.5A) or by RT-PCR (not shown). Therefore, we asked whether TUSC3 is capable of functionally replacing MAGT1 in the context of DENV infection. We found that *MAGT1* knockout Huh 7.5.1 cells transduced with a TUSC3-encoding lentiviral vector were able to support significantly increased DENV propagation compared to cells expressing neither MAGT1 nor TUSC3 (Figure 2.5A). These data demonstrate that the expression of either MAGT1 or TUSC3 is required for DENV propagation, and that these two proteins are functionally redundant in the context of DENV propagation.

We next asked whether the enzymatic activity of MAGT1 or TUSC3 is required for DENV propagation. Expression of catalytically inactive AxxA mutants of MAGT1 or TUSC3 failed to rescue DENV propagation in MAGT1 knockout Huh7.5.1 cells (Figures 2.5A and B), indicating that the oxidoreductase activity of MAGT1 or TUSC3 is required for DENV replication.

We also investigated whether MAGT1 knockout cells expressing single-cysteine active site MAGT1 mutants (CxxA and AxxC) are able to support DENV replication. Some single-cysteine mutants of ER resident oxidoreductases, such as protein disulfide isomerase (PDI), have been shown to retain oxidoreductase activity (125, 126), and single-cysteine MAGT1 mutants can form mixed disulfides with target proteins, demonstrating that they are reactive in cells (88). Interestingly, MAGT1 knockout cells expressing a single cysteine MAGT1 mutant were able to support increased levels of DENV replication compared to knockout cells, albeit at levels lower than with wild-type MAGT1 rescue (Figure 2.5B). This indicates that single cysteine MAGT1 mutants retain significant catalytic activity to support DENV infection. Together, these data demonstrate that the oxidoreductase activity of MAGT1 is required for DENV propagation, and that cells expressing single-cysteine MAGT1 are still able to support DENV replication.

MAGT1 partially localizes to DENV replication compartments

We next performed immunofluorescence microscopy on cells expressing an HA-tagged MAGT1 construct (MAGT1-HA) to visualize the localization of MAGT1 during DENV infection. In uninfected Huh-7 cells, both wild-type MAGT1 and MAGT1 mutants were distributed in an intracellular reticular pattern consistent with ER localization (Figure 2.5C). This supports the evidence that MAGT1 is an ER-localized component of the OST complex, rather than the proposal that MAGT1 contributes to magnesium import at the plasma membrane (88, 127). We also found that the distribution of the mutant MAGT1-AxxA was similar to that of wild-type MAGT1, demonstrating that the inability of cells expressing MAGT1-AxxA to support DENV replication is not due to defects in subcellular localization. DENV infection was associated with partial

colocalization of MAGT1 with viral NS1 protein (Figure 2.5C). Additionally, co-immunopreciptation assays demonstrated MAGT1-AxxA interaction with STT3B, indicating that MAGT1-AxxA's inability to support DENV replication is not due to a defect in association with the OST complex (Figure 2.5D). These data are consistent with previous data showing that the OST localized to sites of DENV induced vesicle packets and replication compartments(26).

NS1 is not detectably different in STT3A, STT3B, and MAGT1 knockout cells

We hypothesize that MAGT1 functions as an oxidoreductase, potentially affecting the folding of a DENV non-structural protein. We asked which DENV proteins could be candidate substrates for MAGT1 oxidoreductase activity. All four DENV serotypes are impaired in their ability to propagate in *STT3B* knockout cells (26), which based on our data must also lack MAGT1 expression. Therefore, we hypothesized that a viral target of MAGT1 oxidoreductase activity should have cysteines exposed to the ER lumen that are conserved across all four serotypes.

Four of the seven nonstructural proteins have cysteine residues predicted to be exposed to the ER lumen: NS1, NS2A, NS4A, and NS4B. Of these proteins, only NS1 and NS4B have cysteines that are conserved across all four DENV serotypes. The DENV protein NS1 forms a dimer in the ER, is secreted as a soluble hexamer, and contains twelve cysteines, six disulfide bonds, and two N-glycosylation sites (128). The DENV protein NS4B contains three cysteines and two N-glycosylation sites (70).

We first investigated whether we could detect any changes in NS1 properties by immunoblotting of NS1 expressed in knockout and wild-type cells. We were unable to detect any changes in NS1 dimerization or glycosylation in STT3A or STT3B knockout cells (Figure 2.6A). We also found that the pattern of NS1 glycosylation was unchanged after performing pulse-chase experiments in *STT3A*, *STT3B,* or *MAGT1/TUSC3* knockout cells (Figure 2.6B). We were also unable to detect any interaction between NS1 and STT3B or MAGT1 by co-immunoprecipitation (not shown). In summary, these data suggest that glycosylation of NS1 is unaffected by the loss of STT3A, STT3B, or MAGT1, and that NS1 is not a target of MAGT1 oxidoreductase activity.

NS4B synthesis is altered in STT3B knockout cells

We next sought to find differences in NS4B exogenously expressed in OST subunit knockout cells by generating tagged constructs expressing C-terminally tagged DENV 2k-NS4B-HA (pNS4B-HA) or 2k-NS4B-V5 (pNS4B-V5). NS4B has been proposed to be glycosylated at two residues, N58 and N62 (70). In 293T cells, we found that the pattern of NS4B-HA glycosylation was altered in cells expressing STT3B-dead compared to wild-type STT3B, with the apparent loss of accumulation of higher molecular weight HA-reactive bands (Figure 2.7A). Additionally, following transient expression of NS4B in Huh7.5.1 cells, we found three specific PNGase F sensitive bands that migrated at a higher molecular weight than unglycosylated NS4B, confirming that NS4B can be partially glycosylated under our experimental conditions (Figure 2.7B). Together this data shows that NS4B glycosylation is primarily mediated by STT3B. Although glycosylation of NS4B is not necessary for viral replication, as catalytically inactive STT3B rescues DENV replication in *STT3B* knockout cells, this finding suggests that NS4B physically interacts with the STT3B OST complex in the ER lumen.

We noticed a consistent reduction in NS4B protein levels in STT3B and MAGT1 knockout cells, and hypothesized that NS4B protein folding may be affected by the loss of STT3B or MAGT1. To measure the steady state levels of NS4B in STT3B knockout cells, we co-transfected a plasmid expressing either NS1 or GFP to control for transfection efficiency and quantitated chemiluminescent band intensities to measure relative levels of NS4B synthesis in STT3B knockout cells. We found a consistent and statistically significant ($p<0.0001$) 20-25% decrease in NS4B band intensity in STT3B knockout cells compared to wild-type controls relative to transfection control (Figure 2.7C). Despite this difference in NS4B steady-state levels, we did not find a difference in the half-life of NS4B in STT3B knockout cells compared to WT (Figure 2.7D), suggesting that the rate of synthesis, and not degradation, of NS4B is altered in STT3B knockout cells.

Together, these data show that NS4B is an STT3B substrate that requires MAGT1 to be efficiently glycosylated. Furthermore, NS4B synthesis appears to be

reduced by the loss of STT3B/MAGT1. Taken together, although NS4B glycosylation is not necessary for DENV infection, these findings suggest that NS4B physically interacts with both STT3B and MAGT1. Furthermore, they suggest that one mechanism by which MAGT1 facilitates DENV propagation may be through promoting efficient synthesis of NS4B.

Close proximity of MAGT1 to NS4B and NS1 during DENV infection

Although our data so far suggested a possible interaction between STT3B/MAGT1 and NS4B, using conventional immunoprecipitation methods, we were unable to demonstrate a stable interaction between MAGT1 and NS4B (not shown). Therefore, we used the engineered peroxidase APEX2 to label proteins in close proximity to MAGT1 during DENV infection. APEX2 catalyzes the biotinylation of proteins within a 5-10nm radius in the presence of biotin-phenol and hydrogen peroxide(129). We generated a construct in which APEX2 was inserted between the signal sequence and MAGT1, placing APEX2 in the ER lumen near the MAGT1 active site. We stably transduced *MAGT1* knockout cells to express the APEX2-MAGT1 fusion protein, and induced APEX2-mediated biotinylation in DENV infected cells. After lysis of the cells, we performed affinity purification of biotinylated proteins using streptavidin beads followed by SDS-PAGE and immunoblotting.

We found that both NS1 and NS4B were specifically biotinylated by APEX2-MAGT1 in DENV infected cells (Figure 2.8). To assess the specificity of APEX2 labeling, we probed for biotinylation of STT3A, which also associates with sites of DENV replication but does not interact with MAGT1 (26, 88), and found that STT3A is not biotinylated by APEX2-MAGT1 under these conditions (Figure 2.8). Similarly, the integral ER membrane protein VAPA is not biotinylated by APEX2-MAGT1. On the other hand, EMC3, another ER protein necessary for flavivirus propagation that was a hit in our screen and interacts with the OST complex (25), was biotinylated. These data are consistent with the model that MAGT1 likely resides at sites of DENV replication and either associates with or is in close physical proximity to DENV non-structural proteins.

The redox status of NS4B is unchanged in the absence of MAGT1

We hypothesized that the NS4B cysteine redox state is modulated by MAGT1. To test this, we used Western blots to examine changes in NS4B migration on SDS-PAGE after treating cell lysates with maleimide-PEG (mPEG), which covalently bonds to free reduced cysteine residues. The mPEG reagent has an average molecular weight of 5 kDa, resulting in a shift in the apparent molecular weight of modified proteins visualized by Western blot. DENV NS4B has three conserved cysteines that may participate in disulfide bonds. As a negative control, we lysed cells in the presence of N-ethylmaleimide (NEM), which covalently blocks all reduced cysteines, rendering them mPEG-nonreactive (Figure 2.9, lanes 1 and 2). As a positive control, we treated lysates with Tris(2-carboxyethyl)phosphine hydrochloride (TCEP), which reduces all cysteines, allowing subsequent mPEG modification of all cysteines (Figure 2.9, lane 5).

mPEG modified NS4B, when expressed in isolation, migrates the same in both wild-type and *STT3B* knockout cells, indicating that MAGT1 does not affect the cysteine redox state of NS4B (Figure 2.9, lanes 3 and 4). Additionally, a fraction of mPEG-modified NS4B (lanes 3 and 4) runs at the same apparent molecular weight as fully reduced TCEP-treated NS4B treated with mPEG (lane 5), indicating that at steady state, a fraction of NS4B molecules contains fully-reduced cysteines. However, another fraction of NS4B is modified by fewer mPEG molecules (lanes 3 and 4), demonstrating that some NS4B molecules may contain oxidized cysteines in the form of intra- or intermolecular disulfide bonds.

While our results indicate that MAGT1 does not modulate NS4B cysteine redox state when expressed in isolation, they do not rule out the possibility that MAGT1 modulates NS4B cysteine redox status transiently and/or in the context of authentic viral infection. Further experiments will have to be carried out to determine whether NS4B disulfide bonds exist during infection.

Discussion

Our results demonstrate the high reproducibility of whole genome CRISPR screens compared to the low overlap among hits from siRNA-based screens for host

cofactors of viral infection. We compared the top hits from our CRISPR screen to those recently published and found that 15 of the top 25 hits from our screen were in the top 1% of the other's (Table 2.1)(26). By contrast, three independent siRNA screens for host dependency factors of DENV infection performed by the same group identified over 150 high confidence hits; however, only 14% of hits from one independent siRNA library overlapped with hits from another siRNA library, even when performed by the same investigators using the same infection conditions (25). This is consistent with meta-analyses demonstrating the low reproducibility of siRNA screens for viral host factors (130).

While there is a high degree of overlap between CRISPR screens for DENV, the number of significant hits is relatively low compared to those obtained from RNAi screens. For example, the pooled results of the three siRNA screens for DENV yielded hundreds of hits whereas our CRISPR screen yielded fewer than 50 significant hits. This may be due in part to some DENV host factors also being necessary for cellular survival or growth. Additionally, using cell survival from lethal viral challenge as a readout is highly stringent and will increase the false-negative rate, as only partial suppression of DENV infection may not be sufficient to protect cells from death. Thus, experimental readouts that can capture intermediate phenotypes are likely to reveal additional host dependency factors for DENV infection.

The events at the endoplasmic reticulum that direct the formation of a functional dengue virus replication organelle remain incompletely understood. In this study, a whole-genome CRISPR screen reveals a non-canonical function of the OST complex that serves to support DENV infection. STT3B, the subunit of the OST complex that provides oligosaccharyltransferase activity, is required to stabilize MAGT1 to support DENV replication. We show that MAGT1, or its homolog TUSC3, provides a catalytic oxidoreductase activity necessary for DENV to replicate.

On the other hand, we find that the N-glycosylation activity of STT3A or STT3B is dispensable for DENV propagation, in agreement with previous findings by Marceau et al. (26). Based on this observation, these authors suggested that the OST complexes serve as structural scaffolds for DENV to replicate. However, it is unclear why both

STT3A- and STT3B-containing OST complexes would be required to serve a scaffolding function for DENV replication. Our data show that STT3B-containing complexes serve more than a structural scaffolding function to support DENV replication, and in fact contribute a direct catalytic activity for DENV replication: namely, the oxidoreductase activity of MAGT1. We propose that the dependency of DENV replication on STT3B without requiring its oligosaccharyltransferase activity is explained by the loss of MAGT1 expression in the absence of STT3B.

Analogous to the dependence of MAGT1 on STT3B for stable expression, some subunits of the STT3A complex require STT3A for stable expression (86). We propose that there may be a specific function granted by the STT3A complex subunits DC2/OSTC or KCP2 that is necessary for DENV replication. In support of this hypothesis, DC2 was a hit in both CRISPR screens(26). However, the precise cellular function of DC2 is unknown.

We have shown that the CxxC catalytic motif of MAGT1 or TUSC3 is required for DENV propagation, and that TUSC3 can functionally replace MAGT1 in the context of DENV infection. Some cell types, including HEK293 cells, express both TUSC3 and MAGT1, while others, including hepatocytes and Huh7.5.1 hepatoma cells, express only MAGT1 (127). Importantly, TUSC3 expression is upregulated in HEK293 cells when *MAGT1* is knocked out (83). Thus, essential but functionally redundant functions of MAGT1 and TUSC3 in DENV replication will not be revealed in cell types capable of expressing both proteins.

We carried out several experiments directed at the hypothesis that viral NS1 and/or NS4B is a substrate of MAGT1, as these viral proteins harbor multiple cysteines conserved across all DENV serotypes that are also predicted to be accessible to MAGT1. We were unable to find any differences in NS1 dimerization or glycosylation in MAGT1 knockout cells compared to wild-type, suggesting that NS1 is correctly folded and processed in the absence of MAGT1. In addition, we probed the disulfide status of NS4B expressed in isolation, and found no apparent differences in NS4B cysteine accessibility to mPEG modification in the absence or presence of MAGT1 activity. Typically, both cysteines in the CxxC active site motif of an oxidoreductase are involved

in catalyzing disulfide bond formation in a target protein. Surprisingly, cells expressing CxxA or AxxC active site mutants of MAGT1 can support DENV propagation. Single-cysteine active site mutants of protein disulfide isomerase (PDI) have been shown to retain partial reductase activity *in vitro*, and are still able to shuffle disulfide bonds and mediate native protein folding (125, 126). Previous studies have shown that a single-cysteine MAGT1 mutant exhibits partial catalytic activity when assessing glycosylation of an STT3B substrate (88). As depicted in Figure 2.10, a single-cysteine reductase can act as a disulfide isomerase by attacking a non-native disulfide bond on a target protein, generating a mixed disulfide between the reductase (here MAGT1) and its target. An alternate cysteine from the target protein then resolves the mixed disulfide, forming the native disulfide bond and releasing the target protein from MAGT1. Single-cysteine MAGT1 could therefore serve as a disulfide isomerase in the context of DENV infection. Alternatively, single-cysteine MAGT1 could function in tandem with another ER-resident oxidoreductase to resolve the mixed disulfide, and generate a correctly folded target substrate. However, this model is not easily reconciled with the observation that either single-cysteine or wild-type MAGT1 is capable of supporting DENV replication, because the majority of wild-type MAGT1 appears to be oxidized in cells, without reduced cysteines to attack disulfide bonds(88). One possibility is that the minor fraction of reduced MAGT1 or TUSC3 is sufficient to support DENV replication.

If MAGT1 does not directly catalyze disulfide bond rearrangement in a DENV protein such as NS4B, another possibility is that MAGT1, though its oxidoreductase activity, recruits a DENV protein to another cellular protein or complex. For example, the OST complex has recently been identified to associate with proteins in the ER membrane complex (EMC), which has been reported to act as a chaperone for multipass transmembrane proteins, of which NS4B is an example (105, 112). In this model, MAGT1, through its oxidoreductase activity, might transiently interact with NS4B, recruiting it to the EMC as an NS4B chaperone. Although we were unable to demonstrate a stable interaction between MAGT1 and DENV non-structural proteins by coimmunoprecipitation, likely due to the transient association between oxidoreductases and their target substrates(131), APEX2-MAGT1 induced biotinylation of both NS4B and

NS1 in DENV infected cells, indicating that MAGT1 interacts with, or is at least in close proximity to, components of the DENV replication organelle in the ER.

Consistent with the possibility that MAGT1 might help to recruit dengue nonstructural proteins to the EMC complex, the rate of NS4B synthesis appears to be reduced in cells lacking MAGT1 and STT3B. While we see only relatively modest reductions in NS4B expression in cells lacking STT3B and MAGT1, one caveat is that NS4B is expressed in isolation in our system. It is possible that loss of MAGT1 may have more detrimental effects on NS4B expression (or the expression of other DENV proteins) in the context of authentic DENV infection. However, the strong inhibition of DENV infection in OST knockout cells prevents accurate assessment of protein expression.

We also found that ZIKV infection is significantly reduced in STT3A or STT3B knockout cells, suggesting that ZIKV may also require the OST complex for efficient infection or replication. However, the other flaviviruses tested did not appear to be dependent on OST complex function, despite the common dependence of most flaviviruses on the host cell ER for replication organelle formation. Interestingly, the NS4B cysteines are not conserved among flaviviruses despite being conserved across all DENV serotypes.

In conclusion, our data demonstrate that the STT3B-containing OST complex serves a catalytic and non-canonical function during DENV replication, and not merely a scaffolding function. We hypothesize that this non-canonical oxidoreductase activity of MAGT1 acts on a DENV non-structural protein, such as NS4B, to mediate efficient synthesis, folding, and/or recruitment of non-structural proteins to specific sites in the ER. Our results improve our understanding the cell biology of DENV infection, and also may potentially guide the development of DENV antivirals that target MAGT1.

Materials and Methods

Pooled CRISPR screen

The Human GeCKOv2 plasmid library was a gift from Feng Zhang, acquired from AddGene. VSV-G pseudotyped GeCKOv2 lentiviruses were generated at the University

of Michigan vector core. In brief, 16 million Huh-7 cells were transduced with the GeCKOv2 A or B lentiviral half-library at an MOI = 0.3 in 10 cm dishes. Cells were selected for 6 d post-transduction with 2 μg/mL puromycin, then infected with DENV-2 16681 at an MOI = 0.1 for 2 weeks. Genomic DNA from surviving cells was harvested using a Quick-gDNA Midi kit (Zymo Research, Irvine, CA). The integrated sgRNAs were amplified using PCR, and Illumina adapters and barcodes were subsequently added by PCR as previously described (121). Sequencing was performed at the University of Michigan sequencing core on a MiSeq (Illumina, San Diego, CA), and data was analyzed using MaGeCK (132).

Plasmids and lentiviral transduction

Individual sgRNAs targeting *STT3A*, *STT3B*, and *MAGT1* were generated in pLENTICRISPRv2 as previously described using the crRNA sequences listed in Table 2.2. The lentiCRISPR - EGFP sgRNA 1 was a gift from Feng Zhang (Addgene plasmid # 51760).

The cDNA clone for *STT3A* was purchased from OriGene (RC201991; Rockville, MD). The cDNA clones for *STT3B* and *MAGT1* were described previously (83). The *TUSC3* gene was cloned by PCR from 293T cDNA. The sgRNA-resistant *STT3A, STT3B*, and *MAGT1* constructs were made using overlap extension PCR to introduce silent mutations either modifying the CRISPR protospacer adjacent motif or sgRNA basepair complementarity. Constructs encoding catalytically inactive *STT3B, STT3B, MAGT1*, and *TUSC3* were generated using overlap extension PCR. These constructs were cloned into the lentiviral expression vector pSMPUW (Cell Biolabs, San Diego, CA). The constructs for expression of pSAP and SHBG have been previously described (133, 134). The pNS1-flag, pNS1-NS2A-V5, and pNS4B-HA constructs were generated by PCR using pD2/IC-30P-NBX as a template (135). Detailed descriptions of construction of these plasmids are available upon request.

Lentiviral expression constructs were used to generate VSV-G pseudotyped lentiviruses and for stable transduction of target cells as described in (136). Knockouts and expression were confirmed by Western blot.

Viruses

The infectious cDNA clone pD2/IC-30P-NBX encoding Dengue virus serotype 2 strain 16681 was used to generate full-length viral RNA, and for construction of a reporter virus and replicon (135). In brief, the luciferase reporter virus luc-DENV was generated by overlap extension PCR, by fusion of a Renilla luciferase (Rluc) with C-terminal self-cleaving 2A peptide to the DENV capsid in a pD2/IC-30P-NBX background. The luciferase reporter replicon was generated as previously described(137). To generate wild-type DENV-2 virus, the pD2/IC-30P-NBX plasmid was linearized with XbaI (New England Biolabs, Ipswich, MA), in vitro transcribed, and capped with the $m^7G(5')ppp(5')A$ cap analog (New England Biolabs) using T7 Megascript (Thermo Fisher Scientific, Waltham, MA). This RNA was transfected into Vero cells using TransIT mRNA reagent (Mirus Bio, Madison, WI). One week post-transfection, supernatant from transfected cells was 0.45 μm filtered and buffered with 20 mM HEPES. Cells were infected by replacing media on the cells with viral supernatant for 4 hr at 37C and 5% CO_2. Afterwards, unbound virus was aspirated and replaced with fresh media. For luciferase reporter assays, cells were infected with the luciferase reporter virus luc-DENV at an MOI = 0.1 for 2 or 3 d and luciferase activity was measured with the Renilla Luciferase Assay System (Promega, Madison, WI) and a Synergy 2 plate reader (BioTek, Winooski, VT).

The recombinant infectious viruses used were as follows:
SINV-GFP, generated from pTE/5'2J/GFP (138), YFV-Venus, generated from pYF17D-5′C25Venus2AUbi (139), WNV-GFP, generated from pBELO-WNV-GFP-RZ ic (140), CHIKV-GFP generated from pCHIKV-LR 5′GFP (141), VEEV-GFP, a TC83 vaccine strain derivative generated from pVEEV/GFP (142), and DENV2-GFP a 16681 strain derivative generated from pDENV2-ICP30P-A-EGFP-P2AUb (143). Viral stocks were generated by electroporation of in vitro-transcribed RNA into WHO Vero cells (for DENV2-GFP) and BHK-21 cells (for SINV, YFV, WNV, CHIKV and VEEV). Zika virus (ZIKV), 2015 Puerto Rican PRVABC59 strain (144), was obtained from the CDC and passaged twice in Huh-7.5 cells.

Multiplicity of infection (MOI) was based on titers obtained on BHK-J cells for SINV, WNV, YFV and VEEV infections, and on Huh-7.5 cells for ZIKV. Titers were not available for YFV, CHIKV and DENV2, therefore different dilutions of viral stocks were tested.

Cells were seeded in a 24-well plate at $5x10^4$ cells/well for ZIKV or at $1x10^5$ cells/well for other viruses. The next day, cells were infected for 90 min at 37˚C in 2% FBS/PBS using a MOI of 1 for SINV, 0.01 and 0.001 for WNV and 0.8 for VEEV. We used a 1:4 dilution for YFV, 1:10000 for CHIKV and 1:5 for DENV-2. Virus inoculum was removed, fresh complete media was added to the cells, and infections allowed to proceed for 10 h for SINV and VEEV, 24 h for CHIKV, 33 h for YFV, 48 h and 72 h for WNV, 58 h for DENV-2 and 48 h and 96 h for ZIKV. Experiments with WNV and CHIKV were carried out under biosafety level 3 containment. Infected cells were detached using Accumax Cell Aggregate Dissociation Medium (eBiosciences). Cells were pelleted, fixed in 2% paraformaldehyde and permeabilized using Cytofix/Cytoperm (BD Biosciences). For ZIKV infected cells, E protein expression was detected with the 4G2 monoclonal antibody (1:500 dilution), followed by incubation with Alexa Fluor 488-conjugated anti-mouse IgG antibody (Invitrogen) at 1:1,000 dilution. All samples were resuspended in 2% FBS/PBS. Fluorescence was monitored by FACS using an LSRII flow cytometer (BD Biosciences). Data were analyzed with FlowJo Software.

Antibodies

Western blots were performed using antibodies against STT3A (12034-1-AP), STT3B (15323-1-AP), MAGT1 (17430-1-AP), and proSaposin (10801-1-AP) from the Proteintech Group (Rosemont, IL). Antibodies against TUSC3 (SAB4503183) and Actin (A5316) were purchased from Sigma Aldrich (St. Louis, MO). The antibody against EMC3 (sc-365903) was purchased from Santa Cruz Biotechnology (Dallas, TX). The antibody against SHBG (MAB2656) was purchased from R&D systems (Minneapolis, MN). The antibody against HA (C29F4) was acquired from Cell Signaling Technology (Danvers, MA). The anti-V5 antibody (R960-25) was purchased from Thermo Fisher

Scientific. The anti-NS1 monoclonal antibody 1F11 was a gift from the Dr. Malasit at the National Center for Genetic Engineering and Biotechnology in Thailand.

Western blotting

Cells were lysed in a buffer containing 20mM Tris pH 7.5, 100mM NaCl, 1% NP-40, 10% glycerol, and 1mM EDTA with the addition of Halt protease inhibitor (Thermo Fisher). Lysates were cleared by centrifugation at 10,000 rpm for 10 minutes at 4C. LDS sample buffer was added and lysates were resolved by SDS-PAGE on 4-12% Bis-Tris NuPAGE Novex gels. Proteins were transferred to PVDF membranes, which were then blocked for 30 min in 5% nonfat dry milk in TBST. Antibodies were added at the following dilutions: STT3A (1:1000), STT3B (1:500), MAGT1 (1:1000), TUSC3 (1:1000), β-actin (1:20000), HA (1:1000), V5 (1:5000), NS1 (1: 100). Membranes were incubated in primary antibody overnight at 4˚C, then subsequently washed 3x with TBST for 15 min each. Membranes were then incubated in blocking buffer with 1:500 of secondary HRP conjugated antibodies (ThermoFisher) for 1 h at room temperature. Blots were then washed and proteins were detected by the addition of SuperSignal West Femto substrate and immediate visualization on a LI-COR (Lincoln, Nebraska) imager or by X-ray film.

APEX labeling and immunoprecipitation

The APEX2-MAGT1 fusion construct was generated by overlap extension PCR. APEX2-mediated biotinylation and enrichment of biotinylated proteins was performed as previously described (145). A modification to the protocol was the addition of 20 mM N-ethylmaleimide (NEM; Sigma Aldrich) to the lysis buffer to preserve native disulfide bonds. 10% of the lysates were reserved to be run as input controls. 1 μg of either V5 or HA antibody was added to immunoprecipitate respectively tagged proteins. Mixtures were rotated for 2 h at 4˚C. 5 μl of Dynabeads protein G (ThermoFisher) were added to each tube and rotated for 1 h at 4˚C. Complexes were washed 3x in 1x PBS with 0.1% Triton X-100. Proteins were eluted in 1x LDS sample buffer with 50mM Tris(2-

carboxyethyl)phosphine hydrochloride (TCEP, Sigma Aldrich). Lysates were then subjected to SDS-PAGE and Western blotting as described above.

Pulse-chase analysis of NS1 glycosylation

HEK293 cells were grown to 60% confluency in 60 mm dishes and transfected with 6 μg of NS1-FLAG expression plasmids using Lipofectamine 2000 (ThermoFisher) in Opti-MEM (ThermoFisher) according to the manufacturer's instruction. After 24 h, NS1 substrates were labeled with Tran^{35}S label (Perkin Elmer, Waltham, MA) by incubation in methionine- and cysteine free media containing 10% dialyzed FBS for 20 min before the addition of 200 µCi/mL of Tran^{35}S label. Cells were labeled for 5 min, then 3.7 mM unlabeled methionine and 0.75 mM unlabeled cysteine were added and cells were incubated for an additional 20 min. Cells were lysed at 4°C by a 30 min incubation with 1 mL of RIPA lysis buffer. Lysates were clarified by centrifugation (2 min at 13,000 rpm) and precleared by incubation for 2 h with rabbit IgG and a mixture of protein A/G Sepharose beads (Santa Cruz Biotechnology) before an overnight incubation with anti-FLAG antibody (Sigma Aldrich). Immunoprecipitates were collected with protein A/G–Sepharose beads then washed five times with RIPA lysis buffer and twice with 10 mM Tris-HCl, pH 7.5 before eluting proteins with gel loading buffer. Where indicated, immunoprecipitated proteins were digested with Endoglycosidase H (New England Biolabs). Dry gels were exposed to a phosphor screen (Fujifilm, Valhalla, NY), and scanned with a Typhoon FLA9000 laser scanner (GE Healthcare, Chicago, IL).

PNGase F digestion and maleimide-PEG assays

Lysates were subjected to PNGase F (New England Biolabs) digestion as suggested by the manufacturer guidelines. Methoxypolyethylene glycol maleimide 5000 (mPEG; Sigma Aldrich) was dissolved in water to a 100 mM stock immediately prior to use. Cells were lysed in lysis buffer with the addition of either 20 mM NEM, 5 mM mPEG, or 0.5 mM TCEP. Lysates were incubated at room temperature for 30 min prior to clearing by centrifugation at 10,000 rpm for 10 min. Supernatants with TCEP added were then

supplemented with 5 mM mPEG to modify the now reduced cysteines. Lysates were resolved by SDS-PAGE and visualized by Western blot as described above.

Half-life quantification and band densitometry

Cells were transfected in 6-well plates, then four hours later trypsinized and plated in 6 wells of a 12-well plate. 24 hours post-transfection, media was replaced with fresh media containing 40 μg/ml cycloheximide (Cell Signaling Technology). Cells were lysed at various time points after cycloheximide treatment in RIPA buffer, and lysates were subjected to Western blot analysis as described. Band densities were quantified using LI-COR Image Studio (LI-COR, Lincoln, NE).

Immunofluorescence

Huh 7.5.1 cells were plated on poly-D-lysine coated coverslips and infected with DENV-2 at an MOI = 0.1 or mock infected. Two days post-infection, cells were fixed in ice cold methanol for 1 h at -20C. Immunostaining with anti-HA (1:200) and anti-NS1 (1:50) antibodies was performed as described previously(146).

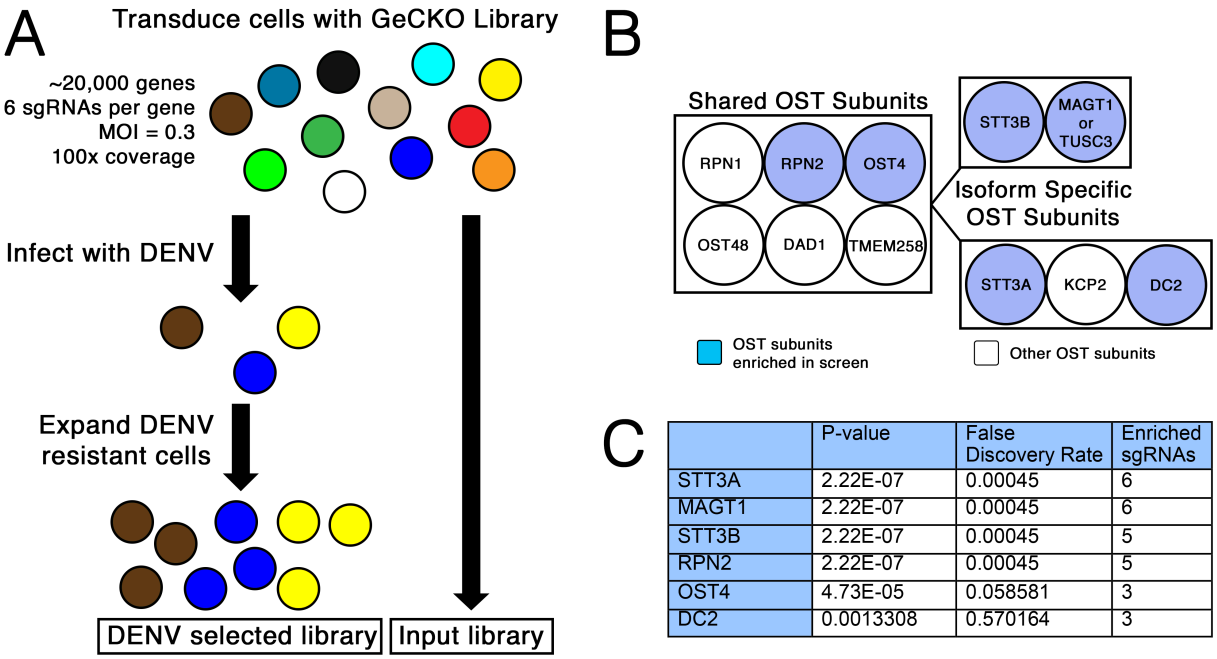

C

	P-value	False Discovery Rate	Enriched sgRNAs
STT3A	2.22E-07	0.00045	6
MAGT1	2.22E-07	0.00045	6
STT3B	2.22E-07	0.00045	5
RPN2	2.22E-07	0.00045	5
OST4	4.73E-05	0.058581	3
DC2	0.0013308	0.570164	3

Figure 2.1. The CRISPR-Cas9 screen reveals the oligosaccharyltransferase complex as essential to DENV propagation. **A**, Depiction of the whole-genome CRISPR screen selecting for knockout cells resistant to dengue virus infection. **B**, Diagram of the two OST complexes that contain either STT3A or STT3B. Subunits of the OST complex shaded in blue were significantly enriched in the screen. **C**, Table of the hits from the screen showing the gene ID, p-value, and false discovery rate as calculated by MaGECK analysis.

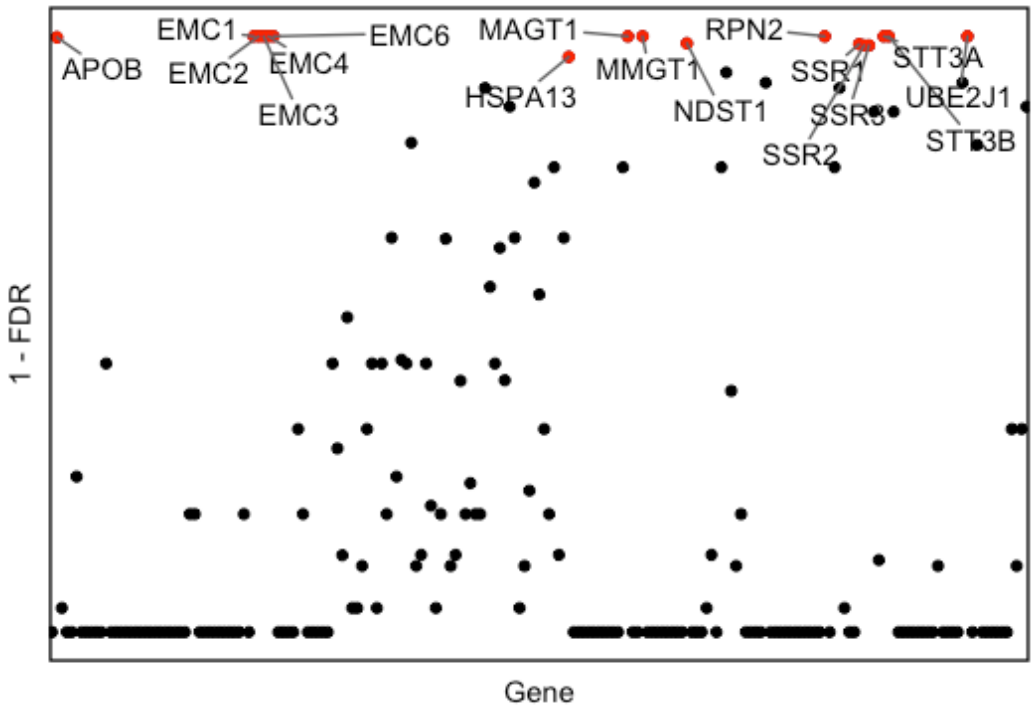

Figure 2.2. Multiple ER resident complexes are necessary for DENV propagation. MaGeCK analysis for the top 200 ranked genes from the screen were plotted, with the gene name plotted on the X-axis and 1- false discovery rate (FDR) on the Y-axis. The top ranked hits are indicated in red and labeled with their gene names.

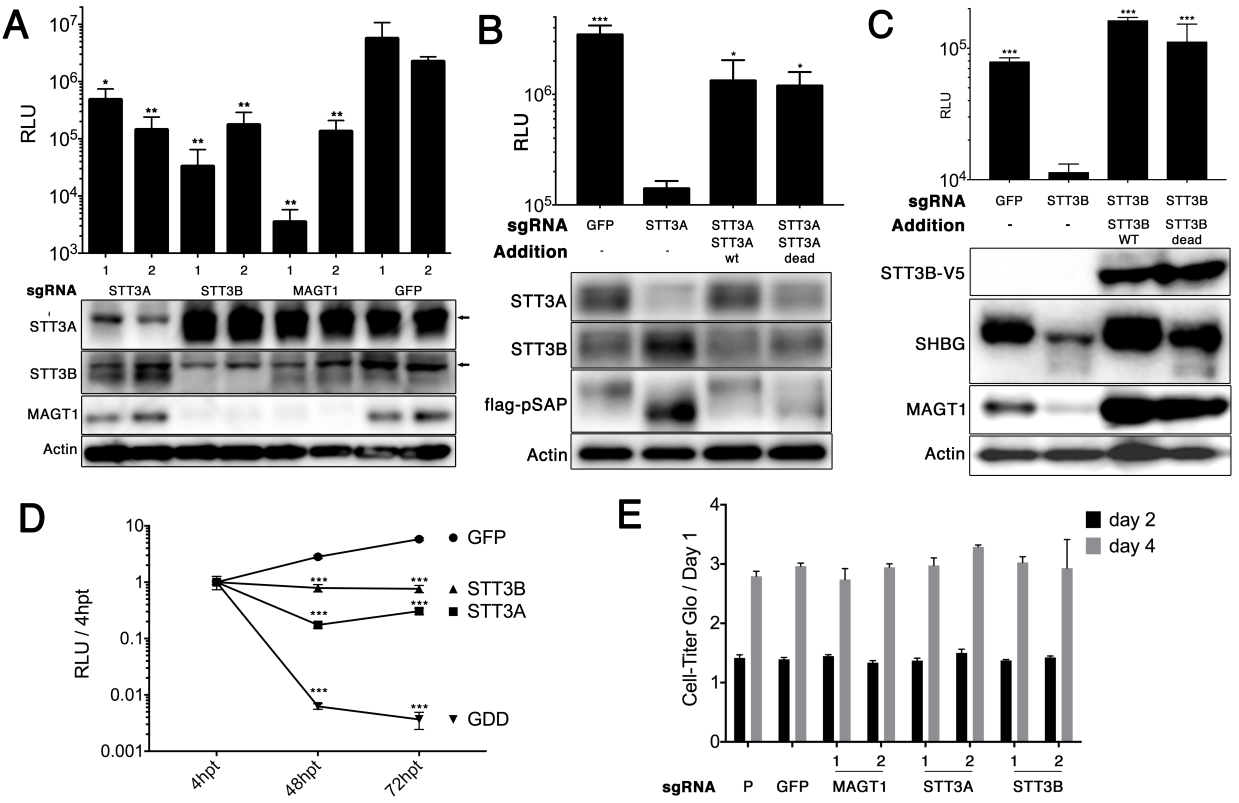

Figure 2.3. The catalytic activities of STT3A or STT3B are not required for DENV replication. A, Huh 7.5.1 cells were transduced with a lentivirus encoding a puromycin resistance marker, Cas9, and a single guide RNA (sgRNA) targeting the indicated genes. The sgRNAs targeting GFP act as a negative control. Two independent sgRNAs (indicated below the bars as "1" or "2") were used per target gene to generate knockout cell pools. Cells were infected with luc-DENV for 3 days and luciferase activity was measured in relative light units (RLU). Below, Western blots for the indicated proteins are shown. Arrows indicate non-specific bands. **B and C**, knockout cell pools were transduced with lentiviral vectors to rescue expression of the indicated protein. "STT3A dead" is a catalytically inactive W526A/D527A double mutant. "STT3B dead" is a catalytically inactive W605A/D606A double mutant with a C-terminal V5 tag. Transient transfection of constructs to express pSAP and SHBG were used to assess STT3A and STT3B catalytic activity. Below, Western blots show the expression of the indicated proteins. **D**, knockout cell pools were transiently transfected with a luc-DENV replicon and luciferase activity was measured at 4, 48, and 72 hours post-transfection (hpt). Data is plotted as a ratio of RLU / 4 hpt to control for transfection efficiency. GDD indicates a polymerase dead replicon with replacement of the GNN active site sequence in the NS5 RNA polymerase by GDD. **E**, cell viability for knockout cell pools was measured by Cell-Titer Glo over the course of 4 days for 3 independent wells. Data are normalized to day 1 values. P indicates the parental Huh7.5.1 cells. For A-E, data are expressed as means with SD for three independent biological replicates. In A-D, statistical significance was determined by Student's t-test, where *p<0.05, **p<0.005, and ***p<0.0005. In A, means were compared to GFP sgRNA #2. In B and C, means were compared to their respective knockouts. In D, means were compared to the GFP control.

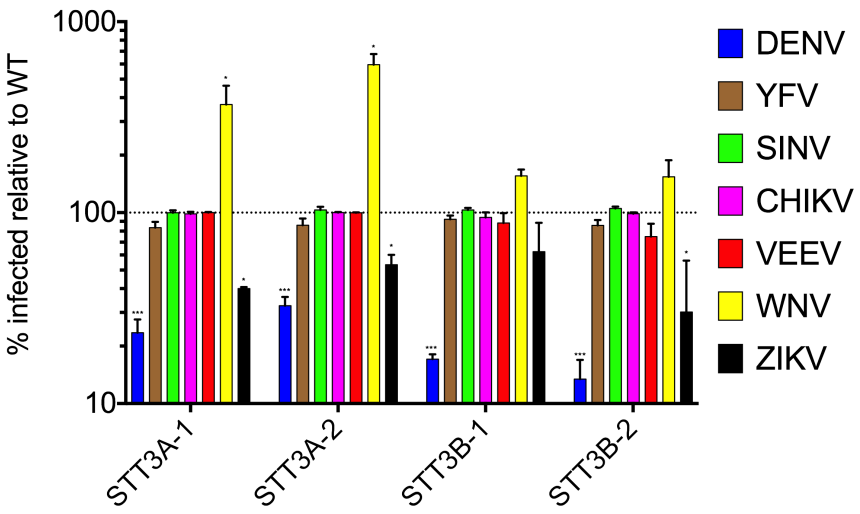

Figure 2.4. Inhibition of flavivirus infection in OST knockout cells. Huh 7.5.1 cells were transduced to express two independent sgRNAs targeting STT3A, STT3B, or one sgRNA targeting GFP as a control. Stably transduced cell pools were then infected with the indicated fluorescent protein-expressing reporter viruses (see Materials and Methods for detailed description of the viruses) and subjected to flow cytometry to measure the number of infected cells. ZIKV infection was detected by immunostaining followed by flow cytometry. Data are plotted as a percentage relative to control cells expressing an sgRNA targeting GFP for three independent infections. Statistical significance was determined by Student's t-test, where means were compared to GFP control, and *p<0.05, **p<0.005, and ***p<0.0005.

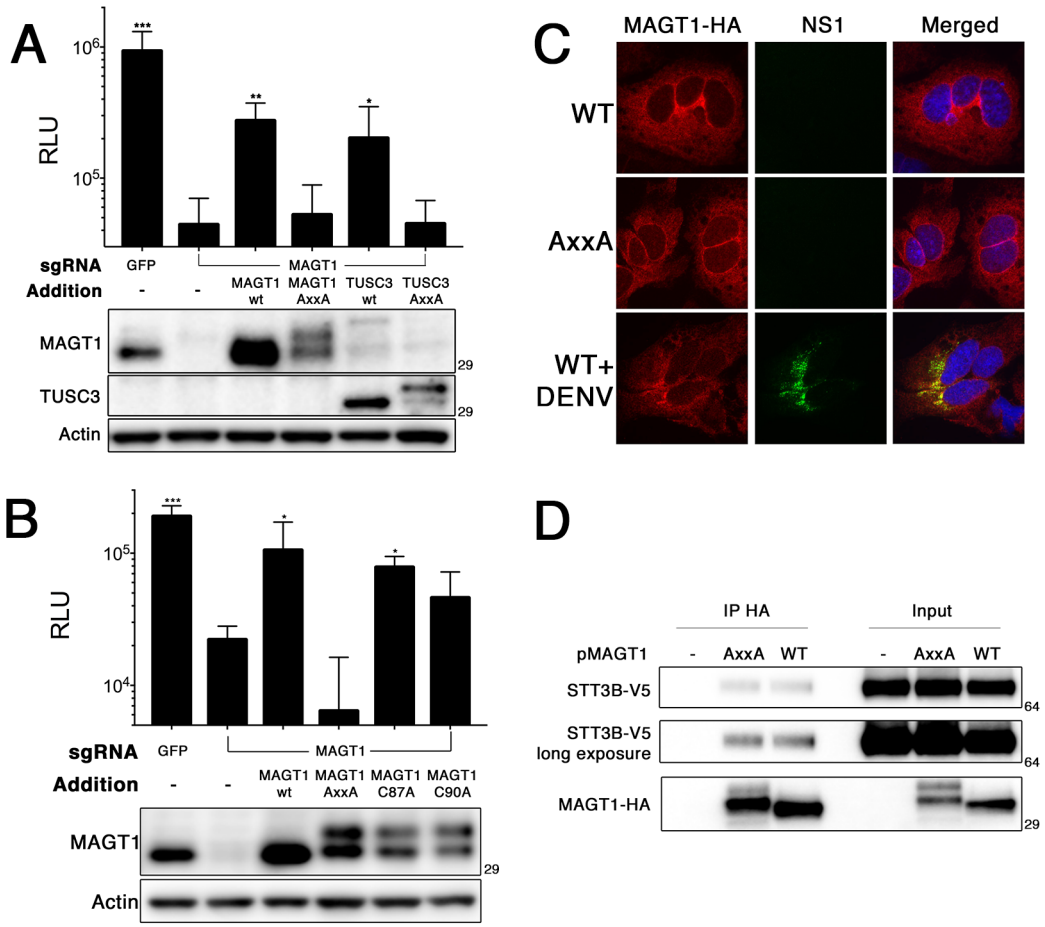

Figure 2.5. The oxidoreductase activity of MAGT1 is required for DENV replication. A, CRISPR modified Huh 7.5.1 MAGT1 knockout cell pools were transduced to express MAGT1 or TUSC3-HA. The AxxA MAGT1 and TUSC3-HA mutants were generated by mutating CxxC active sites to AxxA. Below, Western blots for the indicated proteins are shown. The MAGT1 antibody cross-reacts weakly with TUSC3. **B**, MAGT1 knockout cells were transduced to express MAGT1 mutants with the indicated mutations. Below, Western blots for the indicated proteins are shown. For A and B, cells were infected with luc-DENV and luciferase activity was measured at 3 days post-infection. **C**, immunofluorescence localization of MAGT1 in uninfected cells or two days post-infection with DENV. MAGT1 knockout cells were stably transduced to express HA tagged MAGT1 (WT or AxxA), as indicated on the left. Cells were fixed, permeabilized, and stained with antibodies to the indicated proteins. **D**, 293T cells expressing the indicated MAGT1-HA mutants were transfected to express STT3B-V5. Cells were lysed and co-immunoprecipitation was carried out using an anti-HA antibody. Shown are Western blots detecting the specified proteins. Mutants of MAGT1 migrate as two distinct bands. Data in panels A and B are expressed as means with SD for three independent infections. Statistical significance was determined by Student's t-test, where *p<0.05, **p<0.005, and ***p<0.0005 compared to MAGT1 knockout cells without any additions (lane 2).

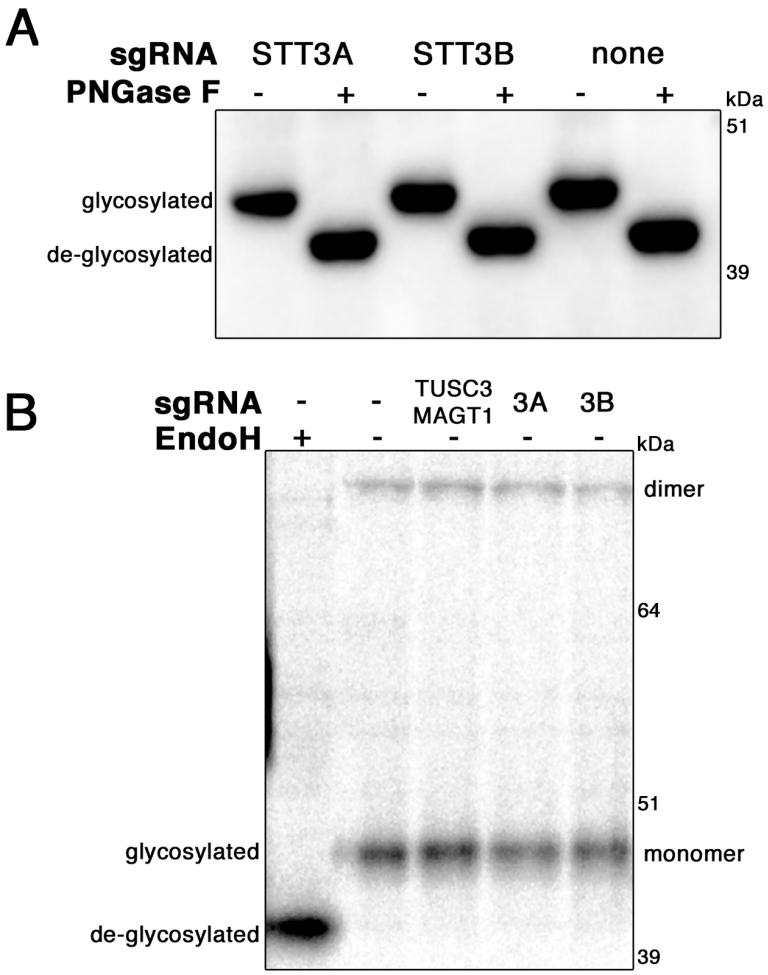

Figure 2.6. NS1 glycosylation and dimerization are unchanged in the absence of STT3A, STT3B, or MAGT1. A, the indicated CRISPR knockout 293T cells were transfected to express NS1-FLAG. Lysates were treated with PNGase F to remove N-linked glycans followed by Western blotting to visualize differences in migration of NS1. The glycosylated and de-glycosylated forms of NS1 are indicated. **B**, A 5 min pulse with ^{35}S-cysteine/methionine was followed by a 20 min chase to visualize differences in the efficiency of NS1 glycosylation and dimerization in CRISPR-edited HEK293 cells. Endoglycosidase H treatment was used to indicate the mobility of unglycosylated NS1 by SDS-PAGE.

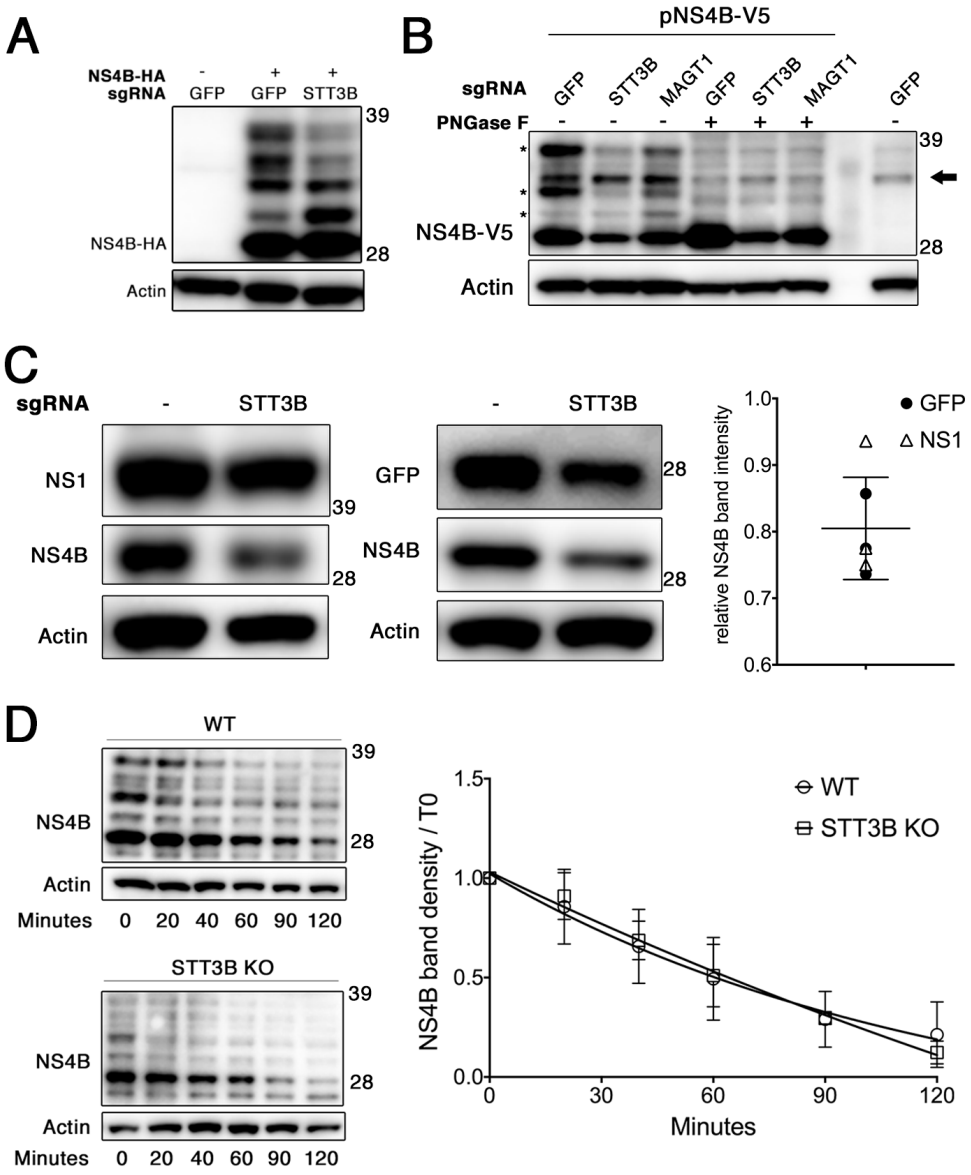

Figure 2.7. Effect of STT3B on NS4B glycosylation and biosynthesis. A, CRISPR modified *STT3B* knockout 293T cell pools were stably transduced to express either wild-type STT3B or STT3B-dead. Cells were transfected to express NS4B-HA, and lysates were resolved by SDS-PAGE and visualized by Western blotting for the indicated proteins. **B**, Huh 7.5.1 cell pools ablated for the indicated genes were transfected to express NS4B-V5 (lanes 1-6) or were mock transfected (lanes 7-12). Lysates were subjected to PNGase F treatment in lanes 3-6 and 10-12 to remove N-linked glycans from proteins, Proteins were resolved by SDS-PAGE and visualized by Western blotting for the indicated proteins. The black arrows indicate nonspecific background bands, and asterisks (*) mark the NS4B specific PNGase F sensitive bands. **B**, the indicated 293T cells were co-transfected to express NS4B-HA and either NS1 or GFP (as transfection controls), and then lysed. Lysates were treated with PNGase F to facilitate quantitation of NS4B protein by removing N-glycans and Western blotting was performed for the indicated proteins. Chemiluminescent band intensities were quantified as NS4B-HA in STT3B knockout cells

relative to NS4B-HA in WT cells compared to the same ratio of GFP or NS1 to control for transfection efficiency. Each point plotted is the quantification of an independent transfection where the open triangles are compared to co-transfection with a plasmid expressing NS1 and closed circles with GFP. The mean and SD plotted are for all points. **C**, the indicated 293T cells were transiently transfected to express NS4B-HA and treated with cycloheximide 24 hours post-transfection to block further translation. Cells were lysed at the indicated times post-cycloheximide treatment and proteins were resolved by Western blotting. To the left are representative blots. The decay curves for 3 independent experiments are shown on the right.

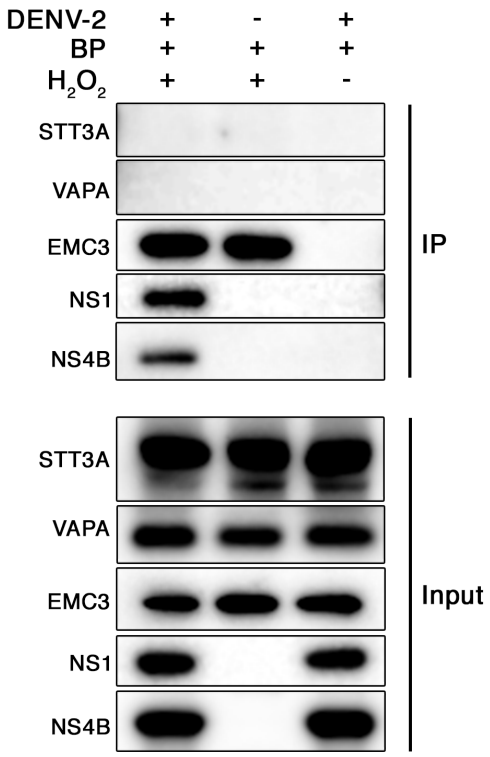

Figure 2.8. MAGT1 is in close proximity to NS4B and NS1 during DENV infection. Huh7.5.1 cells stably transduced to express APEX2-MAGT1 were infected with DENV-2 or mock infected for 2 days. In all conditions, biotin-phenol was added to the cell media for 30 min. Where indicated, APEX2 was activated with hydrogen peroxide for 1 min to biotinylate APEX2-MAGT1 proximal proteins prior to quenching and lysis. The far right lane is a negative control where APEX2 was not activated. Biotinylated proteins were immunoprecipitated with streptavidin beads, and lysates were resolved by SDS-PAGE. Western blotting was performed for the indicated proteins for both the IP samples and the input.

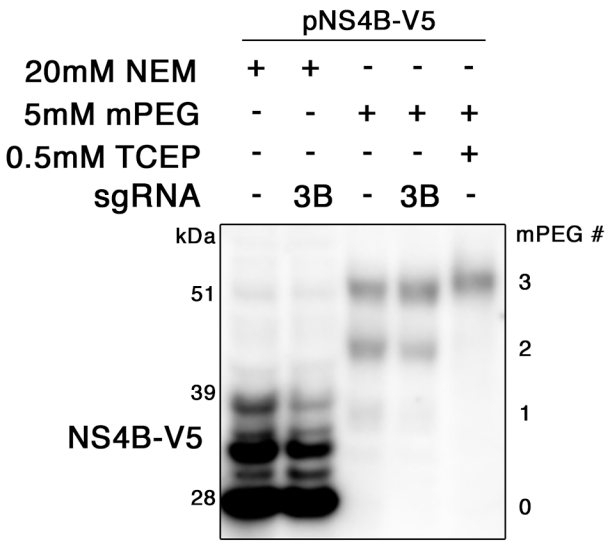

Figure 2.9. The redox status of NS4B is unchanged in the absence of MAGT1.
The indicated CRISPR knockout 293T cells were transfected to express pNS4B-HA. We used STT3B knockout cells to deplete both MAGT1 and TUSC3. Cells were lysed in buffer with the specified additions of NEM, mPEG, or TCEP. Western blots were carried out to determine the migration patterns of NS1 and NS4B in the given conditions. The number of estimated maleimide-PEG modifications is indicated on the right.

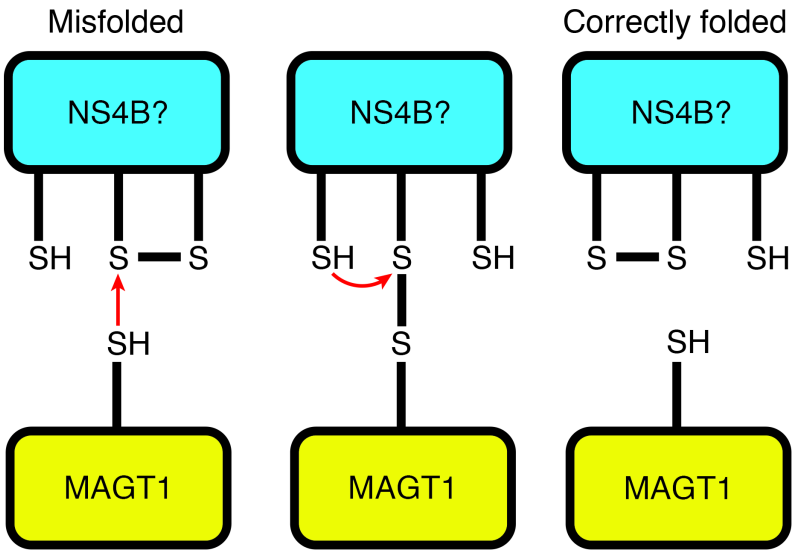

Figure 2.10. A potential model for disulfide isomerization by single-cysteine MAGT1. A MAGT1 mutant containing a single cysteine active site (AxxC or CxxA) is shown in yellow. In blue is a target protein, such as NS4B, which contains multiple cysteines that may form disulfide bonds. This protein has a non-native disulfide arrangement that is identified by MAGT1. Through its active site cysteine, MAGT1 forms a mixed disulfide with the target protein, reducing the incorrect disulfide bond. The correct disulfide bond is then formed by a cysteine from the target protein, resolving the mixed disulfide between MAGT1 and its target.

Table 2.1. List of hits from this and other CRISPR screens. A list of the top 25 significant hits from biological replicates were compared to hits from two previously published screens. Gene names are colored to indicate groups of ER complexes. Yellow indicates genes encoding components of the EMC complex, blue indicates components of the OST complexes, and green indicates components of the ER associated degradation pathway (ERAD). The rank of each hit in independent biological replicates is shown in the second and third columns. The false discovery rate calculated by MAGeCK and the number of sgRNAs classified as a hit by MaGECK in our screen are shown. Hits from our screen that were also identified in the top 25 hits of Marceau *et al.* or the top 150 of Savidis *et al.* are marked with an X.

ID	1st rank	2nd rank	1st FDR	sgRNAs	Top 25 Marceau et al.	Top 150 Savidis et al.
EMC6	1	2	0.00045	6	x	x
STT3A	2	11	0.00045	6	x	x
MAGT1	3	5	0.00045	6	x	
STT3B	4	3	0.00045	5	x	
UBE2J1	5	16	0.00045	6		
EMC3	6	12	0.00045	6	x	x
EMC4	7	17	0.00045	6	x	x
EMC5	8	4	0.00045	5	x	x
EMC1	9	13	0.00045	6	x	x
EMC2	10	7	0.00045	4	x	x
RPN2	11	9	0.00045	5	x	x
APOB	12	10	0.002063	5		
SSR2	15	20	0.015161	4	x	
SSR3	16	14	0.015161	4	x	
HSPA13	17	15	0.033489	4	x	
OST4	18	18	0.058581	3	x	
PRKRA	19	50	0.075	3		
UBE2G2	20	1	0.075	4		
SEC61B	22	6	0.083483	5		x
SSR4	25	48	0.121668	4		
SYVN1	26	8	0.121668	4		
RRBP1	30	21	0.21086	4		
OSTC (DC2)	53	19	0.570164	3	x	
DERL2	74	84	0.768196	4		

Table 2.2. List of guide RNA sequences for OST knockouts. Oligonucleotides were cloned into pLENTICRISPRv2 to generate lentiviruses for CRISPR mediated knockout of specific OST genes.

crRNA sequence	Comment
ACAGACATTCCGAATGTCGA	STT3A-1
AAGGTGGTACGTGACGATGG	STT3A-2
GATGTAAGGCCGCTAAAAGT	STT3B-1
CCAGCGGTTATCATCAACCC	STT3B-2
GAGCGAACATGGCAGCGCGT	MAGT1-1 Forward
AGCAGTGAACATGACGATAA	MAGT1-2 Forward
GGGCGAGGAGCTGTTCACCG	EGFP-1 from Addgene

CHAPTER III

The EMC promotes stable expression of DENV and ZIKV non-structural multi-pass transmembrane proteins to support virus infection

At the time of writing, the majority of this chapter was submitted to Cell Reports for peer review and publication, written by David L. Lin, Takamasa Inoue, Yu-Jie Chen, Aaron Chang, Billy Tsai, and Andrew W. Tai in 2018.

Takamasa Inoue, Yu-Jie Chen, and Aaron Chang performed experiments to show that expression of ZIKV NS4A and NS4B depend on the EMC, and that NS4B ubiquitination is p97 dependent.

The EMC is necessary for DENV replication

The six core subunits of the EMC, EMC1 through EMC6, were identified as host dependency factors for flavivirus infection in four independent screens (12, 24-26). We validated that these EMC subunits were indeed necessary for DENV infection by first generating pooled EMC knockout Huh 7.5.1 cells using CRISPR/Cas9 technology. We found that knockout cells lacking EMC subunits 1, 2, 4, 5, or 6 were significantly reduced in their ability to support DENV infection compared to wild-type control cells (Figure 3.1A).

Using a transient replication assay with a luciferase reporter DENV subgenomic replicon, we found that EMC6 knockout cells supported significantly reduced levels of DENV replication (Figure 3.1B). These data corroborate previous findings, suggesting that EMC depletion inhibits the initial stages of replication (25). By contrast, hepatitis C virus (HCV) infection does not require the EMC (Figure 3.2), demonstrating specificity of viral inhibition by EMC knockout.

We also confirmed that long-term EMC6 depletion leads to the loss of other EMC subunits (Figure 3.1C)(107, 147) without affecting their mRNA levels (Figure 3.3), suggesting that EMC6 is required for the stability of the other EMC subunits. Exogenous expression of a sgRNA-resistant EMC6 construct in EMC6 knockout cells fully restored their ability to support DENV infection, as well as the expression of the other EMC subunits (Figure 3.1C). Collectively, these results demonstrate that the EMC is required to support DENV infection.

The EMC is necessary for expression of flavivirus NS4A and NS4B

The EMC has been shown to act as a multi-pass transmembrane chaperone (100, 105, 106), and has been proposed to function as a transmembrane insertase (107). As the DENV genome encodes several multi-pass transmembrane NS proteins (NS2A, NS2B, NS4A, and NS4B), we hypothesized that the EMC is necessary for the biogenesis of one or more of these NS proteins. To test this, we transfected wild-type and EMC knockout cells to individually express each of the multi-pass transmembrane DENV NS proteins, and assessed the expression level of each of the proteins by immunoblotting. Strikingly, expression of both DENV NS4A and NS4B were significantly reduced in EMC knockout cells compared to wild-type cells (Figures 3.4A and B; quantified in E). By contrast, expression of NS2B was moderately decreased in EMC knockout cells when compared to wild-type cells (Figure 3.4C, quantified in E), while NS2A expression was unaffected by the loss of the EMC (Figure 3.4D, quantified in E). As expected, expression of either soluble NS1 or GFP was also unaffected by the loss of the EMC (Figure 3.4A-E).

To generalize these findings to other flavivirus family members, we performed similar experiments for ZIKV non-structural proteins. As with EMC6 knockout, EMC1 knockdown in HEK 293T cells by siRNA also led to depletion of the other EMC subunits (Figure 3.6). We next transfected wild-type (scrambled siRNA-treated) and EMC1 knockdown cells to express a full-length replication-defective ZIKV polyprotein, and observed a similar reduction in the expression level of NS4B in EMC knockdown cells (Figure 3.4F). However, expression of the viral E protein from the same polyprotein was

unaffected by loss of the EMC, despite also being a multi-pass transmembrane protein (Figure 3.4F). In addition to using the full-length replication-defective ZIKV polyprotein, we also expressed individual ZIKV non-structural proteins. Using this approach, expression of both NS4A and NS4B was significantly reduced in EMC knockdown cells (Figure 3.4H and I), whereas expression of GFP or the multi-pass ER membrane protein BAP31 was unaffected by EMC1 depletion. Interestingly, in contrast to DENV NS2B, expression of ZIKV NS2B was also markedly decreased when EMC1 was knocked down (Figure 3.4G), suggesting a difference in EMC dependency for this NS protein. Taken together, these data suggest that the EMC supports the expression of flavivirus NS proteins, which are necessary for viral replication.

The EMC interacts with flavivirus NS4B

We next performed co-immunoprecipitation (co-IP) experiments using an antibody targeting endogenous EMC4 in cells stably expressing a DENV replicon. Our results revealed that NS4B, but not NS1 or NS2B, significantly co-immunoprecipitated with endogenous EMC4 (Figure 3.4J). Additionally, affinity purification of transfected S-tagged ZIKV NS4B (but not the control S-tagged GFP) co-precipitated with endogenous EMC1 and EMC2 (Figure 3.4K). These results demonstrate that the EMC binds to DENV/ZIKV NS4B.

To further corroborate the physical interaction data, we asked if the EMC might co-localize with the viral NS proteins in cells. To test this, we transduced DENV replicon cells to express FLAG tagged EMC4, then performed immunofluorescence staining and confocal microscopy to visualize localization of the EMC in DENV infected cells. We found strong colocalization of EMC4 with puncta containing NS4A and NS4B (Figure 3.4L). By contrast, EMC4 was diffusely distributed in cells with little NS4A or NS4B staining, suggesting that the EMC is recruited to the DENV replication organelle. These data are consistent with our finding that the EMC interacts with NS4B during DENV replication. Alternatively, we also co-stained DENV replicon cells with NS4B and calnexin, another ER-resident protein, and found that calnexin was not recruited in the same fashion to NS4B positive sites, further reinforcing a role for the EMC at the

replicase (Figure 3.5). Collectively, the evidence supports a model where the EMC is required for flavivirus infection by recruitment to the viral replication organelle, where it directly interacts with NS4A and NS4B to promote their stability.

Mapping determinants of EMC dependence

Given that NS4B engages the EMC, we next sought to identify the specific determinants of NS4B that confer its dependence on the EMC. In addition to its postulated role as a molecular chaperone for multi-pass transmembrane proteins, the EMC also has been shown to function as an insertase for tail-anchored transmembrane proteins, particularly those with weakly hydrophobic transmembrane domains (107). Therefore, we hypothesized that weakly hydrophobic transmembrane domains in NS4A and NS4B might drive their EMC dependence. DENV NS4B harbors an N-terminal 2k signal peptide that is co-translationally cleaved, followed by five predicted hydrophobic helices (Figure 3.7A). Evidence suggests that the three C-terminal helices are membrane-spanning domains (66, 68, 69). By contrast, the first two N-terminal helices have relatively poor hydrophobicity (Figure 3A, pTM1 and pTM2), with one report suggesting that these domains lie on the ER lumenal membrane rather than spanning the lipid bilayer (66). Transmembrane prediction by TMHMM also revealed that the two N-terminal helices exhibit relatively low transmembrane probabilities compared to the three C-terminal helices (Figure 3.7B).

By analogy to tail-anchored transmembrane domains, we hypothesized that the two N-terminal marginally hydrophobic helices in NS4B are targets of EMC activity. To test this idea, we generated plasmids encoding a wild-type DENV 2k-NS4B-GFP fusion protein, a mutant lacking these two helices (Δ32-96), or harboring one or two of the N-terminal hydrophobic segments immediately following the 2k signal sequence (2k-58 and 2k-96) (Figure 3.7A). We co-transfected these plasmids along with NS1-FLAG as a transfection control into wild-type or EMC knockout cells, and assessed their relative levels of expression by immunoblotting. Consistent with previous results, NS4B expression was significantly reduced in EMC knockout cells compared to wild-type cells (Figure 3.7C). However, expression of a GFP tagged or HA tagged NS4B(Δ32-96)

mutant was unaffected by EMC knockout, indicating that loss of these helices rendered NS4B expression independent of the EMC (Figure 3.7C; quantified in D). By contrast, neither NS4B (2k-96) nor NS4B(2k-58) displayed strong EMC dependency when fused to GFP (Figure 3.7C), suggesting that the N-terminal helices of NS4B are not sufficient for EMC dependence. Thus, our results are consistent with the idea that the two N-terminal marginally hydrophobic helices in NS4B are required for recognition by the EMC.

Hydrophobicity as a determinant of EMC dependence

As the Δ32-96 NS4B mutant was insensitive to EMC depletion, we hypothesized that specific mutations to amino acids 32-96, domains containing the two marginally hydrophobic helices, of NS4B could recapitulate the same phenotype. We generated NS4B mutants to swap the hydrophobic residues in pTM1 and pTM2 for lysine to render the domains hydrophilic (Figure 3.8). Similarly, we swapped the polar and charged residues in both domains to leucine, generating more canonical hydrophobic transmembrane domains (Figure 3.8). We transfected WT and EMC knockout cells to express these constructs, then performed Western blots, and quantified their expression levels.

Notably, we found that the glycosylation patterns were significantly different between the mutants. Two glycosylation sites between pTM1 and pTM2, which we found are heavily glycosylated when pTM1 and pTM2 are mutated to increase its hydrophilicity, driving pTM1 and pTM2 into the ER lumen. Indeed, we find that the pTM1+pTM2-to-lysine mutant is highly glycosylated (Figure 3.9). Interestingly, pTM1-to-lysine is heavily glycosylated in wild-type cells, but not in EMC knockout cells (Figure 3.8 and 3.9A). None of the leucine swapped mutants were glycosylated as heavily as the wild-type protein. This data reinforces a model where insertion of pTM1 and pTM2 into the membrane will force the sequons into the cytosolic side of NS4B, where the loop between pTM1 and pTM2 is inaccessible to the ER N-glycosylation machinery (Figure 3.8 and 3.9B).

We found that mutation of either of the transmembrane domains individually was insufficient to drive complete EMC independence (Figure 3.9A-C). We quantified expression levels of each mutant in wild-type and EMC6 knockout cells using band densitometry. Quantification of proteins after PNGase treatment or pre-treatment using this method yielded highly similar results (Figure 3.9C). Mutation of pTM1 and pTM2 to lysine-rich hydrophilic domains slightly but significantly increased its independence on the EMC (Figure 3.9A and C). Mutation of pTM1 to leucine did not affect EMC dependence, while pTM2 to leucine slightly decreased dependence on the EMC (Figure 3.9B and C). Strikingly, mutation of pTM1 and pTM2 to leucine-rich hydrophobic domains dramatically increased its expression in EMC knockout cells, and caused expression to be independent of the EMC (Figure 3.9B and C). Together, these results assert that EMC dependence of NS4B is driven by the marginal hydrophobicity of the first two putative transmembrane domains.

NS4B is degraded via ERAD in the absence of the EMC

Finally, we clarified the fate of destabilized NS4B in the absence of the EMC. As NS4B expression is significantly reduced in EMC knockout/knockdown cells, we asked whether under this depleted condition, NS4B is targeted for proteasomal degradation via the ERAD pathway. To test this, we transduced wild-type and EMC knockout cells to express DENV NS4B-HA, treated them with the proteasome inhibitor MG132, and analyzed the cell lysates by immunoblotting. Importantly, NS4B-HA in EMC6 knockout cells accumulated to levels similar to that of wild-type cells after proteasomal inhibition (Figure 3.10A). This finding suggests that when NS4B is destabilized in the absence of the EMC, it retrotranslocates to the cytosol to be degraded by the proteasome. To further support a role of ERAD in disposing NS4B, we asked if this non-structural protein is in fact polyubiquitinated when the proteasome is inactivated; polyubiquitination of a misfolded ERAD substrate is required for targeting to the proteasome (148). Indeed, in cells treated with MG132, immunoprecipitated DENV NS4B-HA was polyubiquitinated (Figure 3.10B, left panels); a similar result was found for ZIKV NS4B-HA (Figure 3.10B,

right panels). These findings are consistent with an important role of ERAD in degrading NS4B when the integrity of the EMC is compromised.

p97 is an ATPase that normally extracts polyubiquitinated ERAD substrates out of the ER membrane and into the cytosol (149). Because our results implicated a role for ERAD in the removal of NS4B from EMC depleted cells, we asked whether p97 plays a role in promoting flavivirus NS4B degradation in EMC-deficient cells. Accordingly, we co-transfected EMC1 knockdown cells with plasmids encoding wild-type p97 or the dominant-negative p97(p97^{QQ}) (150) along with NS4B from both DENV and ZIKV, and examined NS4B polyubiquitination. Our results demonstrated that in the presence of p97^{QQ}, immunoprecipitated NS4B-HA displayed increased polyubiquitination when compared to cells expressing wild-type p97 (Figure 3.10C and D). These data provide further evidence that in EMC-depleted cells, flavivirus NS4B is misfolded, leading to ERAD recognition, ubiquitination, and proteasomal degradation.

Alanine scanning and truncation analysis of EMC6

EMC6 is highly conserved among metazoans, with no homology to proteins of known function. To date, biochemical analysis of individual EMC subunits has yet to be performed, and thus specific functions of each EMC subunit are unclear. Therefore, we next decided to ask whether EMC activity or assembly was dependent on specific EMC6 residues. We first performed alanine scanning in blocks of 5 consecutive amino acids, and complemented EMC6 knockout cells with C-terminal HA-tagged EMC6 mutants (Figure 3.11).

We confirmed expression of the EMC6 mutants and other EMC subunits by Western blot, and found that expression of any of the EMC6 mutants was sufficient to restore EMC2 or EMC4 expression (Figure 3.11), suggesting that complex assembly is not dependent on a single short contiguous stretch of EMC6 residues. Furthermore, we found that cells expressing any of the EMC6 alanine mutants supported significantly higher luc-DENV infection than cells expressing no EMC6 (Figure 3.11). This data suggests that, as for EMC assembly, that no single short contiguous amino acid stretch is necessary for EMC activity.

Because alanine scanning did not reveal EMC6 functional motifs, we decided to generate truncation mutants to assess whether larger motifs of EMC6 are necessary for EMC activity and complex assembly. The C-terminus of EMC6 is highly conserved among metazoans. Cells expressing EMC6 with a 10 amino acid deletion at the C-terminus were unable to support DENV infection despite partial rescue of EMC2 and EMC4 expression (Figure 3.12A). These data suggest that the C-terminus of EMC6 may be important for EMC activity. Further analysis of the EMC6 C-terminus will reveal whether these residues are critical for complex assembly and EMC activity.

Furthermore, we found that expression of a 20 amino acid N-terminal EMC6 deletion mutant restored EMC2 and EMC4 expression, and luc-DENV infection (Figure 3.12B). Meanwhile, a 40 amino acid N-terminal deletion only minimally restored EMC2 and EMC4 expression, and allowed for a partial but statistically significant rescue of DENV infection (Figure 3.12B). A 60 amino acid N-terminal EMC6 truncation did not express to detectable levels, and as expected did not restore DENV infection or EMC expression (Figure 3.12B). Together, these data suggest that the N terminus of EMC6 is not critical for its function in flavivirus replication or complex assembly.

Discussion

The infection cycles of flaviviruses depend on the ER. Flavivirus infection induces extensive remodeling of the ER membrane to form specialized replication organelles (17, 151). These structures have been proposed to shield viral products, such as double-stranded RNA, from innate immune recognition, and to concentrate factors that promote viral replication. We speculate that another function of these organelles is to generate a specialized environment for polyprotein translation, processing, and folding. The viral polyprotein is translated and processed at the ER, and it has been shown that the cytosolic capsid and NS5 proteins of DENV depend on Hsp70 chaperones for their stability (152). However, whether flaviviral membrane proteins also require cellular chaperones for their folding and stability remains unknown.

The EMC has been identified as a host dependency factor for infection by the flaviviruses DENV, ZIKV, and YFV (12, 24-26). While the functions of the EMC remain

incompletely understood, accumulating evidence indicates that it acts as an ER-localized molecular chaperone for a subset of multi-pass transmembrane proteins (100, 105, 106), as well as a tail-anchored transmembrane protein insertase (107). As the EMC likely acts as a chaperone for multiple cellular membrane proteins, we cannot exclude the possibility that a cellular membrane protein essential for DENV and ZIKV infection is misfolded in EMC-depleted cells. For example, it has been suggested that the EMC is required for expression of a ZIKV entry factor (25). However, this does not exclude a role for the EMC in NS4A and NS4B folding. In fact, several lines of evidence argue that the EMC functions as a molecular chaperone for these viral proteins: (1) both are multi-pass transmembrane proteins expressed on the ER and thus are biologically plausible substrates; (2) the levels of both proteins are specifically reduced by EMC depletion and restored by ERAD/proteasome inhibition; (3) the EMC is recruited to viral replication sites in DENV-replicating cells lacking viral structural proteins; (4) NS4B interacts with the EMC by co-immunoprecipitation analysis.

While expression of NS4A and NS4B are reduced in EMC knockout cells, other DENV NS proteins are relatively unaffected, as are at least some cellular multi-pass transmembrane proteins such as BAP31. While DENV NS2B was relatively unaffected by EMC knockout and did not co-precipitate with the EMC, expression of ZIKV NS2B was significantly reduced. This data lends the possibility that the EMC may be additionally required for expression of different NS proteins for each flavivirus. Furthermore, HCV does not depend on the EMC for infection despite encoding several multi-pass transmembrane proteins. This specificity invokes the obvious question: what are the determinants within multi-pass transmembrane proteins that drive EMC dependence? We showed that deletion of two marginally hydrophobic helices in NS4B leads to a loss of EMC dependence, consistent with the proposal that the EMC recognizes weakly hydrophobic segments in both multi-pass transmembrane and tail-anchored membrane proteins. We speculate that the EMC mediates the native folding of specific proteins with marginally hydrophobic domains, and that in the absence of the EMC, these proteins are recognized by ERAD machinery as misfolded, and thus are degraded.

Our findings regarding EMC function are conceptually in agreement with a recent publication (Shurtleff et al, 2018) concluding, based on ribosome labeling and proteomics in yeast and human cells, that the EMC serves to stabilize multipass transmembrane proteins encoding transmembrane domains enriched for charged residues. However, there was no experimental demonstration that mutation of any putative EMC client could modulate its EMC dependence. Also very interesting was the finding that in EMC-depleted human cells, there was a surprisingly limited number of cellular proteins that displayed significant EMC dependence: only 11 proteins were decreased by 2-fold or more in both EMC2 and EMC4-depleted cells. Our work adds substantially to these findings by the experimental demonstration that the stability of NS4B in EMC-depleted cells depends on two marginally hydrophobic segments. Furthermore, the NS4A and NS4B proteins of both ZIKV and DENV display strong dependence on the EMC for their stability. This is consistent with cells being able to tolerate genetic depletion of EMC subunits while these flaviviruses are not. Finally, the EMC is recruited to sites of viral replication in DENV-replicating cells, consistent with a specific hijacking of this complex during viral infection.

In summary, this work defines a mechanism by which the EMC supports flavivirus replication and provides additional evidence that the EMC functions as a multi-pass transmembrane chaperone. The dependence of multiple flaviviruses on the EMC and on Hsp70 proteins highlights their dependence on ER quality control mechanisms and therefore a shared vulnerability that potentially could lead to broadly antiviral strategies.

Materials and Methods

Plasmids, sgRNAs, and siRNAs

Individual sgRNAs were cloned into the pLENTICRISPRv2 vector for lentiviral transduction to generate EMC knockout cells (Table 3.1). For transient EMC knockdown, Thermo Fisher Predesigned Silencer™ siRNA against KIAA0090 (ID# 122746) was used as an EMC1 siRNA. Allstar negative control siRNA (Qiagen, Hilden, Germany) was used as a scrambled siRNA.

Constructs to express epitope tagged DENV non-structural proteins were generated by PCR using DENV serotype 2 strain 16681 cDNA clone pD2/IC-30P-NBX (135), then cloned into pSMPUW (Cell Biolabs, San Diego, CA) or pCDNA4 (Thermo Fisher Scientific) expression vectors. A full-length infectious cDNA clone of ZIKV from the 2015 Epidemic in Brazil (ZIKV-ICD) was a generous gift from Dr. A. Pletnev (National Institutes of Health, Bethesda, MD) (153). To construct a replication-defective cDNA clone of ZIKV, the NS5 catalytic G664-D665-D666 domain in ZIKV-ICD was mutated to G664-A665-A666 using standard cloning methods. To construct ZIKV non-structural protein expression vectors, the corresponding cDNA sequences were amplified by PCR using ZIKV-ICD as template and inserted into pcDNA3.1(-) in frame with the S tag or S-tagged GFP sequence by standard cloning methods. To construct C-terminal FLAG- or S-tagged GFP expression vectors, the GFP cDNA sequence was inserted into pcDNA3.1(-) in frame with the FLAG or S tag sequence by standard cloning methods.

The WT and dominant negative QQ p97 expression vectors were generous gifts from Dr. Y. Ye (National Institutes of Health) (150). Epitope tagged *EMC6* and *EMC4* were cloned by PCR using 293T cDNA as a template. Mutants of non-structural proteins were generated by overlap extension PCR. Detailed descriptions of these plasmid constructs are available upon request. Lentiviral expression constructs including pSMPUW and pLENTICRISPRv2 were also used to generate VSV-G pseudotyped lentiviral particles for transduction as previously described (136).

Luciferase virus and replicon assays

DENV serotype 2 strain 16681 cDNA clone pD2/IC-30P-NBX was used to generate the luciferase dengue reporter virus as previously described (24). The construction of the luciferase dengue reporter replicon has also been previously reported (146). Luciferase activity was measured using the Renilla luciferase assay system (Promega, Madison, WI). The transient replicon assay was performed as previously described (24). In brief, the luciferase dengue reporter replicon was in vitro transcribed and 5’ capped using T7 Megascript (Thermo Fisher Scientific). RNA was

then transfected into cells using TransIT mRNA reagent (Mirus Bio, Madison, WI). Luciferase activity was measured at 4 hours and 48 hours post-transfection.

Western blotting and band densitometry

For DENV expression constructs, cells were lysed in buffer containing 50 mM Tris, 150 mM NaCl, 1 mM EDTA, 1% SDS, and 5% glycerol, and Halt protease inhibitor (Thermo Fisher Scientific) on ice for 10 min. Lysates were clarified by centrifugation at 10k RCF for 10 min at 4˚C. LDS sample buffer (Thermo Fisher Scientific) was added to the lysate prior to loading the lysate on Bis-Tris NuPAGE Novex gels (Thermo Fisher Scientific).

For ZIKV expression constructs, Flp-In™ T-REx™ 293 cells (Thermo Fisher Scientific) were reverse-transfected with the indicated siRNAs at 50 μM using Lipofectamine RNAi MAX (Thermo Fisher Scientific) and incubated in a 12-well plate. At 48 h post siRNA transfection, cells were co-transfected with ZIKV constructs and GFP-FLAG using PEI and incubated for 24 h. Alternatively, cells were transfected with a vector containing the replication-defective ZIKV-ICD cDNA clone and incubated for 48 h. Cells were then lysed with a buffer containing 50 mM HEPES, 150 mM NaCl, 1% Triton X-100, and 1 mM PMSF, and centrifuged at 16,100 x *g* for 10 min at 4 ºC. The resulting supernatants were subjected to SDS-PAGE.

After electrophoresis, proteins were transferred to a PVDF membrane, then blocked in Tris-buffered saline pH 7.5 with 0.1% Tween-20 (TBST) with 5% BSA for 30 min at room temperature. Primary antibodies were diluted in blocking buffer and incubated with the membrane at 4˚C overnight. Blots were washed three times with TBST for 10 min each, incubated in HRP-conjugated secondary antibody diluted in the same blocking buffer for 1 h, and washed again three times. Bands were visualized by chemiluminescent detection with SuperSignal West Femto (Thermo Fisher Scientific) substrate in a Syngene PXi 6 (Synoptics Limited, Cambridge, UK) imager or developed using traditional X-ray film methods. Band quantification was performed using ImageJ (NIH).

Antibodies

Antibodies used for Western blotting, co-IP, and immunofluorescence are as follows: anti-HA C29F4 from Cell Signaling Technology (Danvers, MA), anti-HA 12CA5 from Santa Cruz Biotechnology (Dallas, TX), anti-DENV-NS2B GTX124246 from Gentex (Irvine, CA), anti-DENV-NS4B GTX103349 from Genetex, anti-DENV-NS4A GTX124249 from Genetex, anti-ZIKV-NS4B GTX133311 from Genetex, anti-S tag AB19321 from Abcam (Cambridge, UK), anti-FLAG F1804 from Sigma Aldrich (St. Louis, MO), anti-p97 PA5-22257 from Thermo Fisher Scientific, anti-Ubiquitin P4D1 from Santa Cruz Biotechnology, anti-GFP D5.1 from Cell Signaling Technology, anti-EMC1 AP10226b from Abgent (San Diego, CA), anti-EMC2 (TTC35) sc-166011 from Santa Cruz Biotechnology, anti-EMC3 (TMEM111) sc-365903 from Santa Cruz Biotechnology, anti-EMC4 PA5-48708 from Thermo Fisher Scientific, anti-EMC4 ab184162 (EPR15081) from Abcam, anti-EMC6 ARP44679_P050 from Aviva Systems Biology (San Diego, CA), anti-Beta actin A5316 from Sigma Aldrich, anti-BAP31 CC-1 from Thermo Fisher Scientific. Anti-S tag agarose beads were used for affinity purification. The anti-NS1 monoclonal antibody was a gift from Dr. Malasit at the National Center for Genetic Engineering and Biotechnology in Thailand. The anti-E protein monoclonal antibody originated from hybridoma 4G2 supernatant.

Proteasomal inhibition and co-immunoprecipitation

For proteasome inhibition assays, MG132 (Sigma Aldrich) was added to the media at 10 μM for 6 h, then cells were lysed in RIPA buffer with 20 mM N-ethylmaleimide (Sigma Aldrich) to inhibit deubiquitinase activity and Halt protease inhibitor, then subjected to IP by anti-HA antibody.

For p97/VCP experiments, Flp-In™ T-REx™ 293 cells were reverse-transfected with EMC1 siRNA at 50 μM using Lipofectamine RNAi MAX and incubated in a 6-well plate. At 48 h post-transfection, cells were further co-transfected with the indicated flavivirus NS4B construct and either one of an empty vector, the WT or dominant negative $p97^{QQ}$ expression vector. Following incubation for 24 h, cells were harvested, lysed with a buffer containing 50 mM HEPES, 150 mM NaCl, 1% Triton X-100, and 1

mM PMSF, and centrifuged at 16,100 x *g* for 10 min at 4 ºC. To immunoprecipitate DENV NS4B-HA, the resulting supernatant fraction was incubated with the anti-HA monoclonal 12CA5 antibody at 4ºC for 2 h, followed by incubation with protein A/G agarose beads. Alternatively, to isolate ZIKV NS4B-S, whole cell lysates were incubated with S protein-conjugated beads at 4ºC for 2 h. After beads were extensively washed with a buffer containing 50 mM HEPES, 150 mM NaCl, and 1% Triton X-100, bound materials were eluted with SDS sample buffer followed by SDS-PAGE and Western blotting for detection.

For Co-IP assays between the EMC and NS4B, cells were lysed in buffer containing 50 mM Tris, 150 mM NaCl, 1% Deoxy Big CHAP detergent (256455, EMD Millipore, Burlington, MA) and Halt protease inhibitor. Lysates were clarified by low speed centrifugation at 10,000 x *g* for 10 min at 4˚C. The monoclonal antibody C29F4 was added for HA immunoprecipitation. For endogenous EMC4 co-IP, the EMC4 monoclonal antibody EPR15081 was added. After addition of antibody, samples were incubated at 4˚C for 1 h. Protein G Dynabeads (Thermo Fisher Scientific) were then added, and samples were again incubated at 4˚C for 1 h. Magnetically isolated beads and bound proteins were washed three times with PBS containing 0.1% Deoxy Big CHAP. Samples were eluted by addition of LDS sample buffer with 50 mM TCEP (Thermo Fisher Scientific) then heated to 95˚C for 10 min.

Immunofluorescence microscopy

Huh 7.5.1 cells stably harboring a DENV replicon encoding puromycin resistance were stably transduced with a lentivirus encoding FLAG-EMC4 and blasticidin resistance. Cells were plated on poly-D-lysine coated coverslips then fixed in ice cold 100% methanol for 20 minutes. Coverslips were washed in PBS, then blocked in PBS with 2% BSA and 0.1% Triton X-100 for 30 minutes. The same blocking buffer was used to dilute the indicated antibodies for immunostaining, and for secondary fluorophore conjugated antibody detection.

Quantification and Statistical Methods

For infection and replicon experiments, each dot represents an individual biological replicate, with bars representing the mean ± SD. For band densitometry, each dot represents an individual Western blot from an independent transfection. Statistics were calculated using Prism 7 (GraphPad Software). Statistical significance was determined by non-parametric Mann Whitney U test as indicated in the figure legends. For all figures, * $p<0.05$, ** $p<0.005$, and *** $p<0.0005$.

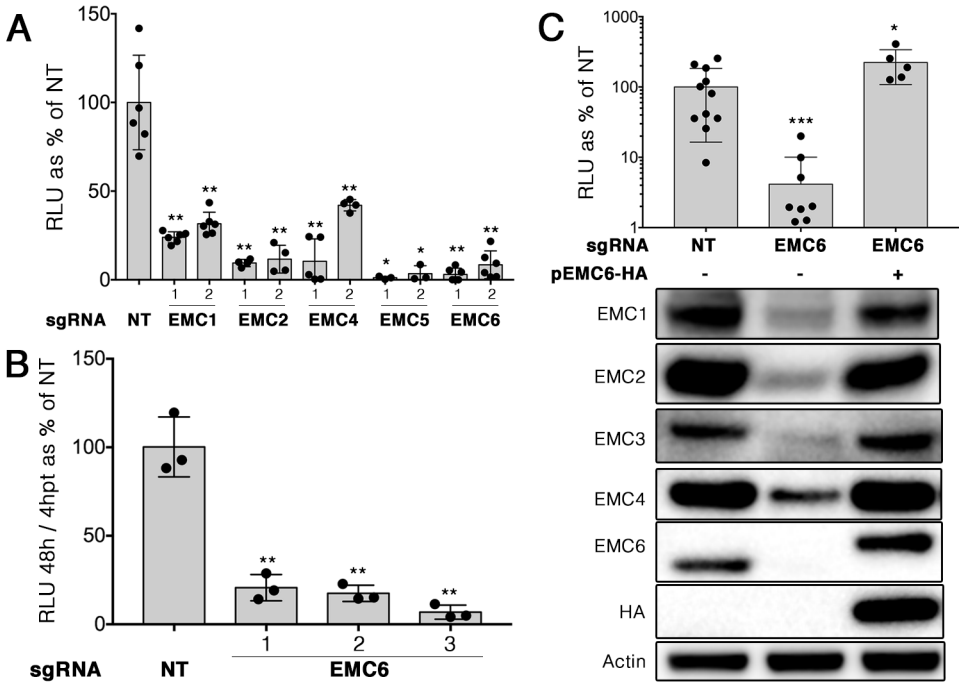

Figure 3.1. DENV requires the EMC for replication. In **A-C,** Huh 7.5.1 cells were stably transduced with pLentiCRISPRv2 lentiviral vectors encoding Cas9 nuclease and a targeting sgRNA to knock out the indicated gene, or a non-targeting (NT) control. In **A**, two independent sgRNAs were used per gene. Cells were then infected with a luciferase reporter DENV (luc-DENV) and luciferase activity was measured 3 d post-infection. In **B**, cells expressing 3 different sgRNAs targeting EMC6 or a NT control were transfected with *in vitro* transcribed RNA encoding a luciferase reporter DENV replicon. Replication was assessed by the ratio between luciferase activity at 48 h vs 4 h post-transfection to control for differences in transfection and translation efficiency. In **C**, EMC6 knockout cells were transduced to express an sgRNA-resistant HA tagged EMC6, then infected with luc-DENV and luciferase activity was measured 3 d post-infection. Duplicate wells were lysed for immunoblotting with the indicated antibodies. For **A-C**, data are plotted as relative luciferase units as a percentage of NT. Each dot represents an independent infection, and bars show means ± SD relative to cells expressing a non-targeting sgRNA control. Statistical significance compared to NT was determined by Mann-Whitney U: *, $p < 0.05$, **, $p < 0.005$, ***, $p < 0.0005$.

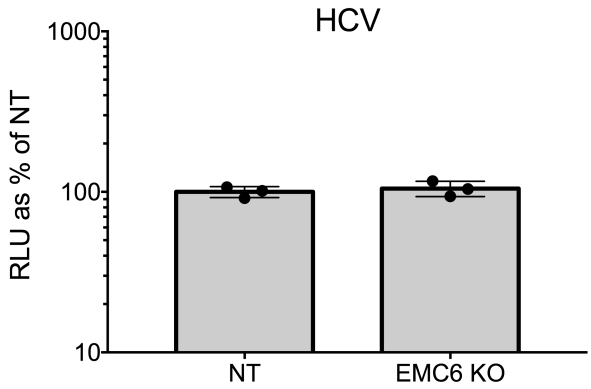

Figure 3.2. Hepatitis C virus replication is unaffected by the loss of the EMC. Huh 7.5.1 cells stably expressing Cas9 nuclease with either a non-targeting (NT) or EMC6 specific sgRNA were infected with HCV encoding a NanoLuc luciferase reporter followed by luciferase activity measurement 3 d later. Each dot represents a biological replicate with bars representing means±SD.

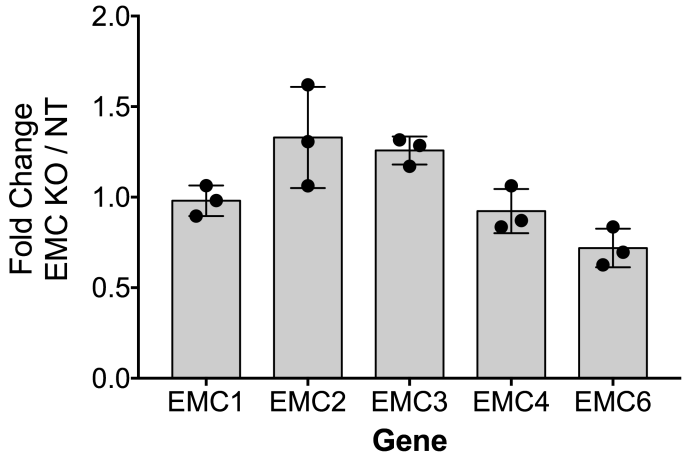

Figure 3.3. Transcription of EMC subunits is unaffected by EMC6 knockout. RNA was extracted from wild-type and EMC6 knockout Huh 7.5.1 cells, then subjected to reverse transcription and qPCR for the indicated genes. Each dot represents a biological replicate with bars showing means±SD.

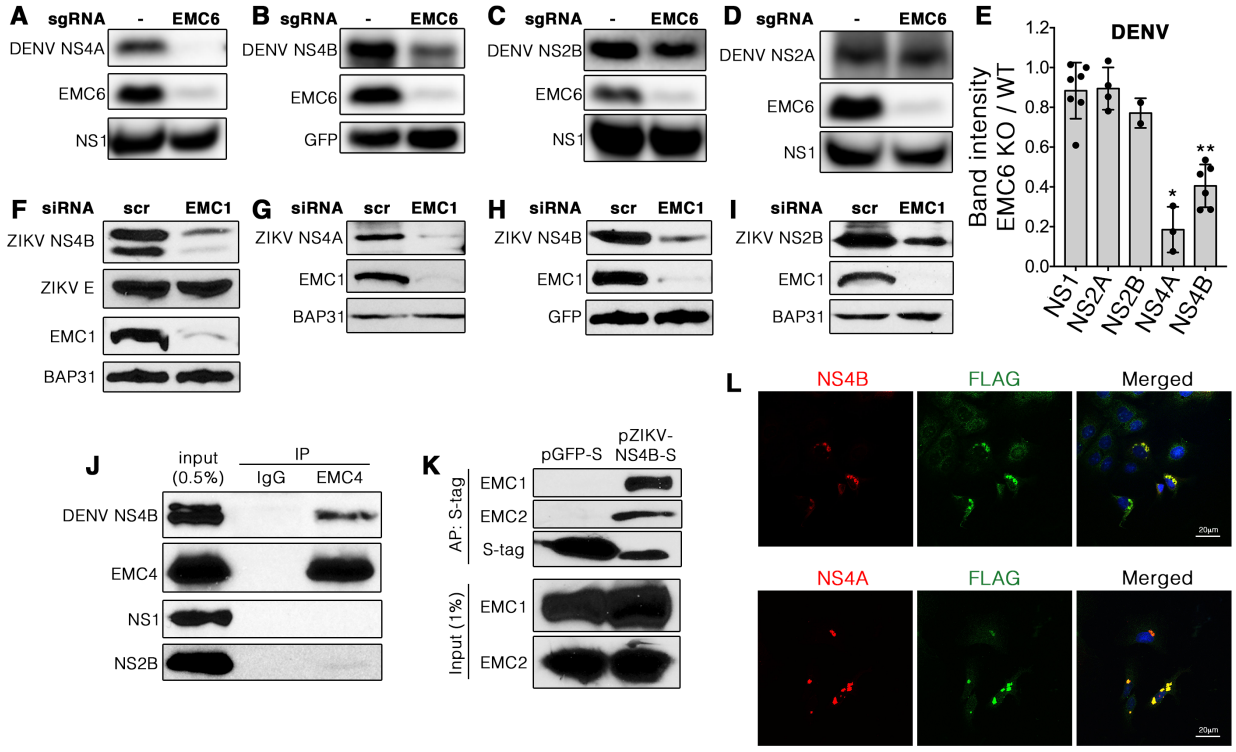

Figure 3.4. Flavivirus NS4A and NS4B are dependent on the EMC for efficient expression. In **A-D**, 293T cell pools stably expressing Cas9 nuclease and a targeting sgRNA to knockout EMC6 were subsequently transiently cotransfected with constructs encoding HA-tagged DENV non-structural proteins and NS1-FLAG (**A-C**) or GFP (**D**) as a transfection control. In **F-I**, 293 cells were transfected with siRNAs against EMC1 or a scrambled control (scr). 48 h later, cells were transfected with a replication-defective full-length ZIKV cDNA in **F** or to express the indicated S-tagged ZIKV nonstructural proteins in **G-I.** For **A-D** and **F-I**, 24 h post-transfection, cells were lysed and proteins were separated by SDS-PAGE followed by Western blotting for the indicated proteins. In **E**, ImageJ was used to quantify band intensities for Western blots of each of the DENV non-structural proteins in EMC6 knockout cells compared to wild-type. Each dot represents a biological replicate, with independent transfections and Western blots. Bars represent means±SD. Mann-Whitney U was performed for statistical significance, with *, $p<0.05$ and **, $p<0.005$ as compared to NS1. In **J**, Huh 7.5.1 cells stably harboring a DENV replicon were lysed and subjected to immunoprecipitation using an anti-EMC4 antibody or an isotype control. Immunoprecipitates were analyzed by immunoblotting with the indicated antibodies. In **K**, 293 cells transiently transfected to express either GFP-S or ZIKV NS4B-S were lysed 24 h later for affinity purification by S-protein conjugated beads and immunoblotting with the indicated antibodies. **L**, stable DENV replicon Huh 7.5.1 cells were transduced to express EMC4-FLAG. Immunostaining was performed for the indicated antigens with DAPI nuclear counterstaining, followed by confocal microscopy.

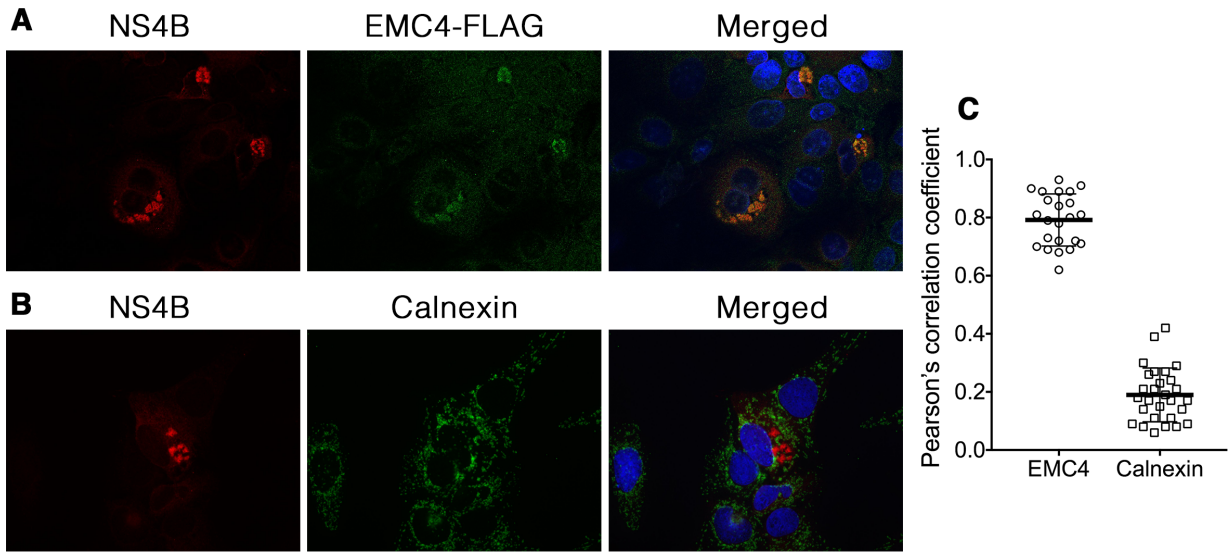

Figure 3.5. The EMC localizes to the DENV replication organelle. In **A** and **B**, Huh-7.5.1 cells were stably transfected with a DENV replicon, then immunostaining was performed against the indicated antigens with DAPI nuclear counterstaining, followed by confocal microscopy. In **C**, quantitation of co-localization between EMC4-FLAG and NS4B or Calnexin and NS4B in replicon cells. Each point represents the Pearson's correlation coefficient for a single cell, with the mean±SD.

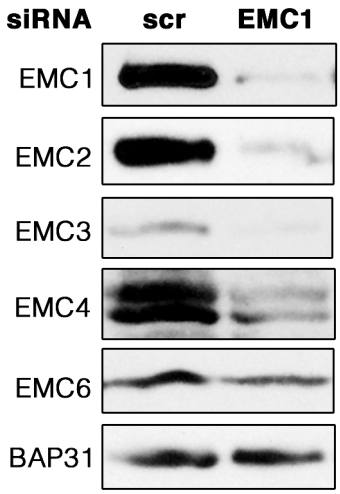

Figure 3.6. EMC1 knockdown results in loss of other EMC subunits. HEK293 cells were transfected with a siRNA against EMC1 or scrambled control (scr) for 48 h. Cells were then lysed and subjected to SDS-PAGE and Western blotting for the indicated proteins.

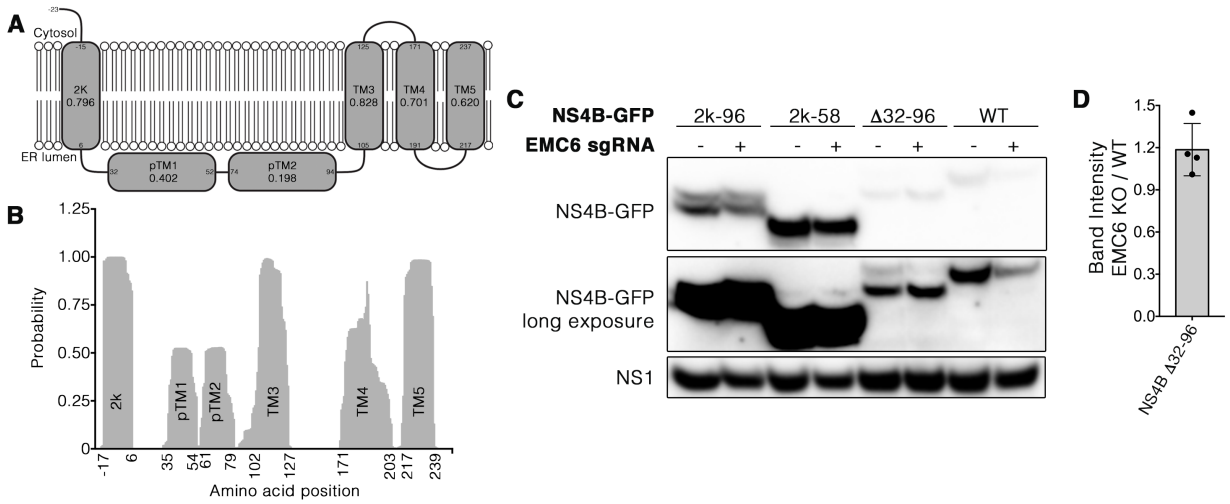

Figure 3.7. Identification of DENV NS4B domains that confer EMC dependence. In **A**, a diagram depicting the putative transmembrane domains in 2k-NS4B (gray bars) as listed in UniprotKB (accession P29990) with relative hydrophobicity scores, which are the average of the "transmembrane tendency scale" values described in (154) for the 20 amino acids in the helix. Values >0.8 indicate "high TM tendency" and values <0.3 indicate "low TM tendency". The numbers within the transmembrane domains indicate amino acid numbers marking the terminal amino acids of each domain. In **B,** TMHMM (155) was used to predict membrane topology, and the resulting probabilities for each residue were plotted where greater values reflect greater transmembrane probability. Amino acid positions at the bottom indicate the terminal amino acids with scores above 0.3 for each predicted transmembrane domain. In **C,** 293T cells stably expressing Cas9 and sgRNA targeting EMC6 were co-transfected to express the indicated C-terminally GFP-tagged NS4B mutants and NS1-FLAG as a transfection control. 2k-96 indicates a C-terminal truncation at amino acid 97. 2k-58 indicates a C-terminal truncation at amino acid 59. Δ32-96 indicates a deletion from 32 to 96. 24 h post-transfection, cells were lysed and proteins were resolved by SDS-PAGE followed by Western blotting for the indicated proteins. In **D**, band intensity for NS4B Δ32-96 in EMC6 knockout cells compared to wild-type cells, where each dot represents an individual biological replicate from independent transfections and Western blots.

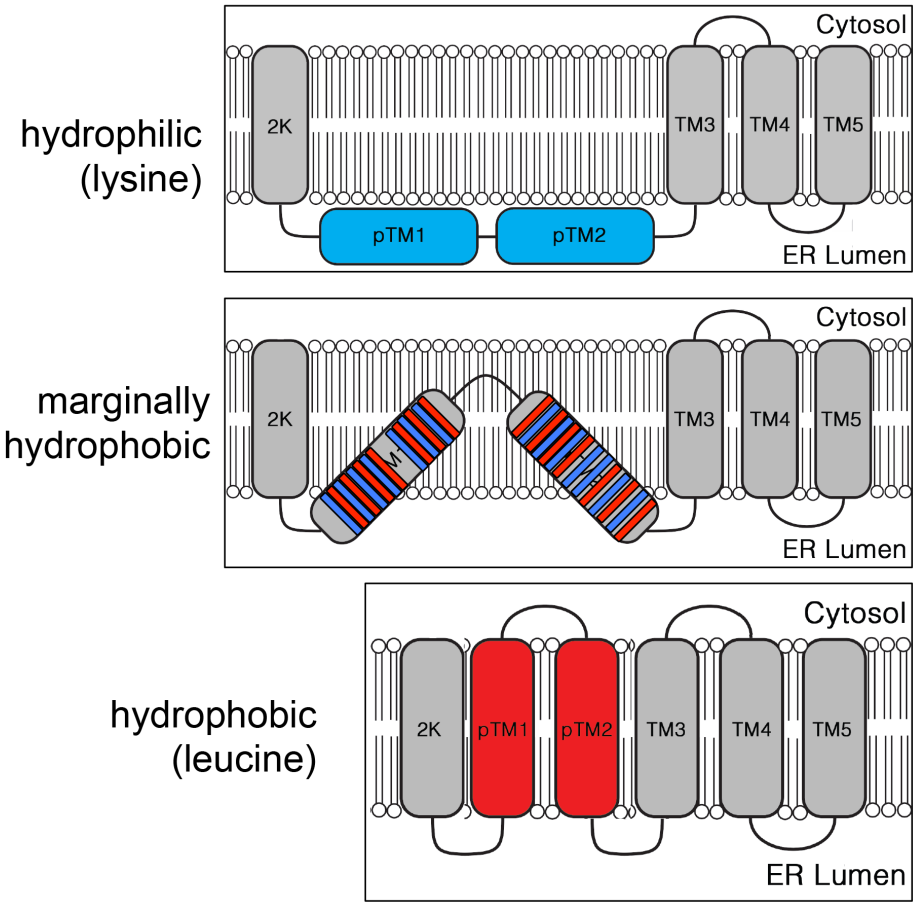

Figure 3.8. Model of hydrophobicity mutants of NS4B. The two NS4B marginally hydrophobic domains pTM1 and pTM2 are speculated to be membrane associated, with red representing hydrophobic residues, and blue representing charged and polar hydrophilic residues. Mutagenesis of the hydrophobic residues to lysine causes a change in topology, and withdrawal of pTM1 and pTM2 from the membrane. Mutation of the charged and polar residues to leucine results in the insertion of the domains into the membrane, as the domains now resemble canonical transmembrane domains.

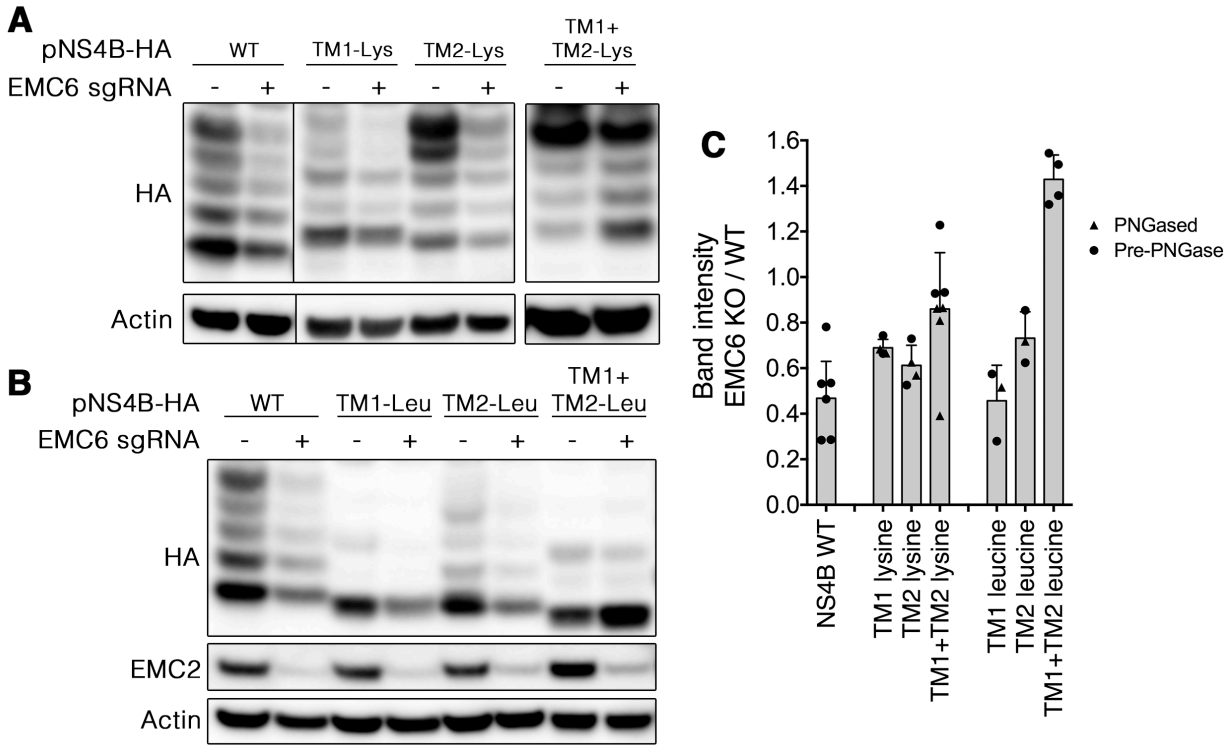

Figure 3.9. NS4B EMC dependence is driven by marginal hydrophobicity. Wild-type or EMC6 knockout 293T cells were transfected to express various NS4B mutants. TM1-Leu indicates R33L, P34L, S36L, T39L, T35L, T36L, T39L mutations. In **A**, TM1-Lys indicates L32K, A35K, A37K, L40K, A42K, V43K, A44K, F47K mutations. In **B**, TM2-Lys indicates L84K, I89K, V91K, L93K, L94K mutations. TM2-Leu indicates TM2: K80L, P83L, S85L, K86L, D88L, P92L mutations. In **C**, bands were quantified by ImageJ and represented as a ratio of EMC6 knockout / wild-type cells. Each point represents a biological replicate with bars representing the means±SD. Triangles represent quantification from blots after PNGase treatment. Circles represent total quantification from blots prior to PNGase.

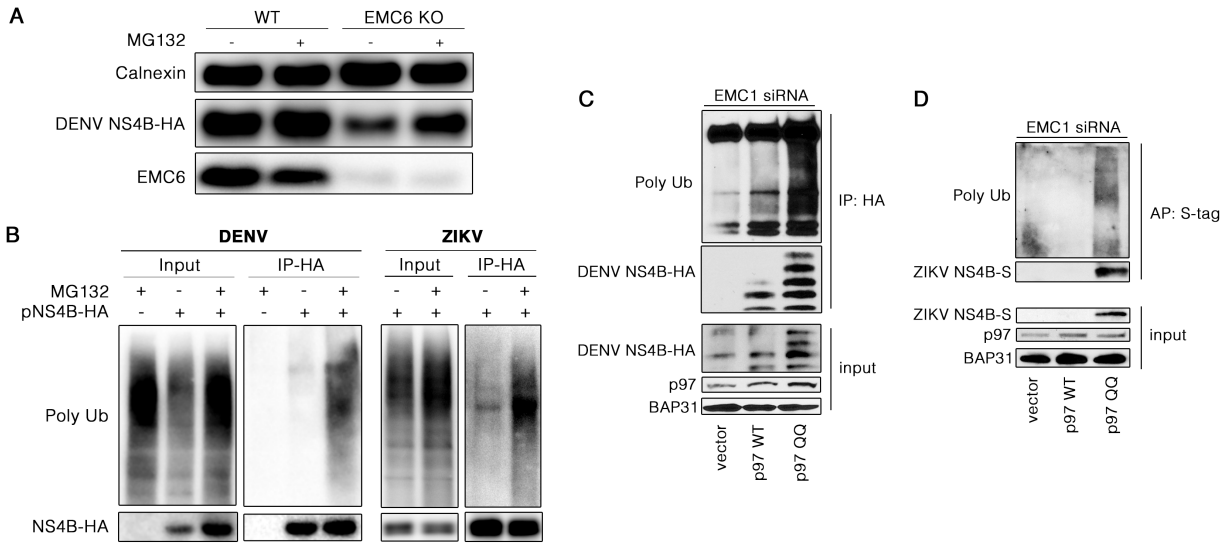

Figure 3.10. NS4B removal in EMC depleted cells is mediated by ERAD. In **A**, wild-type or EMC6 knockout Huh 7.5.1 cells were transduced to express DENV NS4B-HA, then treated with 10 μM MG132 for 6 h prior to lysis. In **B**, EMC6 knockout Huh 7.5.1 cells were stably transduced to express HA tagged DENV NS4B, ZIKV NS4B, or vector, then treated with 10 μM MG132 for 6 h followed by lysis and immunoprecipitation with anti-HA antibody. In **C** and **D**, 293 cells were transfected with a siRNA against EMC1 to deplete the EMC. 48 h later, cells co-transfected to express the indicated p97 constructs or empty vector control with epitope tagged DENV or ZIKV NS4B. 24 h later, cells were lysed and immunoprecipitated for tagged NS4B. In **A-D**, proteins were separated by SDS-PAGE and visualized by Western blotting for the indicated proteins.

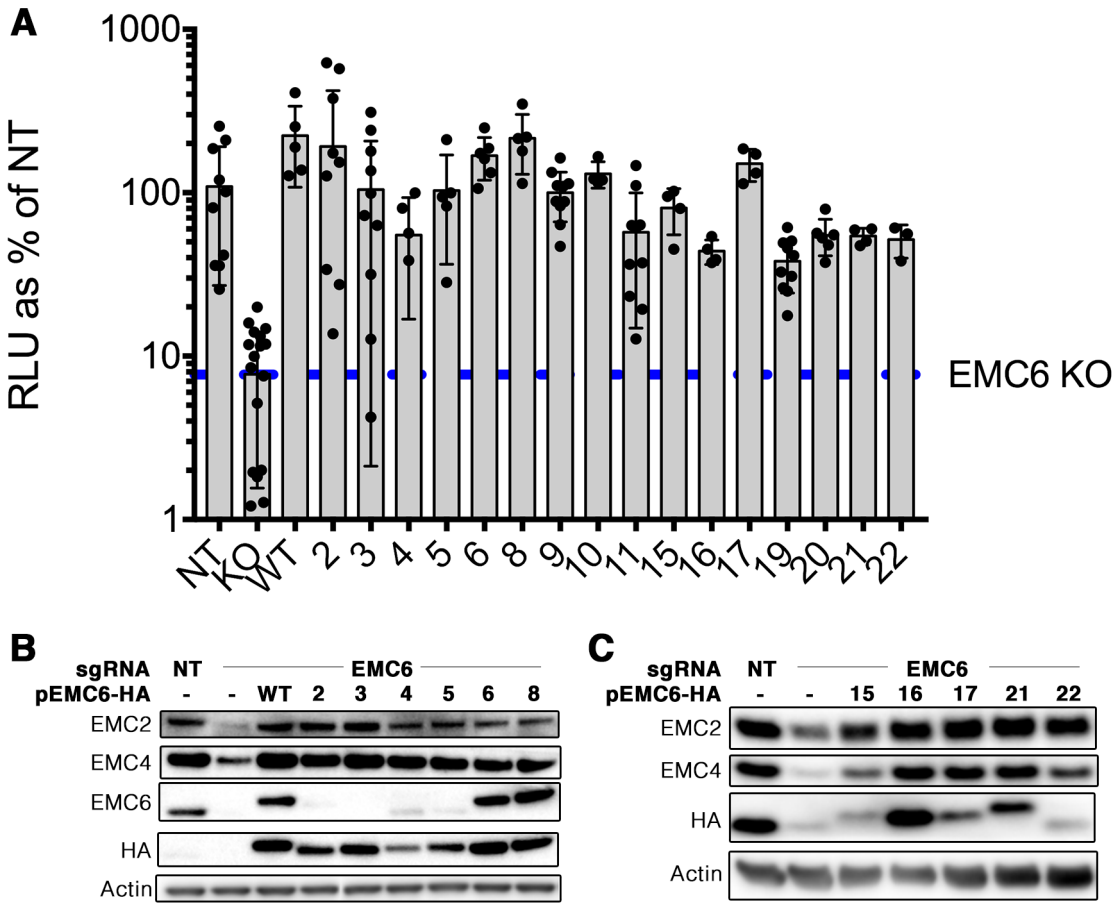

Figure 3.11. Alanine scanning of EMC6. Huh 7.5.1 cells were transduced to express a Cas9 and sgRNA targeting EMC6 or non-targeting control (NT). Cells were then stably transduced again with a lentivirus encoding sgRNA resistant EMC6 harboring alanine mutations at 5 consecutive residues. Numbers 2-22 indicate the position of the 5 amino acid (aa) mutation to EMC6, i.e. 1: aa 1-5, 2: aa 6-10, 3: aa 11-15, etc. KO indicates EMC6 knockout cells transduced with empty vector. WT indicates EMC6 knockout cells transduced with an sgRNA-resistant wild-type EMC6. In **A**, cells were infected with luc-DENV for 2 days, then luciferase activity was measured. Each dot represents an independent biological replicate with bars representing the mean±SD. In **B** and **C**, representative Western blots show the level of expression of each HA-tagged EMC6 mutant as well as EMC2 and EMC4, which are surrogate measures for rest of the EMC.

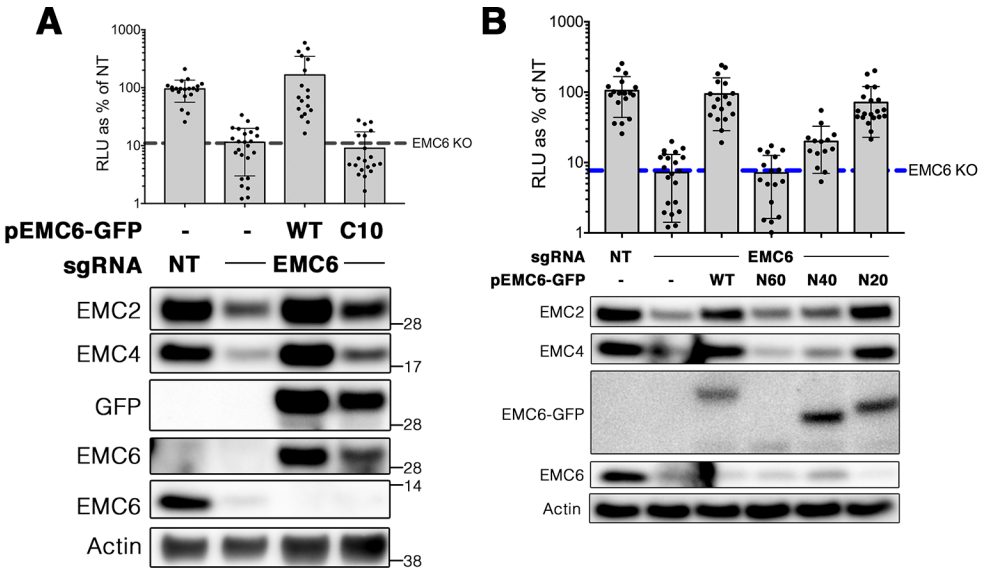

Figure 3.12. The N-terminal 20 amino acids of EMC6 are not required for complex assembly or infection. For **A** and **B,** Huh 7.5.1 cells were transduced to express a Cas9 and sgRNA targeting EMC6 or non-targeting control (NT). Cells were then stably transduced again with a lentivirus encoding sgRNA resistant EMC6 harboring truncations to either the C or N terminus. In **A**, C10 indicates 10 amino acid deletion at the C-terminus. In **B**, N20 represents a 20 amino acid deletion at the N-terminus, etc. Cells were infected with luc-DENV for 2 days, then luciferase activity was measured. Each dot represents an independent biological replicate with bars representing the means±SD. Representative Western blots show the level of expression of each GFP-tagged EMC6 mutant as well as EMC2 and EMC4, surrogate measures for rest of the EMC. WT indicates wild-type EMC6. For N-terminal truncation mutants, EMC6 was C-terminally GFP tagged while C-terminal truncation mutants were N-terminally GFP tagged.

Table 3.1. List of guide RNAs for generating EMC knockout cells. Oligos were annealed and cloned into pLENTICRISPRv2. Constructs were co-transfected into 293Ts to generate VSV-G pseudotyped lentiviruses for stable transduction of target cells.

Sequence	Comments
CACCG AGGCCGAATCATGCGTTCCT	F sgRNA targeting EMC1
AAAC AGGAACGCATGATTCGGCCT C	R sgRNA targeting EMC1
CACCG ACGCATGATTCGGCCTCCAT	F sgRNA targeting EMC1
AAAC ATGGAGGCCGAATCATGCGT C	R sgRNA targeting EMC1
CACCG ATACTCATTCAGCTCCCGAA	F sgRNA targeting EMC2
AAAC TTCGGGAGCTGAATGAGTAT C	R sgRNA targeting EMC2
CACCG TAATGAATATGCTTCTAAGC	F sgRNA targeting EMC2
AAAC GCTTAGAAGCATATTCATTA C	R sgRNA targeting EMC2
CACCG TGCTTGTCCAAGTAACCGAC	F sgRNA targeting EMC4
AAAC GTCGGTTACTTGGACAAGCA C	R sgRNA targeting EMC4
CACCG CAATGGCCCACTTGAAGCGC	F sgRNA targeting EMC4
AAAC GCGCTTCAAGTGGGCCATTG C	R sgRNA targeting EMC4
CACCG AATATGAACTATACCGTAAC	F sgRNA targeting EMC5
AAAC GTTACGGTATAGTTCATATT C	R sgRNA targeting EMC5
CACCG GCATCATGGCGCCGTCGCTG	F sgRNA targeting EMC5
AAAC CAGCGACGGCGCCATGATGC C	R sgRNA targeting EMC5
CACCG ACGGCCGCCTCGCTGATGAA	F sgRNA targeting EMC6
AAAC TTCATCAGCGAGGCGGCCGT C	R sgRNA targeting EMC6
CACCG GACCTCGGTGTCAGCGCTGT	F sgRNA targeting EMC6
AAAC ACAGCGCTGACACCGAGGTC C	R sgRNA targeting EMC6
CACCG CCGGCAATAATCCAGGACGG	F sgRNA targeting EMC6
AAAC CCGTCCTGGATTATTGCCGG C	R sgRNA targeting EMC6

CHAPTER IV

Dominant-negative inhibition of flavivirus infection by heterologous expression of engineered non-structural protein 1.

The experiments to demonstrate inhibition of ZIKV and YFV infection by expression of various NS1 mutants were performed by Stephanie Azzopardi and Margaret R. MacDonald. Natalie McMyn assisted in the cloning of various NS1 constructs.

Introduction

Upon seeing the hits from the initial CRISPR-Cas9 screen, and prior to any characterization of the hits, my initial hypothesis was that loss of STT3A or STT3B would affect the glycosylation of NS1 and potentially its folding or stability, which in turn would prevent DENV replication. I had transduced WT and STT3A or STT3B knockout cells to express NS1, but found that I could not detect any differences in NS1, even using metabolic labeling to visualize nascent NS1 (Figure 2.6B). As a result, that hypothesis was quashed. As I had been in the process of validating hits from the screen by infecting knockout cells with a luciferase reporter DENV, I also decided to infect cells transduced with various NS1 constructs. To my surprise, I found that DENV replication was severely inhibited in cells expressing DENV NS1 harboring an N207A mutation. I decided to explore this phenomenon further, and the following are results that stem from the those observations.

Hypoglycosylated NS1 blocks flavivirus replication in a dominant-negative fashion

We stably transduced Huh 7.5.1 cells to express wild-type DENV-2 or ZIKV NS1, N130A NS1, N207A NS1, or the double mutant N130A N207A NS1, then subsequently

infected them with a luciferase DENV-2 reporter virus (luc-DENV) at an MOI = 0.1. Cells expressing wild-type DENV-2 NS1 (D-WT) supported elevated levels of infection compared to the parental cell line (Figure 4.1A). However, expression of DENV-2 NS1-N207A (D-N207A) or the double mutant N130A N207A (D-ΔGlyco) dramatically reduced levels of infection by 2 logs as compared to the parental cell line (Figure 4.1A). Expression of DENV-2 NS1-N130A (D-N130A), on the other hand, had no effect on the level of DENV-2 infection, demonstrating that the inhibition of DENV-2 infection by hypoglycosylated D-N207A or D-ΔGlyco NS1 is not simply a nonspecific effect of NS1 hypoglycosylation.

Similarly, expression of ZIKV-NS1 wild-type (Z-WT) did not affect levels of DENV-2 infection compared to a vector control (Figure 4.1B). In contrast to DENV-2, ZIKV NS1-N207A (Z-N207A) did not affect DENV infection, while ZIKV NS1-N130A (Z-N130A) or ZIKV NS1-ΔGlyco (Z-ΔGlyco) reduced DENV infection by approximately 20-fold (Figure 4.1B).

Glycosylation of NS1 is dependent upon its insertion into the endoplasmic reticulum (ER) lumen via an N-terminal signal sequence encoded by the C-terminal 22 amino acids of the DENV envelope protein (27). Therefore, we asked whether localization of NS1 in the ER lumen is necessary to block replication by expressing a mutant of DENV NS1 lacking this signal sequence, dubbed ΔSig. We find that ΔSig NS1 remains unglycosylated and migrates at the same size as ΔGlyco NS1 by SDS-PAGE and Western blotting lysates obtained from the intracellular compartment of transduced cells (Figure 4.1A). After infection with luc-DENV, we found that cells expressing ΔSig NS1 supported infection to the same level as control cells. Although the expression level of ΔSig NS1 was lower than that of D-N207A or D-ΔGlyco, this data suggests that hypoglycosylated NS1 can only block DENV propagation if it resides within the ER lumen.

DENV is blocked at the level of replication in NS1-N207A expressing cells

We next sought to determine the step at which DENV infection was impaired in D-N207A and D-ΔGlyco expressing cells. We transfected 293T cells stably expressing

D-N207A or D-WT with a luciferase reporter replicon, which encodes a monocistronic N-terminal luciferase tagged to a DENV subgenomic replicon containing the 7 non-structural proteins required for DENV replication (24, 146). DENV replication was significantly impaired in D-N207A expressing cells compared to D-WT, with approximately 1 log reduction in luciferase activity (Figure 4.2A). This subgenomic replicon also encodes a puromycin gene for stable selection of cells supporting replication of the DENV replicon, so we further performed colony formation assays to determine whether we could recover mutations that allow DENV to replicate in cells expressing D-N207A (Figure 4.2B). Similar to the transient replicon assay, we found a dramatic decrease in the number of puromycin-resistant colonies formed on cells expressing D-N207A compared to D-WT (Figure 4.2B). Additionally, we transduced stable DENV replicon cells with a lentivirus encoding either D-WT or D-N207A and found that 2 weeks post-selection for the replicon and lentivirus, we were able to generate colonies in the D-WT condition, but not with D-N207A, suggesting that the addition of D-N207A can functionally cure cells of a DENV replicon (Figure 4.2C).

In an attempt to identify mutations conferring resistance to D-N207A, we isolated double selected stable D-N207A DENV replicon colonies by ring selection. Western blot analysis showed that of twelve colonies, only three expressed detectable levels of D-N207A; replicon RNA from these cells was cloned and sequenced. In one replicon, we found an I167L mutation in NS1, and another had a K60E mutation in NS2B. In the third colony, the replicon was determined to be wild-type. Using reverse genetics, we introduced NS1-I167L or NS2B-K60E mutations into the subgenomic replicon and repeated the colony formation assay to determine their level of resistance to D-N207A. After transfection of these mutant replicons into NS1 expressing cells, we found that these mutations did not significantly affect colony formation in D-N207A cells, indicating that these mutations did not grant substantial resistance to the dominant-negative effects of D-N207A (Figure 4.2D).

Inhibition by DENV N207A is MOI dependent

We hypothesized that D-N207A and Z-N130A inhibit replication in a trans-dominant manner through heterodimerization with wild-type NS1 molecules expressed from the viral RNA, which in turn blocks replication. In this model, we would predict that the dominant negative inhibition is dependent on the ratio between NS1-N207A and virally encoded NS1-WT. Therefore, we infected cells with increasing MOI to determine whether we could overcome the effect of NS1-N207A. After infection, we measured NS4B viral protein expression by Western blot 2 days post-infection as a surrogate for virus propagation. Additionally, we probed for total NS1, which includes both exogenously expressed and virally encoded NS1.

In WT-NS1 expressing cells, we found that NS4B protein levels were similar across cells infected at MOI 0.1 to 10, suggesting that these cells are already maximally infected at 2 days post infection (Figure 4.3A). However, in D-N207A expressing cells, NS4B expression correlated strongly with MOI, with increasing levels of NS4B at higher MOI (Figure 4.3A). At MOI 0.1, NS4B was undetectable, while at MOI 10, NS4B levels were similar to D-WT expressing cells infected at MOI 0.1. Similar data were found when we measured total NS1 expression (Figure 4.3A). We also show that the exogenously expressed NS1 is present at a level far below that of infection (Figure 4.3A). This data shows that the block in DENV replication by NS1-N207A is dependent on the MOI, indicating that the stoichiometry between virally encoded NS1-WT and D-N207A is critical to the dominant-negative inhibition of replication.

Hypoglycosylated NS1 can heterodimerize with wild-type NS1

As our model predicts that D-N207A forms heterodimers with virally encoded WT NS1, we proceeded to test the ability of the NS1 mutants to form heterodimers with WT NS1 by co-immunoprecipitation (co-IP). We co-transfected cells to express FLAG-tagged D-WT and HA-tagged D-N207A, or vice-versa, performed co-IP with anti-HA antibody, and then performed Western blotting to detect the presence of FLAG. We found that D-WT was able to interact with D-N207A by IP of either D-WT or D-N207A (Figure 4.3B), confirming that the two NS1s are able to heterodimerize. The degree of

dimerization was similar between two D-WT molecules as between D-WT and D-N207A, suggesting that the N207 glycosylation does not play a major role in the dimerization of NS1 (Figure 4.3B). NS1 exists almost exclusively as a dimer within cells, suggesting that these interactions are not due to homodimers forming hexamers (38, 124). Additionally, the level of expression by transient transfection or stable transduction is far below the level of NS1 expression during viral replication (Figure 4.3A), demonstrating that even under relatively low levels of expression, NS1 heterodimers are prevalent.

Because Z-N130A was also capable of inhibiting DENV infection, we performed co-IPs using Z-N130A and DENV NS1. Similarly, we found that Z-N130A could interact with D-WT, though to a significantly lesser degree than two DENV NS1 molecules (Figure 4.3C). We also tested whether a hypoglycosylated DENV NS1 could dimerize with ZIKV NS1, and found that the regardless of glycosylation status, ZIKV NS1 and DENV NS1 could still interact (Figure 4.3C), again suggesting that the glycosylation status of DENV or ZIKV NS1 does not affect hetero- or homo-dimerization within cells.

Engineered NS1 chimeras inhibit DENV infection

We next sought to determine whether we could isolate specific motifs in ZIKV and DENV NS1 that guide Z-N130A and D-N207A to block DENV replication, but not Z-N207A or D-N130A. The exogenously expressed sequences for ZIKV NS1 and DENV-2 NS1 share 54% identity, with 162 of 352 amino acids being different. The N-terminal 129 amino acids share only 43% identity, with 73 residues differing between the two. We hypothesized that specific residues at the N-terminus of NS1 may influence whether the N130A or N207A NS1 proteins are able to inhibit DENV infection. Therefore, we used a classic approach to study differences in homologous proteins through generating chimeric NS1 fusions. We constructed plasmids to express fusion proteins where we swapped the first 129 amino acids from ZIKV NS1 with DENV NS1 (D(1-129)-Z(130-352), now referred to as D-Z) and vice-versa where the first 129 amino acids from DENV NS1 were mutated to ZIKV (Z(1-129)-D(130-352), now referred to as Z-D) (Figure 4.4A).

Western blotting indicated that the Z-D chimeras had an apparent mobility pattern similar to DENV NS1, suggesting that they also were glycosylated as engineered (Figure 4.4C). To our surprise, stably transduced cells expressing chimeric Z-D NS1 dramatically inhibited luc-DENV infection in a glycosylation independent manner, with fully glycosylated Z-D NS1 blocking luc-DENV-2 infection by over 200 fold (Figure 4B). D-Z NS1 also inhibited luc-DENV infection but to a lesser degree, with D-Z WT inhibiting luc-DENV only 5-fold, and D-Z N130A blocking infection by 10-fold. Interestingly, D-Z N207A exhibited the greatest level of inhibition among the D-Z chimeras, with luc-DENV infection reduced approximately 30-fold (Figure 4.4B). We also demonstrated that both of these chimeric NS1s were able to form heterodimers with DENV NS1-WT, further providing evidence that heterodimerization may be important for the inhibition of viral replication (Figure 4.4D).

N207A-NS1 exhibits aberrant localization upon DENV infection

We then performed immunofluorescence microscopy to compare the localization of epitope tagged D-N207A and D-WT after DENV infection. We visualized the exogenously expressed NS1 with antibodies against FLAG or HA and also marked infected cells with an antibody against DENV NS4B. In uninfected cells, D-WT, D-N130A, and D-N207A were distributed in a reticular pattern consistent with their known localization to the ER lumen. Two days post-infection, both D-NS1 and D-N130A localized to distinct foci in infected cells (Figure 4.5A), similar to previous reports where NS1 was localized to replication complexes (46).

By contrast, the morphology and localization of D-N207A were dramatically different from D-WT after DENV infection. In many infected cells, D-N207A appeared in brightly staining accumulations that often appeared filamentous (Figure 4.5A). Importantly, we also noticed that cells not yet expressing visually apparent levels of NS4B also contained these filamentous N207A-positive structures (Figure 4.5A). These cells were frequently found in the immediate vicinity of NS4B-positive cells, suggesting that these cells were undergoing the early stages of infection. By contrast, in cells expressing high levels of NS4B, D-N207A often appeared to distribute in a punctate

pattern more similar to D-WT. The apparent inverse association between the appearance of D-N207A accumulations and the level of NS4B expression is consistent with our model's prediction that the strength D-N207A dominant negative inhibition is a function of the ratio of mutant to WT NS1 levels.

Furthermore, we found that Z-N130A exhibits a filamentous phenotype comparable to D-N207A upon DENV infection, suggesting that the mechanism of inhibition by Z-N130A and D-N207A are similar (Figure 4.5B).

A fraction of NS1 is secreted through the Golgi apparatus as hexamers, therefore we performed co-staining of infected cells with the vesicle marker β-COP, and found that neither D-WT nor D-N207A colocalized with β-COP vesicles after infection, demonstrating that the N207A filaments were not in the Golgi apparatus (Figure 4.5C).

NS1 and other viral non-structural proteins form replication complexes at the ER membrane, which co-localize with calnexin (49). Consistent with these findings, we found that exogenously expressed D-WT accumulated at calnexin positive sites after DENV infection (Figure 4.5D). However, D-N207A filaments did not co-localize with calnexin after infection, suggesting that they reside in a distinct cellular compartment (Figure 4.5D). These filaments often appeared to be excluded from calnexin-positive regions of the ER.

Dimerization as a determinant of the dominant-negative effect

We next wanted to determine whether the ability to form heterodimers was necessary for the dominant-negative inhibition on flavivirus replication by D-N207A. We attempted to generate mutant NS1 that would not dimerize with virally encoded wild-type NS1. We generated a mutant NS1 with 4 substitutions (K182D N191K K227D N234K) at the dimer interface targeting charged and non-conserved residues in an attempt to hinder the formation of NS1 heterodimers (D-WT-4x and D-N207A-4x) (Figure 4.6A). We chose non-conserved residues as we hypothesized that mutations at conserved residues could affect NS1 function and disrupt the dominant-negative phenotype in a mechanism independent of dimerization. However, these four mutations were insufficient to block heterodimerization with wild-type NS1, as detected by co-IP

(Figure 4.6B). Upon infection with luc-DENV, we found that these mutants no longer displayed the same dominant-negative effect as D-N207A (Figure 4.6C). D-WT-4x expressing cells and D-N207A-4x cells supported similar levels of DENV infection, which were slightly reduced compared to parental control (Figure 4.6C).

Engineered NS1 mutants inhibit infection by multiple flaviviruses

We next tested whether these NS1 mutants also exhibit dominant negative activity against other flaviviruses. We tested whether ZIKV or YFV could propagate in cells stably expressing DENV or ZIKV NS1. Using flow cytometry to measure the percentage of infected cells, we found that ZIKV was unaffected by expression of DENV NS1 or glycosylation mutants of DENV NS1 (Figure 4.8A). Like DENV-2, ZIKV was also inhibited by Z-N130A and not by Z-N207A (Figure 4.8A). Surprisingly, we also found that YFV was unable to replicate in cells expressing DENV or ZIKV NS1 regardless of glycosylation status (Figure 4.8B).

Discussion

Despite considerable effort over the past two decades and the recent elucidation of its structure, the molecular mechanisms by which flavivirus NS1 supports both genome replication and virion assembly remain unclear. Part of this mystery includes the role of flavivirus NS1 glycosylation. The strict conservation of NS1 glycosylation at N130 and N207 in all flaviviruses suggests that these sequons play important roles during infection. Furthermore, others have shown that mutant viruses lacking specific NS1 glycosylation sequons are attenuated in vivo and in vitro (31-34, 36). Our data show that expression of mutant NS1 lacking specific glycosylation sequons from both ZIKV and DENV can act in a dominant-negative fashion blocking flavivirus replication.

Importantly, we showed that Z-N130A is a potent inhibitor of multiple flaviviruses including DENV, YFV, and ZIKV, while D-N207A blocks only DENV-2 and other DENV serotypes. This cross-virus inhibition suggests that the exogenously expressed NS1 somehow poisons replication, most likely through heterodimerization with virally encoded NS1. We provided evidence that ZIKV NS1 and DENV NS1 can form

heterodimers, albeit with lower affinity than DENV NS1 homodimers. This difference in affinity also correlates with the degree of inhibition, as D-N207A reduces DENV-2 propagation by about 2-4 fold more than Z-N130A. In addition, inhibition of infection is MOI dependent, suggesting that the ratio of inhibitory NS1 to virally encoded non-structural proteins is a critical determinant of replication inhibition. We cannot exclude the possibility that hypoglycosylated NS1 homodimers can also inhibit infection through a mechanism independent of heterodimerization with virally encoded NS1.

We speculate that inhibitory NS1 molecules block replication in a mechanism that is dependent on interactions with other flavivirus non-structural proteins or host dependency factors. In support of this hypothesis, NS1 mutants display varying specificities in their ability to block flavivirus infection. For example, D-N207A does not block ZIKV infection, but is able to inhibit DENV infection. This suggests that hypoglycosylated NS1 is not nonspecifically detrimental to flavivirus infection, but that inhibitory NS1 heterodimers might block the assembly of the viral replicase or recruitment of a host dependency factor to the viral replication organelle. NS1 has been shown to interact with NS4A and NS4B (41, 47), which may be viral determinants that guide whether NS1 mutants can block infection. We sought but were unable to isolate viral mutations that conferred resistance to inhibitory NS1 proteins.

We also attempted to map NS1 determinants that drive N130A or N207A to exhibit an inhibitory phenotype by generating chimeric ZIKV and DENV NS1 fusion proteins. Simply swapping the first 130 amino acids on fully glycosylated DENV NS1 to ZIKV yielded a potent inhibitor of DENV infection. Likewise, all tested DENV and ZIKV NS1 molecules, both glycosylated and hypoglycosylated, blocked YFV infection. These data suggest that NS1 N-glycosylation and specific amino acid residues are both required for the association of NS1 with non-structural proteins or cellular factors to establish a functional replication complex, and that these interactions can be targets of dominant negative inhibition by NS1 mutants.

We made several attempts to produce NS1 mutants that were unable to form heterodimers to ask whether heterodimerization was necessary for dominant-negative inhibition. Unfortunately, using our co-immunoprecipitation assay, each of these mutants

was still capable of forming heterodimers with NS1-WT. However, D-WT-4x did not enhance DENV infection, and D-N130A-4x but could not efficiently block DENV infection, suggesting that either the NS1-4x mutants are able to heterodimerize with NS1-WT but fail to be recruited to the DENV replication complex, or that these NS1-4x mutants fail to form heterodimers with viral NS1 in the context of viral infection.

One hint at the potential mechanism of inhibition by the dominant-negative NS1 mutants is the altered distribution of inhibitory NS1 in infected cells, but not in uninfected cells. Using immunofluorescence, we were able to detect unusual NS1-positive structures in the early stages of infection of D-N207A and Z-N130A expressing cells, even prior to detectable accumulation of virally encoded proteins. These filamentous structures are reminiscent of those formed in cells expressing the CAP domain of the Bromovirus (BMV) 1a protein, which also functions as a dominant negative inhibitor of BMV replication in a mechanism dependent on multimerization (156). As aberrant NS1 distribution is observed only in the context of viral infection (e.g. not by cotransfection of D-N207A with D-WT or other DENV non-structural proteins), our data suggest that mutant NS1 redistribution is driven by heterodimerization with virally encoded NS1 in the context of polyprotein expression.

We also explored whether rationally designed NS1 chimeras could block flavivirus replication. The Z-D NS1 chimera was a potent inhibitor of DENV, despite being fully glycosylated at N130 and N207. Because ZIKV NS1-WT and DENV NS1-WT did not affect DENV infection, this suggests that the Z-D chimera is functionally distinct from its parental NS1s. The Z-D chimeras displayed possible glycosylation dependence, with N207A or N130A blocking infection to greater degrees than its fully glycosylated counterpart. As wild-type Z-D reduced the level of infection to our assay's limit of detection, future work will determine whether glycosylation of this chimera affects its dominant-negative activity.

The D-Z NS1 chimeras more clearly exhibited a modest but significant degree of glycosylation dependence, with both N130A and N207A inhibiting luc-DENV infection to greater degrees than wild-type. Because D-N207A and Z-N130A both blocked DENV infection, but not D-N130A or Z-N207A, these data suggest that the D-Z NS1 chimeras

may retain properties of both DENV and ZIKV NS1s in their ability to inhibit flavivirus infection.

We are currently exploring whether exogenous expression of engineered NS1 molecules in insect cells can similarly block flavivirus infection. Additionally, we predict that this phenomenon of dominant negative NS1 inhibition may be generalizable to other flaviviruses such as West Nile virus and that engineered NS1 mutants may be useful in controlling flavivirus dissemination. While the mechanism of this dominant-negative inhibition is unclear, this work provides tools to better understand the function of NS1 during viral replication.

Materials and Methods

Plasmids and lentiviral transduction

The DENV serotype 2 strain 16681 cDNA clone pD2/IC-30P-NBX was used as a template for generation of all DENV mutants (135). The ZIKV Paraiba_01/2015 strain cDNA clone ZIKV-ICD was used as a template for generation of the ZIKV mutants (153); the intron inserted into NS1 to enhance genetic stability of the clone was removed by overlap extension PCR prior to generation of mutants and subcloning of ZIKV NS1 into a lentiviral expression vector.

For all mutations, overlap extension PCR was performed to generate mutants that were subsequently cloned into the pSMPUW lentiviral expression vector (Cell Biolabs, San Diego, CA). Detailed descriptions of these constructs are available upon request. Lentiviral expression constructs were used to generate VSV-G-pseudotyped lentiviruses and for stable transduction of target cells as previously described (24). Expression after lentiviral transduction or transient transfection was confirmed by Western blotting.

The DENV 4x NS1 mutants harbor the following mutations: K182D N191K K227D N234K. These residues were chosen based on the crystal structure of the DENV NS1 dimer (PDB: 4O6B).

Viruses and replicons

The infectious DENV serotype 2 strain 16681 cDNA clone pD2/IC-30P-NBX was used to generate full-length viral RNA, and the luciferase reporter virus and replicon as previously described (146). Luc-DENV was titered by fluorescence focus assay using the 4G2 pan-flavivirus anti-envelope antibody to detect infected cells. To generate replicon RNA, linearized cDNA was in vitro transcribed, and capped with the $m^7G(5')ppp(5')A$ cap analog (New England Biolabs) using T7 Megascript (Thermo Fisher Scientific, Waltham, MA). Recombinant infectious virus for YFV-Venus was generated as previously described (139). ZIKV 2015 Puerto Rican PRVABC59 strain (144), was obtained from the CDC and passaged twice in Huh-7.5 cells prior to use in these experiments.

Antibodies

Western blots were performed using antibodies against HA (C29F4) from Cell Signaling Technology (Danvers, MA), and FLAG (F1804) from Sigma Aldrich. The anti-NS1 monoclonal antibody 1F11 was a gift from Dr. Malasit at the National Center for Genetic Engineering and Biotechnology in Thailand. For immunofluorescence assays, immunostaining was performed with anti-DENV-NS4B (Genetex GTX103349) (1:1000), anti-HA (Cell Signaling Technologies C29F4) (1:200), anti-FLAG (Sigma Aldrich F1804) (1:500), anti-NS1 (1:50), anti-calnexin (Santa Cruz Biotechnologies sc-23954) (1:100), or anti-beta-COP (Sigma Aldrich G2279) (1:200).

Flow Cytometry

For analysis of ZIKV and YFV replication, cells were infected at low MOI for 4 days, then fixed with 4% paraformaldehyde prior to analysis by flow cytometry on a BD LSR II flow cytometer. For ZIKV, cells were stained with 4G2 antibody to detect infected cells. For YFV-Venus, cells were directly observed for Venus expression. Data was analyzed using FloJo version 10.2, with the positive gate set such that <1% of uninfected cells resided in the positive gate.

Transient replicon and colony formation assay

Cells were transfected with in vitro transcribed and capped replicon RNA using TransIT-mRNA reagent (Mirus Bio, Madison, WI) in a 6-well plate. For the transient replicon assay, cells were trypsinized 4 h post-transfection, and 50% of the cells were lysed to measure luciferase activity as a surrogate for transfection efficiency normalization, while the remaining cells were re-seeded on a 6-well plate for future luciferase readings. Two or three days post-transfection, cells were lysed and luciferase activity was measured to determine levels of replication.

For the colony formation assay, one day post-transfection of replicon RNA, cells were trypsinized, seeded on 60 mm dishes, and selected using puromycin (for the replicon), blasticidin (for exogenous NS1), or both drugs. One week later, media was removed and cells were washed twice with PBS before crystal violet staining, or colonies were selected using a cloning cylinder for expansion and sequencing.

Co-Immunoprecipitation and Western blotting

For co-IP and Western blotting, cells were lysed in a buffer containing 20mM Tris pH 7.5, 100mM NaCl, 1% Triton X-100, 10% glycerol, and 1mM EDTA with the addition of Halt protease inhibitor. Co-immunoprecipitation and Western blotting was performed as previously described (24).

Immunofluorescence

Cells were plated on poly-D-lysine coated coverslips and fixed in ice cold 100% methanol for 1 h at -20˚C. Coverslips were then blocked in 2% BSA + 0.1% Triton X-100 in 1x PBS for 1 h at room temperature. Primary antibodies were diluted in blocking buffer and immunostaining was performed. Cells were then washed, probed with secondary fluorophore conjugated antibodies, and mounted as previously described (146).

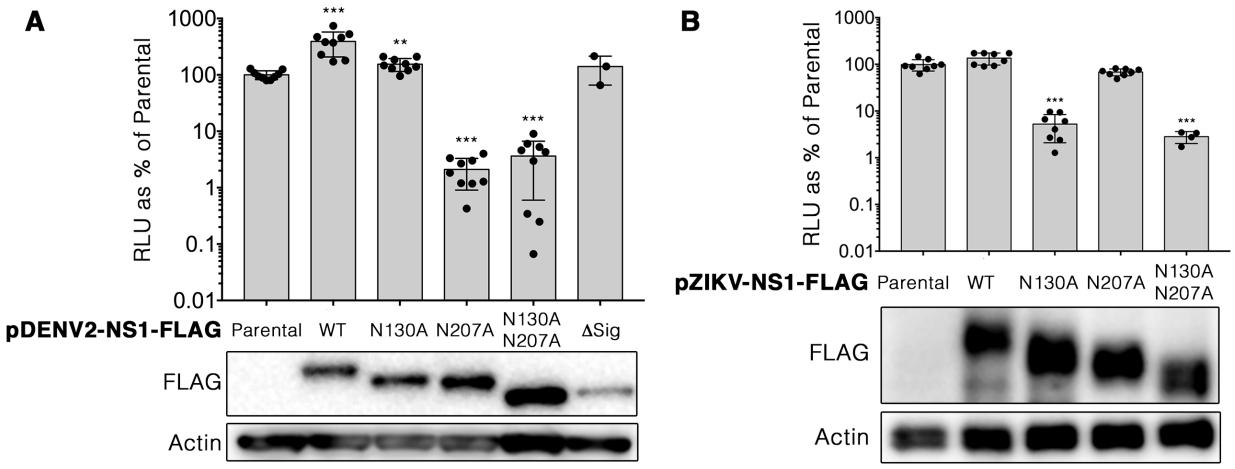

Figure 4.1. Heterologous expression of hypoglycosylated mutants of DENV or ZIKV NS1 blocks DENV-2 propagation. In **A,** Huh 7.5.1 cells were stably transduced to express the indicated DENV NS1 constructs. ΔSig is an NS1 mutant that lacks the N-terminal signal sequence required for insertion of NS1 into the ER lumen and is therefore not glycosylated. Cells were infected with a luciferase reporter DENV at an approximate MOI of 0.1, and luciferase activity was measured 3 d post-infection. In **B**, Huh 7.5.1 cells were stably transduced to express ZIKV NS1 mutants as indicated. The same infection conditions were used as in A. Data are plotted as a percent of the relative luciferase units (RLU) in the parental cell line Huh 7.5.1 where each dot represents a biological replicate. Bars indicate means ± standard deviations. **, $p < 0.005$, ***, $p < 0.0005$ by Mann-Whitney U test compared to Parental**.** Lower panel is a Western blot for NS1 and actin as a loading control.

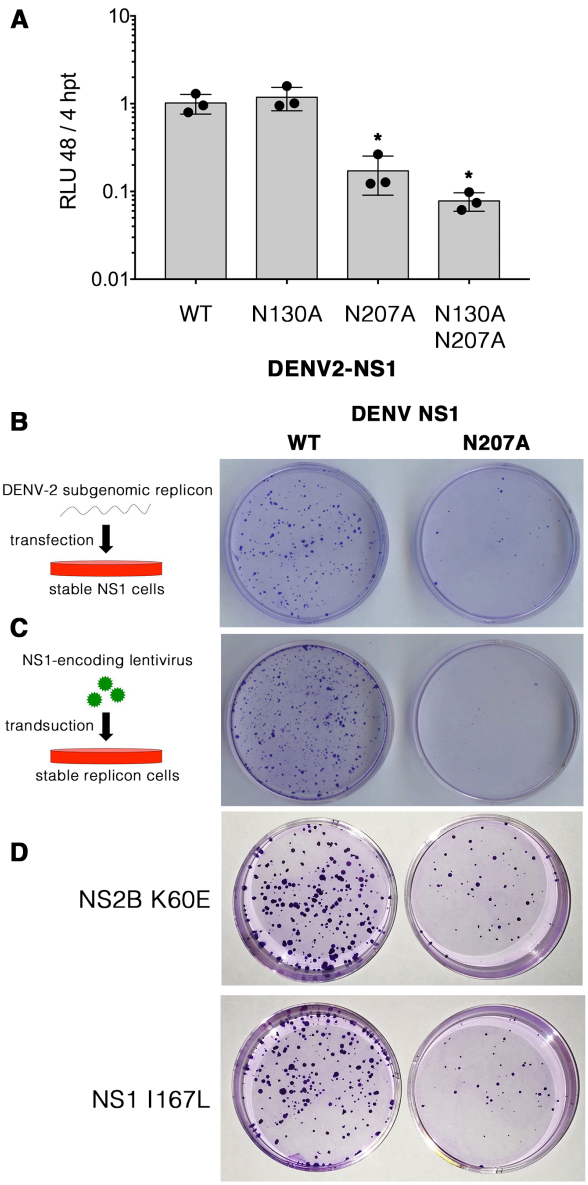

Figure 4.2. NS1 mutants inhibit DENV at the level of replication. In **A**, Huh 7.5.1 cells stably transduced to express the indicated NS1 constructs were transfected with a luciferase DENV replicon, and luciferase activity was measured at 4 hr and 48 hr post-transfection (hpt). Data are plotted as a ratio of relative luciferase units (RLU) to RLU at 4 hpt to control for transfection efficiency. Bars indicate means ± standard deviation. *, $p < 0.05$ by Mann-Whitney U test compared to Parental**.** In **B and D**, 293T cells stably expressing DENV NS1-WT or DENV NS1-N207A (blasticidin-resistant) were transfected with a DENV replicon expressing a puromycin selection marker. 24 hr post-transfection, cells were double selected with blasticidin and puromycin, and colonies were visualized by crystal violet staining 10 d post-selection. In **C**, Huh 7.5.1 cells stably harboring a DENV replicon (puromycin-resistant) were transduced with a lentivirus encoding blasticidin and DENV NS1-WT or NS1-N207A. Cells were double selected 24 hr post-transduction and colonies were visualized by crystal violet staining 10 d post-selection. In **D**, cells were transfected with a DENV replicon harboring the indicated mutation.

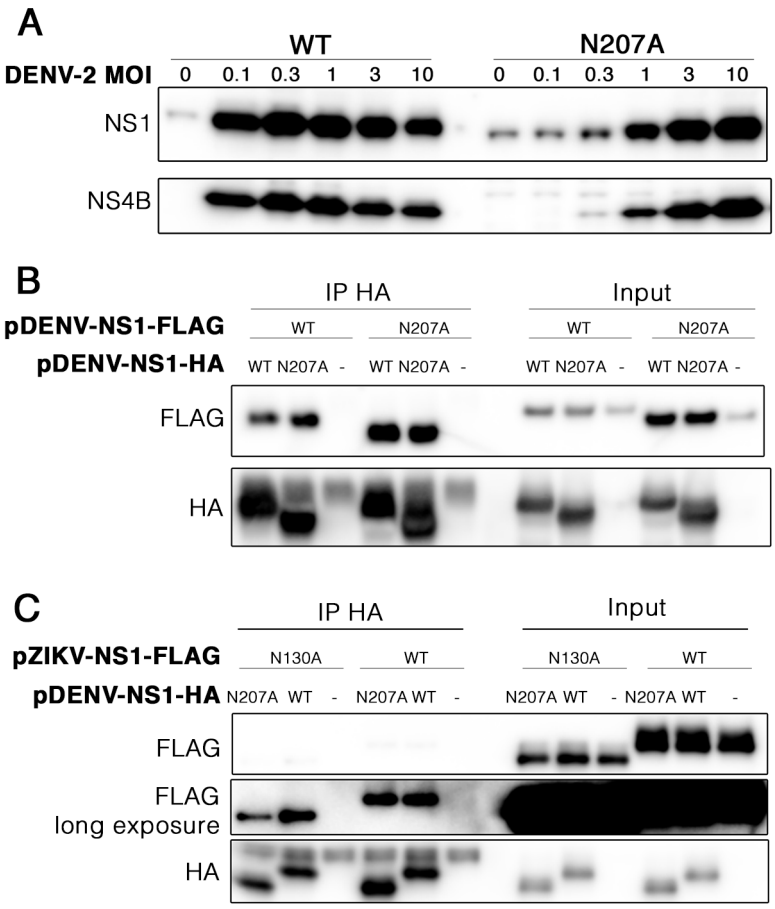

Figure 4.3. ZIKV and DENV NS1 glycosylation mutants can heterodimerize with DENV NS1. In **A,** Huh 7.5.1 cells stably expressing the indicated DENV NS1 constructs were infected with DENV-2 at the indicated MOIs for 48 hr. Cells were lysed for SDS-PAGE and Western blotting for total NS1 and NS4B as measures of viral infection and to demonstrate the relative levels of exogenous NS1 expression (in uninfected cells) compared to virally encoded NS1. In **B and C**, 293T cells were co-transfected to express plasmids expressing the indicated NS1 constructs. Co-immunoprecipitation of HA-NS1 was followed by SDS-PAGE and Western blotting for FLAG-NS1. In **C,** the interaction between ZIKV and DENV NS1 is relatively weak, requiring a longer exposure to visualize FLAG.

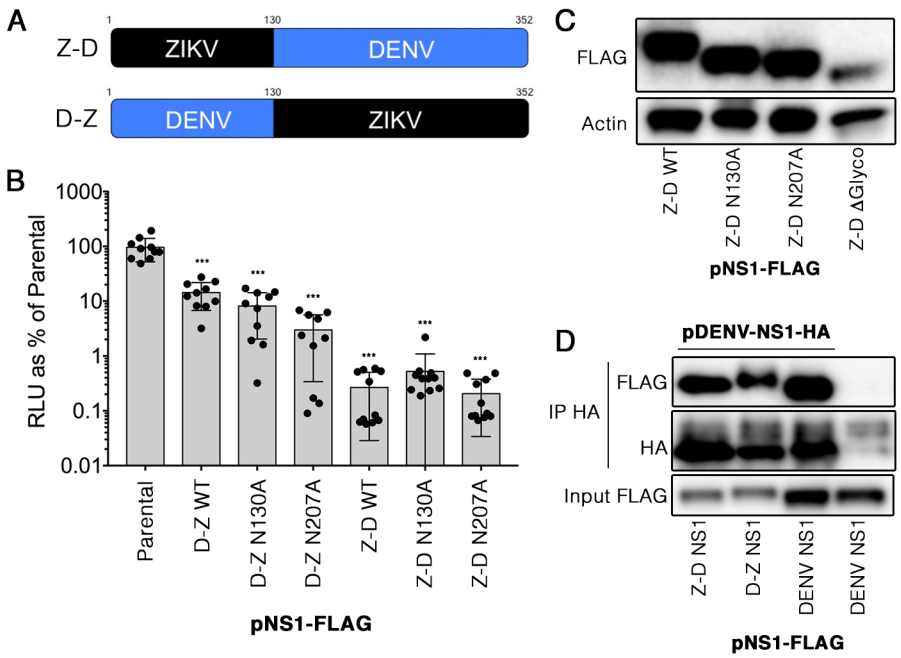

Figure 4.4. Engineered chimeric NS1 constructs inhibit DENV replication. In **A,** a schematic for the NS1 chimeras. The Z-D NS1 harbors ZIKV amino acids 1-129, and DENV amino acids 130-352. The D-Z NS1 harbors DENV amino acids 1-129, and ZIKV amino acids 130-352. In **B**, Huh 7.5.1 cells stably expressing FLAG tagged chimeric NS1 constructs were infected with a luciferase reporter DENV and luciferase activity was measured 3 d post-infection. Data are plotted as a percent of the relative luciferase units (RLU) from the parental Huh 7.5.1 cell line where each dot represents a biological replicate. Bars indicate means ± standard deviations. ***, $p < 0.0005$ by Mann-Whitney U test compared to Parental**.** In **C**, Western blots show the migration pattern of the chimeric NS1 constructs. In **D**, 293T cells were co-transfected to express the indicated NS1 constructs. Immunoprecipitation of HA-NS1 was followed by SDS-PAGE and Western blotting for FLAG-NS1.

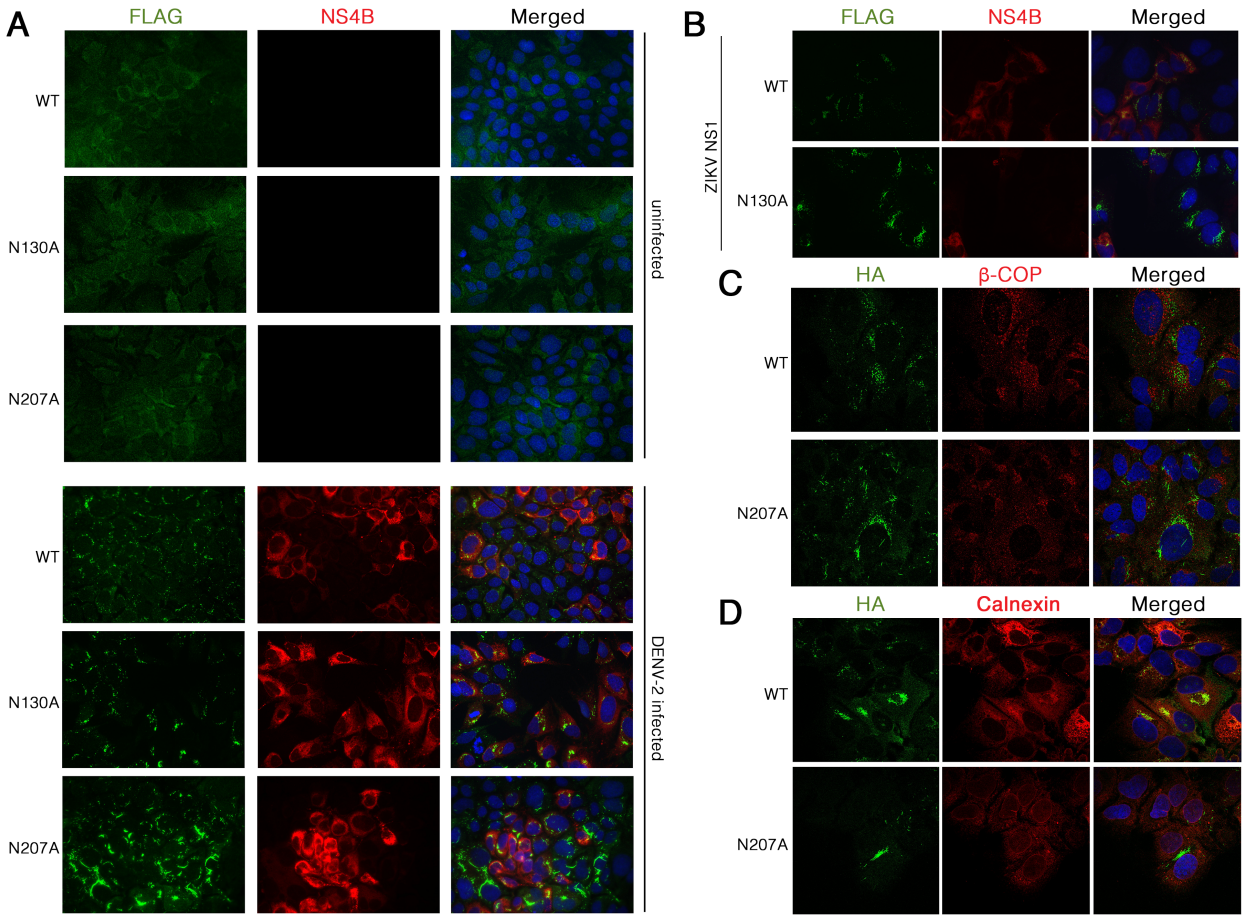

Figure 4.5. Mutant NS1 constructs form filamentous accumulations in DENV-infected cells. In **A, C and D,** Huh 7.5.1 cells stably expressing FLAG or HA tagged DENV NS1 WT, N130A, or N207A were either mock infected or infected with DENV-2 for 3 d at MOI = 1. In **B**, Huh 7.5.1 cells stably expressing FLAG tagged ZIKV NS1 WT or N130A were infected with DENV-2 for 3 d at MOI = 1. In **A-D**, cells were then fixed, permeabilized, and immunostained with antibodies against the indicated protein. Nuclei were visualized by DAPI counterstaining. In **A**, slides were visualized by epifluorescence microscopy. In **B**-**D**, slides were visualized by confocal microscopy.

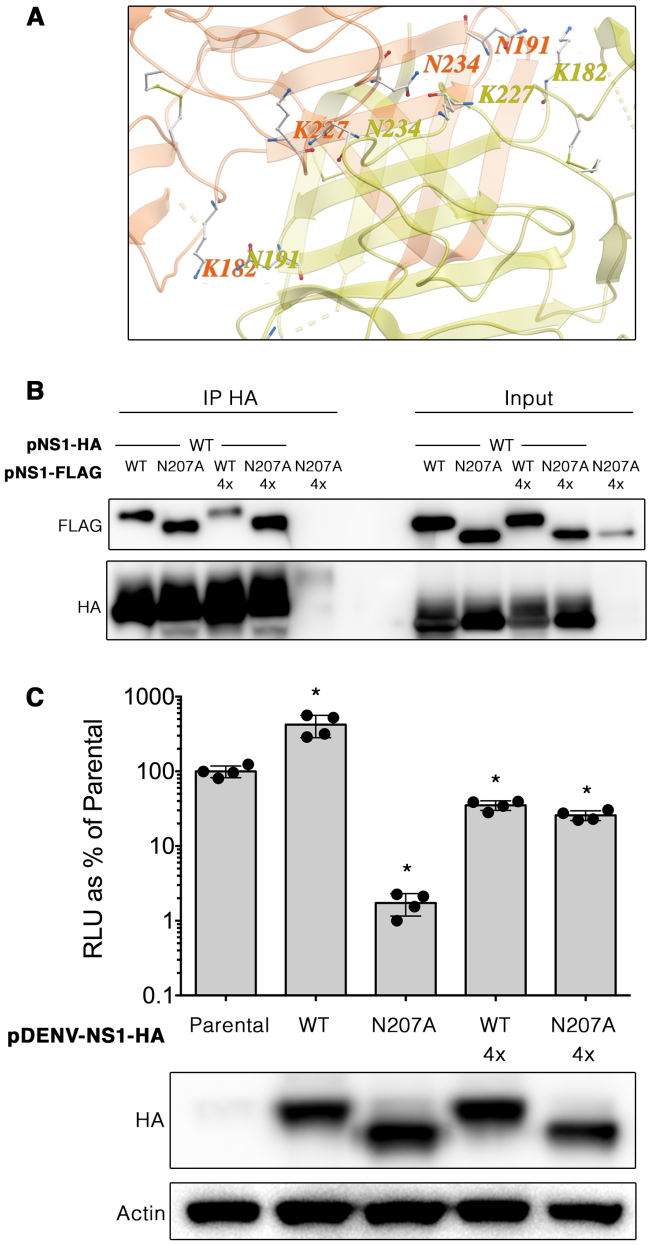

Figure 4.6. Mutations to the NS1 dimer interface do not interfere with heterodimerization, but impair glycosylation-dependent inhibition of DENV replication. In **A**, the four mutated residues of the 4x NS1 mutants are depicted on the crystal structure of the DENV NS1 dimer where one NS1 monomer is colored in yellow and the other in orange. In **B and C**, the 4x indicates 4 mutations: K182D N191K K227D N234K. In **B**, 293T cells were co-transfected to express plasmids expressing the indicated NS1 constructs. Immunoprecipitation of DENV NS1-HA was followed by SDS-PAGE and Western blotting for the indicated proteins. In **C**, Huh 7.5.1 cells stably expressing the indicated mutants were infected with a luciferase reporter DENV for 3 d when luciferase activity was measured, and plotted as a percentage of the Parental. Western blots below the graph show expression patterns for each of the mutants. *, $p<0.05$ by Mann-Whitney U test compared to Parental.

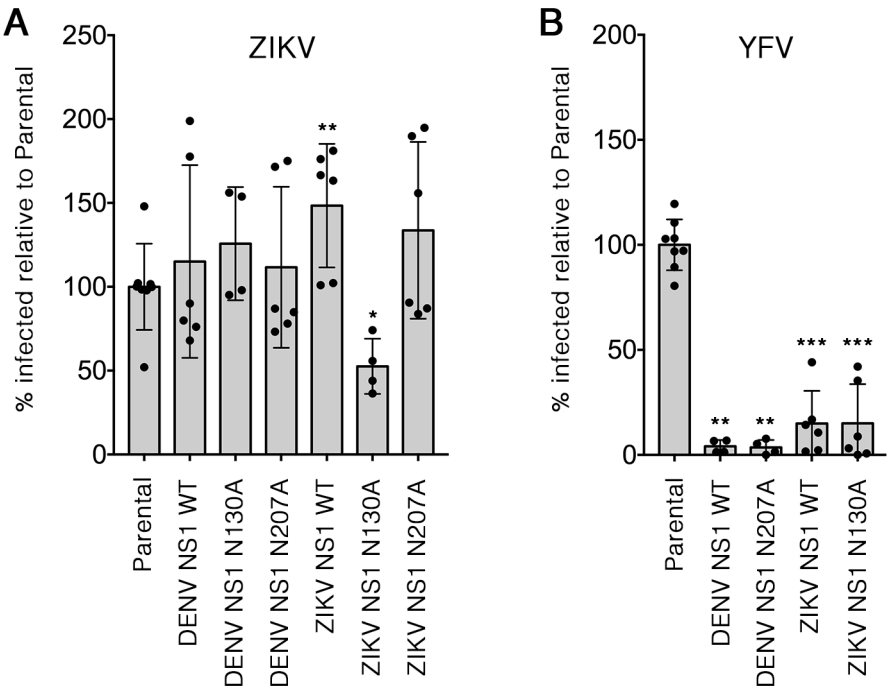

Figure 4.7. Cross-flavivirus inhibition by expression of engineered NS1 constructs. In **A**, Huh 7.5.1 cells expressing the indicated NS1 constructs were infected with ZIKV for 2 d, then fixed and immunostained for E protein as a marker of infection. Flow cytometry was then used to quantify the percentage of infected cells. In **B**, the indicated cells were infected with a Venus expressing reporter YFV. Cells were fixed, and then flow cytometry was used to measure a percentage of cells expressing Venus. Data are plotted as a percentage of infected cells normalized to Parental Huh 7.5.1 control cells, with each dot representing an independent infection and bars representing the mean with standard deviations. *, $p<0.05$, **, $p<0.005$, ***, $p < 0.0005$ by Mann-Whitney U test compared to Parental**.**

CHAPTER V

Concluding remarks and future directions

The OST and EMC

We showed that both the OST and EMC are important cellular factors necessary for DENV replication. Furthermore, we provide evidence that NS4B is a likely target of both of these complexes. While the specific role of the OST in this process is unclear, we showed that the EMC is important for NS4B biogenesis and folding, and the EMC likely interacts with the two N-terminal marginally hydrophobic helices of NS4B and mediates their proper folding. We speculate that the reduced biogenesis of NS4B in EMC knockout cells is due to alterations in folding, leading to recognition and subsequent degradation by ERAD machinery.

While we have invested significant effort to probe the nature of NS4B's dependence on the EMC, we have yet to clarify how NS4A is also EMC dependent. Similar to NS4B, NS4A contains a marginally hydrophobic domain at its N-terminus in the form of an amphipathic helix. Truncation and mutagenesis of NS4A will reveal whether the hydrophobicity of this domain is important for its association with the EMC.

To this point, we have not specifically ruled out impaired translation as a cause for reduced biosynthesis of NS4B. However, because EMC knockout does not result in changes to the expression of other DENV structural and non-structural proteins, overall translation is likely relatively unaffected. We also show that in the context of the full ZIKV polyprotein, the N-terminal E protein is unaffected by loss of the EMC, but NS4B expression is significantly reduced. However, it is still possible that translation of specific proteins is impaired in EMC knockout cells, and further experiments using metabolic labeling will shed light on this possibility.

While the folding of NS4B is difficult to directly measure using readily available assays, the combined biochemical data suggest that NS4B folding is affected by loss of the EMC or OST. The glycosylation status of NS4B in OST and EMC knockout cells is altered, suggesting that either those complexes are directly responsible for NS4B glycosylation, or that the sequons normally accessible to the OST are inaccessible in the absence of the OST or EMC. For example, the glycosylation pattern of TM2-Lys NS4B mutant is drastically different between WT and EMC knockout cells, even in the presence of both STT3A and STT3B OSTs (Figure 3.9). This data would suggest that the sequons exhibit differential sequon accessibility to the ER lumen in the presence or absence of the EMC. This further implies an alteration in NS4B transmembrane helix insertion into the membrane, and a difference in folding. The accessibility of sequons is a useful measure of protein folding, however, the inability to directly probe which helices are membrane inserted limits the extent to which we can biochemically demonstrate that the EMC is a transmembrane protein chaperone. Hopefully, future in vitro assays will be able to more specifically interrogate the folding of NS4B in the presence and absence of the EMC or OST.

Many questions remain about the nature of the association between the OST and EMC in both cell biology and flavivirus infection. As both complexes have been shown to act co-translationally, perhaps the EMC is responsible for recruitment of substrates to the OST or vice versa. Future experiments will also reveal the kinetics of OST and EMC substrate recognition, and uncover interesting aspects of transmembrane protein folding.

Alanine scanning and truncation mutagenesis of EMC6 revealed important domains for EMC stability and function. Similar experiments with other EMC subunits will be critical to identifying EMC residues important for its function. Additionally, a high-resolution structure of the EMC would provide critical biochemical data, which can be used for targeted mutagenesis and inhibitor design. Further experiments characterizing how each EMC subunit contributes to EMC function will be critical to understanding how it engages marginally hydrophobic transmembrane substrates, but not proteins with canonical transmembrane helices.

Dominant-negative inhibition by NS1 mutants

We showed that exogenous expression of a single NS1 mutant inhibits flavivirus infection. Future experiments can help identify the mechanism by which NS1 blocks replication, and grant important insight to the function of NS1 during replication. First, we speculate that heterodimerization of the NS1 mutant with wild-type viral NS1 is important for its inhibition. Expression of a homodimeric NS1 mutant could address this question, perhaps through expression of a tandem NS1 construct. Second, the evidence suggests that the interaction of NS1 with other non-structural proteins likely mediates its inhibition. It is possible that adaptive mutations to viral non-structural proteins could grant resistance to the dominant-negative inhibition by these NS1 mutants. While our attempts to generate resistant replicons were unsuccessful, future experiments passaging virus may provide some valuable insight.

The filamentous distribution of these NS1 mutants after infection indicates that the physical structure of the replication organelle may be affected early during infection. Ultrastructural analysis of infected cells by electron microscopy would provide meaningful data on the subcellular localization of these filaments. Another way to characterize these filaments is to use an NS1-APEX fusion protein to label and identify nearby proteins by mass-spectrometry, thus identifying the compartment where the filaments reside. One major hurdle to these approaches is the heterogeneity of filament formation, which appears to be somewhat stochastic upon infection.

The translational application of these NS1 mutants has also been brought into question. The most feasible application of these mutants is through expression in mosquito vectors, which would theoretically grant the mosquito resistance to flavivirus infection, and prevent the transmission of the virus to people. Initial experiments will determine whether these NS1 mutants can prevent flavivirus replication in mosquito and insect cells. If these NS1 mutants can inhibit replication in mosquito cells, then the next obvious step would be to generate transgenic mosquitos expressing NS1 that is inherited via gene drive. By contrast, if these NS1 mutants inhibit replication in human cells but not insect cells, this data would provide strong evidence that NS1 mutants act as dominant-negative inhibitors via a human cellular host factor.

Conclusions

We demonstrated that pooled CRISPR-Cas9 screens are a highly reproducible, robust, and powerful tool for generating hypotheses. This technology can be rapidly applied to ask about genes that are important for various cellular processes, including viral infection. The identification of the EMC and MAGT1 as DENV host factors provides a strong fundamental basis for the design of inhibitors that can be used as antiviral therapeutics. Most importantly, the characterization of the EMC and its biochemistry are critical findings that contribute our understanding of cell biology.

BIBLIOGRAPHY

1. Kraemer MU, Sinka ME, Duda KA, Mylne AQ, Shearer FM, Barker CM, Moore CG, Carvalho RG, Coelho GE, Van Bortel W, Hendrickx G, Schaffner F, Elyazar IR, Teng HJ, Brady OJ, Messina JP, Pigott DM, Scott TW, Smith DL, Wint GR, Golding N, Hay SI. 2015. The global distribution of the arbovirus vectors Aedes aegypti and Ae. albopictus. Elife 4:e08347.
2. Naish S, Dale P, Mackenzie JS, McBride J, Mengersen K, Tong S. 2014. Climate change and dengue: a critical and systematic review of quantitative modelling approaches. BMC Infect Dis 14:167.
3. Colon-Gonzalez FJ, Fezzi C, Lake IR, Hunter PR. 2013. The effects of weather and climate change on dengue. PLoS Negl Trop Dis 7:e2503.
4. Colon-Gonzalez FJ, Harris I, Osborn TJ, Steiner Sao Bernardo C, Peres CA, Hunter PR, Lake IR. 2018. Limiting global-mean temperature increase to 1.5-2 degrees C could reduce the incidence and spatial spread of dengue fever in Latin America. Proc Natl Acad Sci U S A 115:6243-6248.
5. Messina JP, Brady OJ, Scott TW, Zou C, Pigott DM, Duda KA, Bhatt S, Katzelnick L, Howes RE, Battle KE, Simmons CP, Hay SI. 2014. Global spread of dengue virus types: mapping the 70 year history. Trends Microbiol 22:138-46.
6. Bhatt S, Gething PW, Brady OJ, Messina JP, Farlow AW, Moyes CL, Drake JM, Brownstein JS, Hoen AG, Sankoh O, Myers MF, George DB, Jaenisch T, Wint GR, Simmons CP, Scott TW, Farrar JJ, Hay SI. 2013. The global distribution and burden of dengue. Nature 496:504-7.
7. Acosta EG, Castilla V, Damonte EB. 2009. Alternative infectious entry pathways for dengue virus serotypes into mammalian cells. Cell Microbiol 11:1533-49.
8. Cruz-Oliveira C, Freire JM, Conceicao TM, Higa LM, Castanho MA, Da Poian AT. 2015. Receptors and routes of dengue virus entry into the host cells. FEMS Microbiol Rev 39:155-70.
9. Screaton G, Mongkolsapaya J, Yacoub S, Roberts C. 2015. New insights into the immunopathology and control of dengue virus infection. Nat Rev Immunol 15:745-59.
10. Khromykh AA, Westaway EG. 1997. Subgenomic replicons of the flavivirus Kunjin: construction and applications. J Virol 71:1497-505.
11. Diamond MS, Pierson TC. 2015. Molecular Insight into Dengue Virus Pathogenesis and Its Implications for Disease Control. Cell 162:488-92.
12. Zhang R, Miner JJ, Gorman MJ, Rausch K, Ramage H, White JP, Zuiani A, Zhang P, Fernandez E, Zhang Q, Dowd KA, Pierson TC, Cherry S, Diamond MS.

2016. A CRISPR screen defines a signal peptide processing pathway required by flaviviruses. Nature 535:164-8.
13. Luo D, Xu T, Hunke C, Gruber G, Vasudevan SG, Lescar J. 2008. Crystal structure of the NS3 protease-helicase from dengue virus. J Virol 82:173-83.
14. Xu T, Sampath A, Chao A, Wen D, Nanao M, Chene P, Vasudevan SG, Lescar J. 2005. Structure of the Dengue virus helicase/nucleoside triphosphatase catalytic domain at a resolution of 2.4 A. J Virol 79:10278-88.
15. Dong H, Chang DC, Hua MH, Lim SP, Chionh YH, Hia F, Lee YH, Kukkaro P, Lok SM, Dedon PC, Shi PY. 2012. 2'-O methylation of internal adenosine by flavivirus NS5 methyltransferase. PLoS Pathog 8:e1002642.
16. Yap TL, Xu T, Chen YL, Malet H, Egloff MP, Canard B, Vasudevan SG, Lescar J. 2007. Crystal structure of the dengue virus RNA-dependent RNA polymerase catalytic domain at 1.85-angstrom resolution. J Virol 81:4753-65.
17. Welsch S, Miller S, Romero-Brey I, Merz A, Bleck CK, Walther P, Fuller SD, Antony C, Krijnse-Locker J, Bartenschlager R. 2009. Composition and three-dimensional architecture of the dengue virus replication and assembly sites. Cell Host Microbe 5:365-75.
18. Chen S, Wu Z, Wang M, Cheng A. 2017. Innate Immune Evasion Mediated by Flaviviridae Non-Structural Proteins. Viruses 9.
19. den Boon JA, Ahlquist P. 2010. Organelle-like membrane compartmentalization of positive-strand RNA virus replication factories. Annu Rev Microbiol 64:241-56.
20. Chatel-Chaix L, Bartenschlager R. 2014. Dengue virus- and hepatitis C virus-induced replication and assembly compartments: the enemy inside--caught in the web. J Virol 88:5907-11.
21. Paul D, Bartenschlager R. 2015. Flaviviridae Replication Organelles: Oh, What a Tangled Web We Weave. Annu Rev Virol 2:289-310.
22. Roth H, Magg V, Uch F, Mutz P, Klein P, Haneke K, Lohmann V, Bartenschlager R, Fackler OT, Locker N, Stoecklin G, Ruggieri A. 2017. Flavivirus Infection Uncouples Translation Suppression from Cellular Stress Responses. MBio 8.
23. Heaton NS, Moshkina N, Fenouil R, Gardner TJ, Aguirre S, Shah PS, Zhao N, Manganaro L, Hultquist JF, Noel J, Sachs D, Hamilton J, Leon PE, Chawdury A, Tripathi S, Melegari C, Campisi L, Hai R, Metreveli G, Gamarnik AV, Garcia-Sastre A, Greenbaum B, Simon V, Fernandez-Sesma A, Krogan NJ, Mulder LCF, van Bakel H, Tortorella D, Taunton J, Palese P, Marazzi I. 2016. Targeting Viral Proteostasis Limits Influenza Virus, HIV, and Dengue Virus Infection. Immunity 44:46-58.
24. Lin DL, Cherepanova NA, Bozzacco L, MacDonald MR, Gilmore R, Tai AW. 2017. Dengue Virus Hijacks a Noncanonical Oxidoreductase Function of a Cellular Oligosaccharyltransferase Complex. MBio 8.
25. Savidis G, McDougall WM, Meraner P, Perreira JM, Portmann JM, Trincucci G, John SP, Aker AM, Renzette N, Robbins DR, Guo Z, Green S, Kowalik TF, Brass AL. 2016. Identification of Zika Virus and Dengue Virus Dependency Factors using Functional Genomics. Cell Rep 16:232-46.

26. Marceau CD, Puschnik AS, Majzoub K, Ooi YS, Brewer SM, Fuchs G, Swaminathan K, Mata MA, Elias JE, Sarnow P, Carette JE. 2016. Genetic dissection of Flaviviridae host factors through genome-scale CRISPR screens. Nature 535:159-63.
27. Falgout B, Chanock R, Lai CJ. 1989. Proper processing of dengue virus nonstructural glycoprotein NS1 requires the N-terminal hydrophobic signal sequence and the downstream nonstructural protein NS2a. J Virol 63:1852-60.
28. Hafirassou ML, Meertens L, Umana-Diaz C, Labeau A, Dejarnac O, Bonnet-Madin L, Kummerer BM, Delaugerre C, Roingeard P, Vidalain PO, Amara A. 2017. A Global Interactome Map of the Dengue Virus NS1 Identifies Virus Restriction and Dependency Host Factors. Cell Rep 21:3900-3913.
29. Somnuke P, Hauhart RE, Atkinson JP, Diamond MS, Avirutnan P. 2011. N-linked glycosylation of dengue virus NS1 protein modulates secretion, cell-surface expression, hexamer stability, and interactions with human complement. Virology 413:253-64.
30. Whiteman MC, Li L, Wicker JA, Kinney RM, Huang C, Beasley DW, Chung KM, Diamond MS, Solomon T, Barrett AD. 2010. Development and characterization of non-glycosylated E and NS1 mutant viruses as a potential candidate vaccine for West Nile virus. Vaccine 28:1075-83.
31. Tajima S, Takasaki T, Kurane I. 2008. Characterization of Asn130-to-Ala mutant of dengue type 1 virus NS1 protein. Virus Genes 36:323-9.
32. Pryor MJ, Gualano RC, Lin B, Davidson AD, Wright PJ. 1998. Growth restriction of dengue virus type 2 by site-specific mutagenesis of virus-encoded glycoproteins. J Gen Virol 79 (Pt 11):2631-9.
33. Crabtree MB, Kinney RM, Miller BR. 2005. Deglycosylation of the NS1 protein of dengue 2 virus, strain 16681: construction and characterization of mutant viruses. Arch Virol 150:771-86.
34. Muylaert IR, Chambers TJ, Galler R, Rice CM. 1996. Mutagenesis of the N-linked glycosylation sites of the yellow fever virus NS1 protein: effects on virus replication and mouse neurovirulence. Virology 222:159-68.
35. Flamand M, Megret F, Mathieu M, Lepault J, Rey FA, Deubel V. 1999. Dengue virus type 1 nonstructural glycoprotein NS1 is secreted from mammalian cells as a soluble hexamer in a glycosylation-dependent fashion. J Virol 73:6104-10.
36. Fan J, Liu Y, Yuan Z. 2014. Critical role of Dengue Virus NS1 protein in viral replication. Virol Sin 29:162-9.
37. Wallis TP, Huang CY, Nimkar SB, Young PR, Gorman JJ. 2004. Determination of the disulfide bond arrangement of dengue virus NS1 protein. J Biol Chem 279:20729-41.
38. Winkler G, Randolph VB, Cleaves GR, Ryan TE, Stollar V. 1988. Evidence that the mature form of the flavivirus nonstructural protein NS1 is a dimer. Virology 162:187-96.
39. Akey DL, Brown WC, Dutta S, Konwerski J, Jose J, Jurkiw TJ, DelProposto J, Ogata CM, Skiniotis G, Kuhn RJ, Smith JL. 2014. Flavivirus NS1 structures

reveal surfaces for associations with membranes and the immune system. Science 343:881-5.
40. Scaturro P, Cortese M, Chatel-Chaix L, Fischl W, Bartenschlager R. 2015. Dengue Virus Non-structural Protein 1 Modulates Infectious Particle Production via Interaction with the Structural Proteins. PLoS Pathog 11:e1005277.
41. Youn S, Li T, McCune BT, Edeling MA, Fremont DH, Cristea IM, Diamond MS. 2012. Evidence for a genetic and physical interaction between nonstructural proteins NS1 and NS4B that modulates replication of West Nile virus. J Virol 86:7360-71.
42. Xu X, Song H, Qi J, Liu Y, Wang H, Su C, Shi Y, Gao GF. 2016. Contribution of intertwined loop to membrane association revealed by Zika virus full-length NS1 structure. EMBO J 35:2170-2178.
43. Hall RA, Khromykh AA, Mackenzie JM, Scherret JH, Khromykh TI, Mackenzie JS. 1999. Loss of dimerisation of the nonstructural protein NS1 of Kunjin virus delays viral replication and reduces virulence in mice, but still allows secretion of NS1. Virology 264:66-75.
44. Pryor MJ, Wright PJ. 1993. The effects of site-directed mutagenesis on the dimerization and secretion of the NS1 protein specified by dengue virus. Virology 194:769-80.
45. Pryor MJ, Wright PJ. 1994. Glycosylation mutants of dengue virus NS1 protein. J Gen Virol 75 (Pt 5):1183-7.
46. Mackenzie JM, Jones MK, Young PR. 1996. Immunolocalization of the dengue virus nonstructural glycoprotein NS1 suggests a role in viral RNA replication. Virology 220:232-40.
47. Lindenbach BD, Rice CM. 1999. Genetic interaction of flavivirus nonstructural proteins NS1 and NS4A as a determinant of replicase function. J Virol 73:4611-21.
48. Giraldo MI, Vargas-Cuartas O, Gallego-Gomez JC, Shi PY, Padilla-Sanabria L, Castano-Osorio JC, Rajsbaum R. 2018. K48-linked polyubiquitination of dengue virus NS1 protein inhibits its interaction with the viral partner NS4B. Virus Res 246:1-11.
49. Young LB, Melian EB, Khromykh AA. 2013. NS1' colocalizes with NS1 and can substitute for NS1 in West Nile virus replication. J Virol 87:9384-90.
50. Cervantes-Salazar M, Angel-Ambrocio AH, Soto-Acosta R, Bautista-Carbajal P, Hurtado-Monzon AM, Alcaraz-Estrada SL, Ludert JE, Del Angel RM. 2015. Dengue virus NS1 protein interacts with the ribosomal protein RPL18: This interaction is required for viral translation and replication in Huh-7 cells. Virology 484:113-126.
51. Kanlaya R, Pattanakitsakul SN, Sinchaikul S, Chen ST, Thongboonkerd V. 2010. Vimentin interacts with heterogeneous nuclear ribonucleoproteins and dengue nonstructural protein 1 and is important for viral replication and release. Mol Biosyst 6:795-806.
52. Avirutnan P, Zhang L, Punyadee N, Manuyakorn A, Puttikhunt C, Kasinrerk W, Malasit P, Atkinson JP, Diamond MS. 2007. Secreted NS1 of dengue virus

attaches to the surface of cells via interactions with heparan sulfate and chondroitin sulfate E. PLoS Pathog 3:e183.
53. Beatty PR, Puerta-Guardo H, Killingbeck SS, Glasner DR, Hopkins K, Harris E. 2015. Dengue virus NS1 triggers endothelial permeability and vascular leak that is prevented by NS1 vaccination. Sci Transl Med 7:304ra141.
54. Glasner DR, Ratnasiri K, Puerta-Guardo H, Espinosa DA, Beatty PR, Harris E. 2017. Dengue virus NS1 cytokine-independent vascular leak is dependent on endothelial glycocalyx components. PLoS Pathog 13:e1006673.
55. Libraty DH, Young PR, Pickering D, Endy TP, Kalayanarooj S, Green S, Vaughn DW, Nisalak A, Ennis FA, Rothman AL. 2002. High circulating levels of the dengue virus nonstructural protein NS1 early in dengue illness correlate with the development of dengue hemorrhagic fever. J Infect Dis 186:1165-8.
56. Avirutnan P, Hauhart RE, Somnuke P, Blom AM, Diamond MS, Atkinson JP. 2011. Binding of flavivirus nonstructural protein NS1 to C4b binding protein modulates complement activation. J Immunol 187:424-33.
57. Liu J, Liu Y, Nie K, Du S, Qiu J, Pang X, Wang P, Cheng G. 2016. Flavivirus NS1 protein in infected host sera enhances viral acquisition by mosquitoes. Nat Microbiol 1:16087.
58. Roosendaal J, Westaway EG, Khromykh A, Mackenzie JM. 2006. Regulated cleavages at the West Nile virus NS4A-2K-NS4B junctions play a major role in rearranging cytoplasmic membranes and Golgi trafficking of the NS4A protein. J Virol 80:4623-32.
59. Stern O, Hung YF, Valdau O, Yaffe Y, Harris E, Hoffmann S, Willbold D, Sklan EH. 2013. An N-terminal amphipathic helix in dengue virus nonstructural protein 4A mediates oligomerization and is essential for replication. J Virol 87:4080-5.
60. Hung YF, Schwarten M, Hoffmann S, Willbold D, Sklan EH, Koenig B. 2015. Amino Terminal Region of Dengue Virus NS4A Cytosolic Domain Binds to Highly Curved Liposomes. Viruses 7:4119-30.
61. Hung YF, Schwarten M, Schunke S, Thiagarajan-Rosenkranz P, Hoffmann S, Sklan EH, Willbold D, Koenig BW. 2015. Dengue virus NS4A cytoplasmic domain binding to liposomes is sensitive to membrane curvature. Biochim Biophys Acta 1848:1119-26.
62. Zou J, Xie X, Wang QY, Dong H, Lee MY, Kang C, Yuan Z, Shi PY. 2015. Characterization of dengue virus NS4A and NS4B protein interaction. J Virol 89:3455-70.
63. Lee CM, Xie X, Zou J, Li SH, Lee MY, Dong H, Qin CF, Kang C, Shi PY. 2015. Determinants of Dengue Virus NS4A Protein Oligomerization. J Virol 89:6171-83.
64. Li Y, Lee MY, Loh YR, Kang C. 2018. Secondary structure and membrane topology of dengue virus NS4A protein in micelles. Biochim Biophys Acta 1860:442-450.
65. Miller S, Kastner S, Krijnse-Locker J, Buhler S, Bartenschlager R. 2007. The non-structural protein 4A of dengue virus is an integral membrane protein inducing membrane alterations in a 2K-regulated manner. J Biol Chem 282:8873-82.

66. Miller S, Sparacio S, Bartenschlager R. 2006. Subcellular localization and membrane topology of the Dengue virus type 2 Non-structural protein 4B. J Biol Chem 281:8854-63.
67. Nemesio H, Palomares-Jerez F, Villalain J. 2012. NS4A and NS4B proteins from dengue virus: membranotropic regions. Biochim Biophys Acta 1818:2818-30.
68. Li Y, Wong YL, Lee MY, Li Q, Wang QY, Lescar J, Shi PY, Kang C. 2016. Secondary Structure and Membrane Topology of the Full-Length Dengue Virus NS4B in Micelles. Angew Chem Int Ed Engl 55:12068-72.
69. Li Y, Kim YM, Zou J, Wang QY, Gayen S, Wong YL, Lee le T, Xie X, Huang Q, Lescar J, Shi PY, Kang C. 2015. Secondary structure and membrane topology of dengue virus NS4B N-terminal 125 amino acids. Biochim Biophys Acta 1848:3150-7.
70. Naik NG, Wu HN. 2015. Mutation of Putative N-Glycosylation Sites on Dengue Virus NS4B Decreases RNA Replication. J Virol 89:6746-60.
71. Zou J, Lee le T, Wang QY, Xie X, Lu S, Yau YH, Yuan Z, Geifman Shochat S, Kang C, Lescar J, Shi PY. 2015. Mapping the Interactions between the NS4B and NS3 proteins of dengue virus. J Virol 89:3471-83.
72. Xie X, Wang QY, Xu HY, Qing M, Kramer L, Yuan Z, Shi PY. 2011. Inhibition of dengue virus by targeting viral NS4B protein. J Virol 85:11183-95.
73. Zmurko J, Neyts J, Dallmeier K. 2015. Flaviviral NS4b, chameleon and jack-in-the-box roles in viral replication and pathogenesis, and a molecular target for antiviral intervention. Rev Med Virol 25:205-23.
74. Umareddy I, Chao A, Sampath A, Gu F, Vasudevan SG. 2006. Dengue virus NS4B interacts with NS3 and dissociates it from single-stranded RNA. J Gen Virol 87:2605-14.
75. Chatel-Chaix L, Cortese M, Romero-Brey I, Bender S, Neufeldt CJ, Fischl W, Scaturro P, Schieber N, Schwab Y, Fischer B, Ruggieri A, Bartenschlager R. 2016. Dengue Virus Perturbs Mitochondrial Morphodynamics to Dampen Innate Immune Responses. Cell Host Microbe 20:342-356.
76. McArthur MA, Suderman MT, Mutebi JP, Xiao SY, Barrett AD. 2003. Molecular characterization of a hamster viscerotropic strain of yellow fever virus. J Virol 77:1462-8.
77. Grant D, Tan GK, Qing M, Ng JK, Yip A, Zou G, Xie X, Yuan Z, Schreiber MJ, Schul W, Shi PY, Alonso S. 2011. A single amino acid in nonstructural protein NS4B confers virulence to dengue virus in AG129 mice through enhancement of viral RNA synthesis. J Virol 85:7775-87.
78. Wicker JA, Whiteman MC, Beasley DW, Davis CT, Zhang S, Schneider BS, Higgs S, Kinney RM, Barrett AD. 2006. A single amino acid substitution in the central portion of the West Nile virus NS4B protein confers a highly attenuated phenotype in mice. Virology 349:245-53.
79. Puig-Basagoiti F, Tilgner M, Bennett CJ, Zhou Y, Munoz-Jordan JL, Garcia-Sastre A, Bernard KA, Shi PY. 2007. A mouse cell-adapted NS4B mutation attenuates West Nile virus RNA synthesis. Virology 361:229-41.

80. Hanley KA, Manlucu LR, Gilmore LE, Blaney JE, Jr., Hanson CT, Murphy BR, Whitehead SS. 2003. A trade-off in replication in mosquito versus mammalian systems conferred by a point mutation in the NS4B protein of dengue virus type 4. Virology 312:222-32.
81. Shental-Bechor D, Levy Y. 2008. Effect of glycosylation on protein folding: a close look at thermodynamic stabilization. Proc Natl Acad Sci U S A 105:8256-61.
82. Shrimal S, Cherepanova NA, Gilmore R. 2015. Cotranslational and posttranslocational N-glycosylation of proteins in the endoplasmic reticulum. Semin Cell Dev Biol 41:71-8.
83. Cherepanova NA, Gilmore R. 2016. Mammalian cells lacking either the cotranslational or posttranslocational oligosaccharyltransferase complex display substrate-dependent defects in asparagine linked glycosylation. Sci Rep 6:20946.
84. Yan Q, Lennarz WJ. 2002. Studies on the function of oligosaccharyl transferase subunits. Stt3p is directly involved in the glycosylation process. J Biol Chem 277:47692-700.
85. Ruiz-Canada C, Kelleher DJ, Gilmore R. 2009. Cotranslational and posttranslational N-glycosylation of polypeptides by distinct mammalian OST isoforms. Cell 136:272-83.
86. Roboti P, High S. 2012. The oligosaccharyltransferase subunits OST48, DAD1 and KCP2 function as ubiquitous and selective modulators of mammalian N-glycosylation. J Cell Sci 125:3474-84.
87. Shrimal S, Cherepanova NA, Gilmore R. 2017. DC2 and KCP2 mediate the interaction between the oligosaccharyltransferase and the ER translocon. J Cell Biol 216:3625-3638.
88. Cherepanova NA, Shrimal S, Gilmore R. 2014. Oxidoreductase activity is necessary for N-glycosylation of cysteine-proximal acceptor sites in glycoproteins. J Cell Biol 206:525-39.
89. Mohorko E, Owen RL, Malojcic G, Brozzo MS, Aebi M, Glockshuber R. 2014. Structural basis of substrate specificity of human oligosaccharyl transferase subunit N33/Tusc3 and its role in regulating protein N-glycosylation. Structure 22:590-601.
90. Kelleher DJ, Gilmore R. 1997. DAD1, the defender against apoptotic cell death, is a subunit of the mammalian oligosaccharyltransferase. Proc Natl Acad Sci U S A 94:4994-9.
91. Cherepanova N, Shrimal S, Gilmore R. 2016. N-linked glycosylation and homeostasis of the endoplasmic reticulum. Curr Opin Cell Biol 41:57-65.
92. Wilson CM, Magnaudeix A, Yardin C, Terro F. 2011. DC2 and keratinocyte-associated protein 2 (KCP2), subunits of the oligosaccharyltransferase complex, are regulators of the gamma-secretase-directed processing of amyloid precursor protein (APP). J Biol Chem 286:31080-91.
93. Graham DB, Lefkovith A, Deelen P, de Klein N, Varma M, Boroughs A, Desch AN, Ng ACY, Guzman G, Schenone M, Petersen CP, Bhan AK, Rivas MA, Daly MJ, Carr SA, Wijmenga C, Xavier RJ. 2016. TMEM258 Is a Component of the

Oligosaccharyltransferase Complex Controlling ER Stress and Intestinal Inflammation. Cell Rep 17:2955-2965.
94. Pfeffer S, Dudek J, Gogala M, Schorr S, Linxweiler J, Lang S, Becker T, Beckmann R, Zimmermann R, Forster F. 2014. Structure of the mammalian oligosaccharyl-transferase complex in the native ER protein translocon. Nat Commun 5:3072.
95. Wilson CM, Kraft C, Duggan C, Ismail N, Crawshaw SG, High S. 2005. Ribophorin I associates with a subset of membrane proteins after their integration at the sec61 translocon. J Biol Chem 280:4195-206.
96. Wilson CM, High S. 2007. Ribophorin I acts as a substrate-specific facilitator of N-glycosylation. J Cell Sci 120:648-57.
97. Wilson CM, Roebuck Q, High S. 2008. Ribophorin I regulates substrate delivery to the oligosaccharyltransferase core. Proc Natl Acad Sci U S A 105:9534-9.
98. Sanjay A, Fu J, Kreibich G. 1998. DAD1 is required for the function and the structural integrity of the oligosaccharyltransferase complex. J Biol Chem 273:26094-9.
99. Dumax-Vorzet A, Roboti P, High S. 2013. OST4 is a subunit of the mammalian oligosaccharyltransferase required for efficient N-glycosylation. J Cell Sci 126:2595-606.
100. Jonikas MC, Collins SR, Denic V, Oh E, Quan EM, Schmid V, Weibezahn J, Schwappach B, Walter P, Weissman JS, Schuldiner M. 2009. Comprehensive characterization of genes required for protein folding in the endoplasm. Science.
101. Christianson JC, Olzmann JA, Shaler TA, Sowa ME, Bennett EJ, Richter CM, Tyler RE, Greenblatt EJ, Harper JW, Kopito RR. 2012. Defining human ERAD networks through an integrative mapping strategy. Nat Cell Biol 14:93-105.
102. Shurtleff MJ, Itzhak DN, Hussmann JA, Schirle Oakdale NT, Costa EA, Jonikas M, Weibezahn J, Popova KD, Jan CH, Sinitcyn P, Vembar SS, Hernandez H, Cox J, Burlingame AL, Brodsky J, Frost A, Borner GH, Weissman JS. 2018. The ER membrane protein complex interacts cotranslationally to enable biogenesis of multipass membrane proteins. Elife 7.
103. Anghel SA, McGilvray PT, Hegde RS, Keenan RJ. 2017. Identification of Oxa1 Homologs Operating in the Eukaryotic Endoplasmic Reticulum. Cell Rep 21:3708-3716.
104. Goytain A, Quamme GA. 2008. Identification and characterization of a novel family of membrane magnesium transporters, MMgT1 and MMgT2. Am J Physiol Cell Physiol 294:C495-502.
105. Satoh T, Ohba A, Liu Z, Inagaki T, Satoh AK. 2015. dPob/EMC is essential for biosynthesis of rhodopsin and other multi-pass membrane proteins in Drosophila photoreceptors. Elife 4.
106. Richard M, Boulin T, Robert VJ, Richmond JE, Bessereau JL. 2013. Biosynthesis of ionotropic acetylcholine receptors requires the evolutionarily conserved ER membrane complex. Proc Natl Acad Sci U S A 110:E1055-63.
107. Guna A, Volkmar N, Christianson JC, Hegde RS. 2018. The ER membrane protein complex is a transmembrane domain insertase. Science 359:470-473.

108. Kudze T, Mendez-Dorantes C, Jalloh CS, McClellan AJ. 2018. Evidence for interaction between Hsp90 and the ER membrane complex. Cell Stress Chaperones.
109. Lahiri S, Chao JT, Tavassoli S, Wong AK, Choudhary V, Young BP, Loewen CJ, Prinz WA. 2014. A conserved endoplasmic reticulum membrane protein complex (EMC) facilitates phospholipid transfer from the ER to mitochondria. PLoS Biol 12:e1001969.
110. Shen X, Kan S, Hu J, Li M, Lu G, Zhang M, Zhang S, Hou Y, Chen Y, Bai Y. 2016. EMC6/TMEM93 suppresses glioblastoma proliferation by modulating autophagy. Cell Death Dis 7:e2043.
111. Li Y, Zhao Y, Hu J, Xiao J, Qu L, Wang Z, Ma D, Chen Y. 2013. A novel ER-localized transmembrane protein, EMC6, interacts with RAB5A and regulates cell autophagy. Autophagy 9:150-63.
112. Bagchi P, Inoue T, Tsai B. 2016. EMC1-dependent stabilization drives membrane penetration of a partially destabilized non-enveloped virus. Elife 5.
113. Ma H, Dang Y, Wu Y, Jia G, Anaya E, Zhang J, Abraham S, Choi JG, Shi G, Qi L, Manjunath N, Wu H. 2015. A CRISPR-Based Screen Identifies Genes Essential for West-Nile-Virus-Induced Cell Death. Cell Rep 12:673-83.
114. Sessions OM, Barrows NJ, Souza-Neto JA, Robinson TJ, Hershey CL, Rodgers MA, Ramirez JL, Dimopoulos G, Yang PL, Pearson JL, Garcia-Blanco MA. 2009. Discovery of insect and human dengue virus host factors. Nature 458:1047-50.
115. Echeverri CJ, Beachy PA, Baum B, Boutros M, Buchholz F, Chanda SK, Downward J, Ellenberg J, Fraser AG, Hacohen N, Hahn WC, Jackson AL, Kiger A, Linsley PS, Lum L, Ma Y, Mathey-Prevot B, Root DE, Sabatini DM, Taipale J, Perrimon N, Bernards R. 2006. Minimizing the risk of reporting false positives in large-scale RNAi screens. Nat Methods 3:777-9.
116. Birmingham A, Anderson EM, Reynolds A, Ilsley-Tyree D, Leake D, Fedorov Y, Baskerville S, Maksimova E, Robinson K, Karpilow J, Marshall WS, Khvorova A. 2006. 3' UTR seed matches, but not overall identity, are associated with RNAi off-targets. Nat Methods 3:199-204.
117. Bushman FD, Malani N, Fernandes J, D'Orso I, Cagney G, Diamond TL, Zhou H, Hazuda DJ, Espeseth AS, Konig R, Bandyopadhyay S, Ideker T, Goff SP, Krogan NJ, Frankel AD, Young JA, Chanda SK. 2009. Host cell factors in HIV replication: meta-analysis of genome-wide studies. PLoS Pathog 5:e1000437.
118. Jinek M, Chylinski K, Fonfara I, Hauer M, Doudna JA, Charpentier E. 2012. A programmable dual-RNA-guided DNA endonuclease in adaptive bacterial immunity. Science 337:816-21.
119. Gasiunas G, Barrangou R, Horvath P, Siksnys V. 2012. Cas9-crRNA ribonucleoprotein complex mediates specific DNA cleavage for adaptive immunity in bacteria. Proc Natl Acad Sci U S A 109:E2579-86.
120. Mali P, Esvelt KM, Church GM. 2013. Cas9 as a versatile tool for engineering biology. Nat Methods 10:957-63.
121. Sanjana NE, Shalem O, Zhang F. 2014. Improved vectors and genome-wide libraries for CRISPR screening. Nat Methods 11:783-4.

122. Shalem O, Sanjana NE, Hartenian E, Shi X, Scott DA, Mikkelsen TS, Heckl D, Ebert BL, Root DE, Doench JG, Zhang F. 2014. Genome-scale CRISPR-Cas9 knockout screening in human cells. Science 343:84-7.
123. Apte-Sengupta S, Sirohi D, Kuhn RJ. 2014. Coupling of replication and assembly in flaviviruses. Curr Opin Virol 9C:134-142.
124. Muller DA, Young PR. 2013. The flavivirus NS1 protein: molecular and structural biology, immunology, role in pathogenesis and application as a diagnostic biomarker. Antiviral Res 98:192-208.
125. Walker KW, Lyles MM, Gilbert HF. 1996. Catalysis of oxidative protein folding by mutants of protein disulfide isomerase with a single active-site cysteine. Biochemistry 35:1972-80.
126. Laboissiere MC, Sturley SL, Raines RT. 1995. The essential function of protein-disulfide isomerase is to unscramble non-native disulfide bonds. J Biol Chem 270:28006-9.
127. Zhou H, Clapham DE. 2009. Mammalian MagT1 and TUSC3 are required for cellular magnesium uptake and vertebrate embryonic development. Proc Natl Acad Sci U S A 106:15750-5.
128. Watterson D, Modhiran N, Young PR. 2016. The many faces of the flavivirus NS1 protein offer a multitude of options for inhibitor design. Antiviral Res 130:7-18.
129. Lam SS, Martell JD, Kamer KJ, Deerinck TJ, Ellisman MH, Mootha VK, Ting AY. 2015. Directed evolution of APEX2 for electron microscopy and proximity labeling. Nat Methods 12:51-4.
130. Houzet L, Jeang KT. 2011. Genome-wide screening using RNA interference to study host factors in viral replication and pathogenesis. Exp Biol Med (Maywood) 236:962-7.
131. Hatahet F, Ruddock LW. 2007. Substrate recognition by the protein disulfide isomerases. FEBS J 274:5223-34.
132. Li W, Xu H, Xiao T, Cong L, Love MI, Zhang F, Irizarry RA, Liu JS, Brown M, Liu XS. 2014. MAGeCK enables robust identification of essential genes from genome-scale CRISPR/Cas9 knockout screens. Genome Biol 15:554.
133. Bocchinfuso WP, Ma KL, Lee WM, Warmels-Rodenhiser S, Hammond GL. 1992. Selective removal of glycosylation sites from sex hormone-binding globulin by site-directed mutagenesis. Endocrinology 131:2331-6.
134. Shrimal S, Gilmore R. 2015. Reduced expression of the oligosaccharyltransferase exacerbates protein hypoglycosylation in cells lacking the fully assembled oligosaccharide donor. Glycobiology 25:774-83.
135. Huang CY, Butrapet S, Moss KJ, Childers T, Erb SM, Calvert AE, Silengo SJ, Kinney RM, Blair CD, Roehrig JT. 2010. The dengue virus type 2 envelope protein fusion peptide is essential for membrane fusion. Virology 396:305-15.
136. Salloum S, Wang H, Ferguson C, Parton RG, Tai AW. 2013. Rab18 binds to hepatitis C virus NS5A and promotes interaction between sites of viral replication and lipid droplets. PLoS Pathog 9:e1003513.
137. Heaton NS, Perera R, Berger KL, Khadka S, Lacount DJ, Kuhn RJ, Randall G. 2010. Dengue virus nonstructural protein 3 redistributes fatty acid synthase to

sites of viral replication and increases cellular fatty acid synthesis. Proc Natl Acad Sci U S A 107:17345-50.
138. Frolova EI, Fayzulin RZ, Cook SH, Griffin DE, Rice CM, Frolov I. 2002. Roles of nonstructural protein nsP2 and Alpha/Beta interferons in determining the outcome of Sindbis virus infection. J Virol 76:11254-64.
139. Yi Z, Sperzel L, Nurnberger C, Bredenbeek PJ, Lubick KJ, Best SM, Stoyanov CT, Law LM, Yuan Z, Rice CM, MacDonald MR. 2011. Identification and characterization of the host protein DNAJC14 as a broadly active flavivirus replication modulator. PLoS Pathog 7:e1001255.
140. McGee CE, Shustov AV, Tsetsarkin K, Frolov IV, Mason PW, Vanlandingham DL, Higgs S. 2010. Infection, dissemination, and transmission of a West Nile virus green fluorescent protein infectious clone by Culex pipiens quinquefasciatus mosquitoes. Vector Borne Zoonotic Dis 10:267-74.
141. Tsetsarkin K, Higgs S, McGee CE, De Lamballerie X, Charrel RN, Vanlandingham DL. 2006. Infectious clones of Chikungunya virus (La Reunion isolate) for vector competence studies. Vector Borne Zoonotic Dis 6:325-37.
142. Atasheva S, Krendelchtchikova V, Liopo A, Frolova E, Frolov I. 2010. Interplay of acute and persistent infections caused by Venezuelan equine encephalitis virus encoding mutated capsid protein. J Virol 84:10004-15.
143. Schoggins JW, Dorner M, Feulner M, Imanaka N, Murphy MY, Ploss A, Rice CM. 2012. Dengue reporter viruses reveal viral dynamics in interferon receptor-deficient mice and sensitivity to interferon effectors in vitro. Proc Natl Acad Sci U S A 109:14610-5.
144. Lanciotti RS, Lambert AJ, Holodniy M, Saavedra S, Signor Ldel C. 2016. Phylogeny of Zika Virus in Western Hemisphere, 2015. Emerg Infect Dis 22:933-5.
145. Hung V, Udeshi ND, Lam SS, Loh KH, Cox KJ, Pedram K, Carr SA, Ting AY. 2016. Spatially resolved proteomic mapping in living cells with the engineered peroxidase APEX2. Nat Protoc 11:456-75.
146. Wang H, Perry JW, Lauring AS, Neddermann P, De Francesco R, Tai AW. 2014. Oxysterol-binding protein is a phosphatidylinositol 4-kinase effector required for HCV replication membrane integrity and cholesterol trafficking. Gastroenterology 146:1373-85 e1-11.
147. Tang X, Snowball JM, Xu Y, Na CL, Weaver TE, Clair G, Kyle JE, Zink EM, Ansong C, Wei W, Huang M, Lin X, Whitsett JA. 2017. EMC3 coordinates surfactant protein and lipid homeostasis required for respiration. J Clin Invest 127:4314-4325.
148. Ruggiano A, Foresti O, Carvalho P. 2014. Quality control: ER-associated degradation: protein quality control and beyond. J Cell Biol 204:869-79.
149. Stein A, Ruggiano A, Carvalho P, Rapoport TA. 2014. Key steps in ERAD of luminal ER proteins reconstituted with purified components. Cell 158:1375-1388.
150. Ye Y, Meyer HH, Rapoport TA. 2003. Function of the p97-Ufd1-Npl4 complex in retrotranslocation from the ER to the cytosol: dual recognition of nonubiquitinated polypeptide segments and polyubiquitin chains. J Cell Biol 162:71-84.

151. Cortese M, Goellner S, Acosta EG, Neufeldt CJ, Oleksiuk O, Lampe M, Haselmann U, Funaya C, Schieber N, Ronchi P, Schorb M, Pruunsild P, Schwab Y, Chatel-Chaix L, Ruggieri A, Bartenschlager R. 2017. Ultrastructural Characterization of Zika Virus Replication Factories. Cell Rep 18:2113-2123.
152. Taguwa S, Maringer K, Li X, Bernal-Rubio D, Rauch JN, Gestwicki JE, Andino R, Fernandez-Sesma A, Frydman J. 2015. Defining Hsp70 Subnetworks in Dengue Virus Replication Reveals Key Vulnerability in Flavivirus Infection. Cell 163:1108-1123.
153. Tsetsarkin KA, Kenney H, Chen R, Liu G, Manukyan H, Whitehead SS, Laassri M, Chumakov K, Pletnev AG. 2016. A Full-Length Infectious cDNA Clone of Zika Virus from the 2015 Epidemic in Brazil as a Genetic Platform for Studies of Virus-Host Interactions and Vaccine Development. MBio 7.
154. Zhao G, London E. 2006. An amino acid "transmembrane tendency" scale that approaches the theoretical limit to accuracy for prediction of transmembrane helices: relationship to biological hydrophobicity. Protein Sci 15:1987-2001.
155. Krogh A, Larsson B, von Heijne G, Sonnhammer EL. 2001. Predicting transmembrane protein topology with a hidden Markov model: application to complete genomes. J Mol Biol 305:567-80.
156. Diaz A, Gallei A, Ahlquist P. 2012. Bromovirus RNA replication compartment formation requires concerted action of 1a's self-interacting RNA capping and helicase domains. J Virol 86:821-34.